FEASIBILITY OF VERY DEEP BOREHOLE DISPOSAL OF US NUCLEAR DEFENSE WASTES

By

Frances Elizabeth Dozier

B.S., Civil and Environmental Engineering (2009)

University of Maryland College Park

SUBMITTED TO THE DEPARTMENT OF NUCLEAR SCIENCE
AND ENGINEERING
IN PARTIAL FULFILLMENT OF THE REQUIREMENTS FOR THE DEGREE OF

MASTER OF SCIENCE IN NUCLEAR SCIENCE AND ENGINEERING
AT THE
MASSACHUSETTS INSTITUTE OF TECHNOLOGY

SEPTEMBER 2011

Signature of Author: _____
Frances Elizabeth Dozier
Department of Nuclear Science and Engineering
August 8, 2011

Certified by _____
Michael J. Driscoll
Professor Emeritus of Nuclear Science and Engineering
Thesis Supervisor

Certified by _____
Jacopo Buongiorno
Associate Professor of Nuclear Science and Engineering
Thesis Reader

Accepted by _____
Mujid S. Kazimi
TEPCO Professor of Nuclear Engineering
Chair, Department Committee on Graduate Students

FEASIBILITY OF VERY DEEP BOREHOLE DISPOSAL OF

US NUCLEAR DEFENSE WASTES

By Frances Elizabeth Dozier

Submitted to the Department of Nuclear Science and Engineering on August 5, 2011 in partial fulfillment of the requirements of the degree of Master of Science in Nuclear Science and Engineering

Abstract

This thesis analyzes the feasibility of emplacing DOE-owned defense nuclear waste from weapons production into a permanent borehole repository drilled ~4 km into granite basement rock. Two canister options were analyzed throughout the thesis: the canister currently used by the DOE for vitrified defense waste and a reference canister with a smaller diameter. In a thermal analysis, the maximum temperatures attained by the rock surrounding the waste, waste form, canister, liner, and gaps during the post-emplacement period were calculated. From this data, simple analytic equations were formed that can be used to calculate the maximum temperature differences for both defense waste and spent fuel when one does not want to repeat the analysis. Canister corrosion and waste form dissolution analyses were performed using Pourbaix diagrams. Finally, the cost and time for drilling the borehole and emplacing the defense waste were calculated.

The temperature change in the granite is 15.1°C for the reference canister and 45.7°C for the DOE Canister. The resulting maximum temperature at the bottom of the borehole is 135.1°C (reference canister) and 165.7°C (DOE canister) for the bounding defense waste. The centerline temperature for the borosilicate glass waste package is approximately 150°C for the reference canister and 207°C for the DOE canister. Because of the thermodynamic properties, overall corrosion resistance, and reasonable cost, pure copper was shown to be the best borehole outer canister material. High-chromium stainless steel could also be a good option for borehole canisters because it has been shown to be highly corrosion-resistant in environments similar to predicted borehole environments. Cesium ion was found to have the highest concentration in the borehole environment. However, the relatively low half life of the most abundant cesium isotope suggests that the cesium would decay before the canister is breached. For the reference canister, the drilling and emplacement costs are not expected to exceed $46/kg of vitrified waste and the total disposal cost was found to be $153/kg of vitrified waste. The total cost of disposal of defense waste in DOE containers is not expected to exceed $53/kg of vitrified waste. Based on these analyses, disposal of vitrified defense waste in deep boreholes is expected to be technically and economically feasible.

Thesis Supervisor: Michael J. Driscoll
Title: Professor Emeritus of Nuclear Science and Engineering

Thesis Reader: Jacopo Buongiorno
Title: Associate Professor of Nuclear Science and Engineering

Acknowledgements

As my thesis advisor, Professor Michael Driscoll provided patient guidance and a vast array of knowledge. His dedication to furthering the borehole repository concept is inspiring. Professor Jacopo Buongiorno was also instrumental in providing thoughtful explanations and technical expertise.

This thesis would not have been possible without the generous support of the Defense Nuclear Facilities Safety Board. I am grateful to Steven Stokes for serving as my mentor and providing valuable advice.

I would like to thank my father, Jerry Dozier, for teaching me to pursue my dreams and stretch my limits. Equal thanks to my mother, Tami Dozier, for passing on to me her natural curiosity and passion. Thank you both for your endless encouragement and unconditional support.

Finally, I would like to thank my grandmothers for helping to form me into the woman I have become. Thank you to my paternal grandmother and namesake, Frances Dozier, for giving me an amazing example of unshakable faith and solid work ethic. Thank you to my maternal grandmother, Elizabeth Smith, for encouraging me to seek balance, yet remain strong in all my endeavors.

Table of Contents

List of Tables

List of Figures

1 Introduction

1.1 Objective of the Thesis

Boreholes drilled several kilometers into crystalline basement rock remain a contender for the disposal of high-level nuclear waste, whether intact fuel assemblies or defense wastes. This project examines the feasibility of employing boreholes as a permanent repository for U.S. Department of Energy (DOE)-owned defense nuclear wastes (DNW). First, the DNW and defense waste package are described along with applicable properties of the borehole environment. The feasibility study considers the thermal behavior of defense waste and compares it to the behavior of spent nuclear fuel. Appropriate canister materials are also studied in relation to the borehole environment. The chemical behavior and solubility of the DNW is also analyzed. Finally, total cost and time required to dispose of the DNW is calculated.

1.2 Topic Motivation

In March 2010, DOE filed a motion to withdraw the Nuclear Regulatory Commission license application for the High Level Waste Repository at Yucca Mountain in Nevada. The waste that would have been stored at the Yucca Mountain Repository is currently held in temporary storage units at nuclear power plant sites and temporary storage areas designed by U.S. government contractors for waste from weapons development and naval reactors.[1] There is currently no alternative repository specified by the DOE for this waste. This provides the motivation for studying other promising disposal technologies.

One option is disposal in very deep boreholes drilled into crystalline continental bedrock for permanent deposition. Deep borehole disposal is a good alternative to a shallow mined

repository for several reasons. First, at emplacement depths (~2-4 km in this thesis), the environment is geochemically reducing.[2] This limits solubility and ensures low mobility of radionuclides[3] as shown in Chapter 5 of this thesis. The boreholes are also modular so boreholes can be drilled as additional repository space becomes necessary. Finally, the borehole disposal concept has widespread applicability because crystalline basement rocks with less than 1 km of sedimentary overburden are fairly common in the United States and world-wide.[4] These inherent benefits of borehole disposal can be augmented by choosing a site with desirable rock properties and environmental conditions (refer to Chapter 2).

Commonly mentioned disadvantages for a borehole repository are possible confinement breach by rise of hot water plumes (addressed in Section 2.5), expense (addressed in Chapter 6), and difficult retrievability.[5] Other disadvantages include possible inability of prior characterization and subsequent modeling, short life of engineered barriers and lack of licensing protocol.[6] These disadvantages are addressed to various degrees in several publications, but are considered outside the scope of this thesis.

This thesis focuses on disposing DNW in a borehole repository. In addition to the usual benefits of a borehole repository mentioned in this section, a DNW-specific borehole has the added benefit of irretrievability. Retrievability is desirable for spent fuel because changes in political or economic climates could make spent fuel reprocessing an attractive option. If this were the case, spent fuel retrieval from a borehole would be necessary. Although retrievability could be possible for waste in a borehole,[7] it would be expensive. Therefore, because a vast majority of the useful nuclides have been removed from the defense waste (refer to Section 2.2), even if reprocessing was employed in the U.S., the DNW would not need to be retrieved. This provides

an additional benefit of disposing of DNW in a borehole instead of a geologic repository like that at Yucca Mountain.

1.3 The History of the Borehole Concept

Boreholes were briefly considered by the United States for irretrievable plutonium weapon pit entombment in the 1990's.[8] The feasibility of borehole disposal was also analyzed in Sweden, as an alternative for their mined repository.[9] However, these and other borehole repository efforts were abandoned. This was due in part to the lack of drilling experience to suitable depths at that time.[10] Since then, most investigations of deep borehole disposal have been confined to Sheffield University in the United Kingdom, and the Massachusetts Institute of Technology and Sandia National Laboratories in the U.S. Improved drilling technology makes borehole repository study more attractive than in previous decades. Also, international interest in Enhanced Geothermal Systems that involve deep wells drilled into hot, dry rock has provided additional information applicable to deep borehole repository studies.[11]

In addition to general feasibility studies, several aspects of deep borehole repositories have been analyzed at the Massachusetts Institute of Technology. Borehole canister designs,[12] lateral emplacement[13] and other emplacement methods,[14] minor actinide disposal,[15] and effective thermal conductivity measurements in boreholes,[16] are topics of MIT theses from the last decade. The International Atomic Energy Agency, Sandia National Laboratories and Sheffield University have also published recent studies on borehole disposal of nuclear waste.

1.4 Arrangement of the Thesis

1.4.1 Description of Environment and Waste Form: Chapter 2

Chapter 2 describes the bounding waste generated from weapons production in the U.S. This is the waste with the maximum radiochemical composition from the Waste Treatment Plant at Hanford Site. It was expected to provide the maximum radioactive source term, on a canister basis, for the Yucca Mountain Nuclear Waste Repository. This waste will be mixed with molten borosilicate glass and allowed to cool at the Waste Treatment Plant, once begins operation (it is currently under construction). The history, radiological inventory, glass composition, and waste form for this bounding waste is described in this chapter.

Chapter 2 also discusses the proposed borehole configuration and environment that will be used for the remainder of the thesis. The repository configuration includes the dimensions of the proposed canister, as well as the depths associated with various aspects of the borehole repository design (such as the plug length, sedimentary overburden, borehole depth, etc.). The borehole environment section includes a discussion on the mechanisms of transport for nuclides that are assumed to escape from the waste canister. The environment section also includes an overview of the environmental parameters that do not directly affect nuclide transport, but are important in understanding the thermal, chemical, and mechanical behavior of the borehole (heat capacity, pH, reduction potential, etc.). The environmental parameters included in Chapter 2 are appropriate predictions; however, site characterization must occur prior to extensive borehole design.

1.4.2 Thermal Analysis: Chapter 3

One of the principal constraints of the feasibility of deep borehole disposal is the maximum temperature attained by the rock surrounding the waste during the post-emplacement period. Therefore, the maximum temperature change between the far field granite and the granite directly surrounding the borehole filled with emplaced waste is calculated in the thermal analysis. Temperature changes in the waste string, waste package canister, and gaps are also found. It is also valuable to find the time at which this maximum temperature occurs. To calculate these values, first, the decay heat of the vitrified waste was correlated with a model. Then, this model was used as in input for the integral representation of the temperature change from an infinite line source. The integral was approximated using Riemann sums, giving the temperature change between the borehole wall directly outside the waste package and the far field granite.

1.4.3 Waste Canister Corrosion Analysis: Chapter 4

Prospective canister materials including copper, tantalum, titanium, aluminum, iron, chromium, nickel, and their alloys were evaluated for suitability in the borehole environment through a literature review and a stability analysis using Pourbaix diagrams. The ideal waste canister should be corrosion resistant in a borehole environment to prevent possible release of nuclides. A robust canister is especially important for vitrified waste because the borosilicate glass used to vitrify defense waste dissolves much faster than spent fuel in geologic environments.[17] The stable form of the metal of the ideal canister should also be insoluble in a borehole environment. Copper is the canister material chosen for repositories in several other countries,[18] but other metal options are included in this analysis. The sections in Chapter 4 provide some of the

benefits and disadvantages of using various canister materials and a comparison of the corrosion susceptibility of each canister material using Pourbaix diagrams.

1.4.4 Waste Form Dissolution Analysis: Chapter 5

To understand the degradation behavior of the waste form (DNW vitrified in borosilicate glass), a literature review and chemical analysis were performed. The literature review outlines the experimental research conducted on waste form behavior in conditions similar to the borehole environment. The chemical analysis is twofold. First, to understand the leaching of the nuclides, Pourbaix diagrams were created for several nuclides in defense waste. The diagrams were used to determine the stable form of the nuclide in the borehole environment. The Common Thermodynamic Database[19] was used to determine the reaction associated with the stable form. In the second portion of the chemical analysis, the solubility product was used to find the maximum soluble concentration of each nuclide in the borehole environment. The maximum soluble concentration would only be the actual nuclide concentration in the borehole if the system were allowed to reach equilibrium; time is not considered in the calculation. Also, the calculation did not account for elements that would be in the water surrounding the borehole (other than the calcium, sodium, and chloride implicit in the Pourbaix diagrams). In reality, all nuclides and glass former constituents would be leaching concurrently and this will affect the actual concentration of each element.

1.4.5 Cost and Time for Disposal Analysis: Chapter 6

Part of analyzing the feasibility of borehole disposal of DNW is understanding the time and costs associated with disposal activities. For this reason, V-DeepBoRe (a Monte Carlo simulation-based cost model for borehole construction and waste package emplacement)[20] was modified to

create V-DeepBoRe-II. This model calculates the required time and cost of drilling, filling, and plugging a vertical borehole filled with vitrified waste canisters. These costs were added to the vitrification and package fabrication costs for vitrified waste to get a total cost for disposal of vitrified DNW. V-DeepBoRe-II was also utilized to generate a data set that was used to create diameter-dependent cost equations. These equations were used to extrapolate from smaller diameter canisters to predict the costs of the borehole disposal of the canisters currently employed at the Defense Waste Processing Facility and the ones designed for the Waste Treatment Plant.

1.4.6 Conclusions and Future Work: Chapter 7

In closing the thesis, the repository design, analyses, and evaluation tools are summarized and recommendations are made for future research for borehole repositories in general and DNW in borehole repositories in particular.

1.4.7 Appendices

Appendix A gives 6 combinations of DNW. The first 2 compositions are the nuclide concentrations in the Waste Treatment Plant bounding and average wastes. The other 4 compositions are the wastes associated with the Defense Waste Processing Facility. The glass former compositions are also given in Appendix A. Appendix B shows all of the MATLAB codes and spreadsheets used in the thermal analysis. Appendix C gives the Pourbaix diagrams and maximum soluble concentration calculations of several nuclides in DNW. Appendix D gives instructions and codes to use in V-DeepBoRe-II.

2 Description of Environment and Waste Form

2. 1 Chapter Introduction

This chapter outlines the assumptions and background information necessary to analyze the feasibility of very deep borehole emplacement as a disposal strategy for U.S. defense waste. This information includes a borehole repository reference geometry, a description of the bounding defense nuclear waste and its form, as well as the geological and chemical attributes and nuclide transport mechanisms of the granite borehole environment. These assumptions and characteristics are used in the analyses in the chapters which follow.

2.2 Description of Bounding Defense Waste

2.2.1 Brief History of US Weapons Complex

In 1942, the United States began to develop the technology that would enable the creation of nuclear weapons under the U.S. Army Corps of Engineers Manhattan Engineer District (called the Manhattan Project).[21] Over the next few decades, stockpiling nuclear weapons employed a manufacturing process that created large volumes of waste. Although the nation currently owns and maintains nuclear weapons, a vast majority of the weapons production activities have been suspended.[22]

During the extensive weapons manufacturing effort of the mid-to-late twentieth century, plutonium and uranium were separated to be used in weapons production.[23] The separations process involves dissolving spent nuclear fuel rods and targets in acid and separating out the plutonium and uranium using a set of chemical processes.[24] Waste generated by chemical separations processes accounted for more than 85% of the radioactive content generated in the

weapons production activities.[25] For this reason, the waste remaining after chemical separations of plutonium and uranium is the main waste source considered in this thesis.

For much of the history of the U.S. Weapons Complex, the separated product (the plutonium and uranium) had the highest priority; therefore, the remaining wastes were handled in ways that seemed appropriate at the time.[26] For example, waste from chemical reprocessing (in the form of liquid, sludge, or "saltcake")[27] was stored in single-shelled underground tanks at Hanford and Savannah River Sites.[28] However, tank storage is not regarded as adequate disposal and it is necessary to immobilize the waste prior to permanent disposal.[29] For this reason, the Defense Waste Processing Facility at Savannah River Site was constructed and the Waste Treatment Plant at Hanford Site is under construction. These facilities are designed to immobilize (solidify) the high-level waste from the tanks by mixing the waste with borosilicate glass.[30] When cooled, this creates the borosilicate glass logs discussed in section 2.3.

The DOE owns approximately 100 million gallons of high-level waste, as defined by the Atomic Energy Act of 1954.[31] DOE also owns hundreds of millions of gallons of transuranic waste, low-level waste, by product material, mixed low-level waste, and other waste. Of this waste, 89% of the radioactive content is from weapons programs. Wastes from reprocessing fuel from nuclear-powered naval vessels is also considered defense wastes.[32] Thus, there is significant variability in what could be called defense waste. However, for the purposes of this thesis, DNW is defined as the waste vitrified at the Defense Waste Processing Facility and the waste slated to be vitrified at the Waste Treatment Plant.

2.2.2 Bounding Defense Waste Composition

Waste from DOE tank 241-AZ-101 to be vitrified at the Waste Treatment Plant at Hanford Site is used to provide a conservative model for DNW. This tank holds the waste with the highest gamma dose, fissile material content, and decay heat because the waste was generated from the neutralization of wastes from reprocessing the highest burn-up and shortest decayed fuel from the N-Reactor at Hanford Site.[33] The waste in this tank was found to have the maximum chemical and radiochemical composition for Waste Treatment Plant waste and was expected to provide the maximum radioactive source term, on a canister basis, for the Yucca Mountain Nuclear Waste Repository.[34] Therefore, it is considered the bounding DNW for borehole disposal as well. Table 2-1 provides the concentrations of nuclides in this waste in curies per cubic meter (Ci/m^3).[35] It is important to note that most of these nuclides do not occur in the DNW as elemental metal; most are in the form of metal oxides. The elements are given instead of the oxides in table 2.1 so that the specific isotopes can be specified.

Table 2.1: Concentrations of Nuclides in Bounding Defense Waste

Isotope	Element	DNW [Ci/m³]	Isotope (con't)	Element (con't)	DNW [Ci/m³] (con't)	Isotope (con't)	Element (con't)	DNW [Ci/m³] (con't)
227	Ac	0.00012	93	mNb	3	126	Sn	0.48235
241	Am	396.639	59	Ni	0.41681	90	Sr	77058.8
243	Am	0.08403	63	Ni	45.8824	99	Tc	19.4118
14	C	0.1042	237	Np	0.21008	229	Th	0
242	Cm	0.35798	231	Pa	0.00036	232	Th	0.00013
243	Cm	0.05227	238	Pu	2.06723	232	U	0.00043
244	Cm	1.16807	239	Pu	17.8992	233	U	0.00176
60	Co	17.8992	240	Pu	5.40336	234	U	0.01227
134	Cs	230.252	241	Pu	158.824	235	U	0.00047
137	Cs	93277.3	242	Pu	0.00083	236	U	0.00099
152	Eu	6.15966	226	Ra	0.00001	238	U	0.00849
154	Eu	213.445	228	Ra	0.00005	90	Y	77058.8
155	Eu	275.63	106	Ru	6.0084	93	Zr	4.84034
129	I	0	125	Sb	158.824			
137	mBa	88235.3	79	Se	0.07689			
113	mCd	35.2101	151	Sm	3268.91			

The concentrations of nuclides for bounding Defense Waste Processing Facility waste is included in Appendix A. However, this was found to create a smaller radioactivity source term per canister than the waste described in table 2.1, therefore, it is not considered the bounding waste for borehole disposal. Average compositions of Waste Treatment Plant and Defense Waste Processing Facility waste are also included in Appendix A for comparison purposes.

2.2.3 Differences Between Hanford Waste and Savannah River Site Waste

Although the DNW at both Hanford and Savannah River Site was produced from the aqueous separations processes involved in generating weapons-grade material, the processes used at each site were slightly different. The only separation process employed at Savannah River was the

PUREX (Plutonium and Uranium Recovery by EXtraction) process.[36] PUREX and its modifications remain the standard method of aqueous separations and is currently employed at commercial reprocessing facilities including La Hague in France and other facilities world-wide.[37] Hanford also employed PUREX for weapons material extraction, but also used Bismuth Phosphate and Redox processes,[38] which were both made obsolete by PUREX. These processes were less efficient and produced more waste per fuel rod than PUREX.[39] Hanford also reprocessed some additional waste to recover uranium, cesium, and strontium. Thus, Hanford has 55 distinct waste types and Savannah River has 17. The compositions of the bounding and average wastes for Hanford (to be vitrified at the Waste Treatment Plant) and Savannah River (to be vitrified at the Defense Waste Processing Facility) are included in Appendix A.

2.3 Description of Waste Form

The defense waste form is considered, for this thesis, to be the borosilicate glass logs produced at Defense Waste Processing Facility and Waste Treatment Plant. Glass was chosen over a crystalline material because non-crystalline glass is a less uniformly coordinated solid and offers a variety of atom sites for solution of a wide range of elements.[40] Borosilicate glass was chosen because it can melt at relatively low temperatures (less than 900^{o}C) and can be poured controllably at a desired viscosity.[41] Disadvantages of borosilicate glass are that it can devitrify when under high local stresses and can be more soluble in ground water than crystalline forms of similar chemistry.[42] Nonetheless, both the Defense Waste Processing Facility and Waste Treatment Plant are designed to vitrify defense waste in borosilicate glass; a change from this waste form would be costly and require significant design changes.

In all waste considered in this thesis, the nuclides are assumed to account for 45% of the total mass of the borosilicate glass logs. The actual loading of the radionuclides may vary up to 45% by mass;[43] however, to ensure a conservative decay heat analysis (refer to Chapter 3), the maximum nuclide loading is assumed for all waste. Therefore, the remaining 55% of waste form mass is composed of glass formers. The masses and relative percentages of the glass formers in the bounding waste from Hanford is included in table 2.2. The glass formers that compose 55% by mass of the average Hanford waste are included in Appendix A. The glass former composition for Savannah River waste is unavailable; however, it is expected to be similar to the compositions in table 2.2 and will also encompass 55% by mass of the waste form.

Table 2.2: Glass Former Composition for Bounding Hanford Defense Waste

	Mass of Glass Former (kg)	Percentage of Waste Form by Mass
Al_2O_3	108.22	3.83%
B_2O_3	166.13	5.88%
Fe_2O_3	52.00	1.84%
Li_2O_3	65.21	2.31%
Na_2O	288.12	10.20%
SiO_2	866.61	30.68%
Total Glass Formers	1553.78	55.00%
Total Glass Mass	2810.92	

2.4 Repository Geometry

The next step in analyzing the feasibility of disposing of defense waste in deep boreholes is to determine a repository geometry design. The reference depths (emplacement zone, plug zone,

and total depth) used in this thesis was based on that created by Ian Hoag.[44] Although others have specified a 2 km sedimentary overburden,[45] Hoag assumes that a suitable granite formation can be found within 1 km of the surface, allowing for a 2 km emplacement zone in a 4 km hole.

Two waste canisters are analyzed in this thesis. The first waste canister (filled with the vitrified DNW) is assumed to have an outer diameter of 340 mm and a height of 5 m and is based on Ian Hoag's design.[46] The second waste canister is the canister currently employed by DOE at the Defense Waste Processing Facility and designed for use by DOE at the Waste Treatment Plant. The Hoag canister, as it will be referred to in this thesis, is smaller than the DOE canister and has been shown to be a feasible for borehole emplacement. The DOE canister is 3 m or 4.5 m in height and has a larger diameter (0.61 m).[47] Because of the large diameter, special considerations must be made for understanding the cost and feasibility of emplacement (refer to Chapter 6). It should be noted that the DOE canister is currently being employed at the Defense Waste Processing Facility, but because the Waste Treatment Plant has not been constructed yet, the Hoag canister could be used at the Waste Treatment Plant. This provides flexibility in the actual design canister used in a borehole repository.

The waste canister will be surrounded by a borehole liner casing, which serves as liner to prevent the waste canister from becoming stuck in the hole.[48] Hoag specifies H40 Steel as the final casing material.[49] Additional research should ensure that galvanic coupling does not occur between the casing and the waste canister and increase corrosion rates.

Additional information on the drilling and emplacement procedure and cost can be found in Chapter 6. Figure 2.1 shows the dimensions specified by Hoag that will be used in this thesis. Figure 2.2 shows the dimensions of the DOE canister. Table 2.3 gives the inner and outer

diameters of each radial element of the borehole repository design. The diameters given reflect the configuration after canister emplacement and the borehole is sealed by a plug in the upper zone.

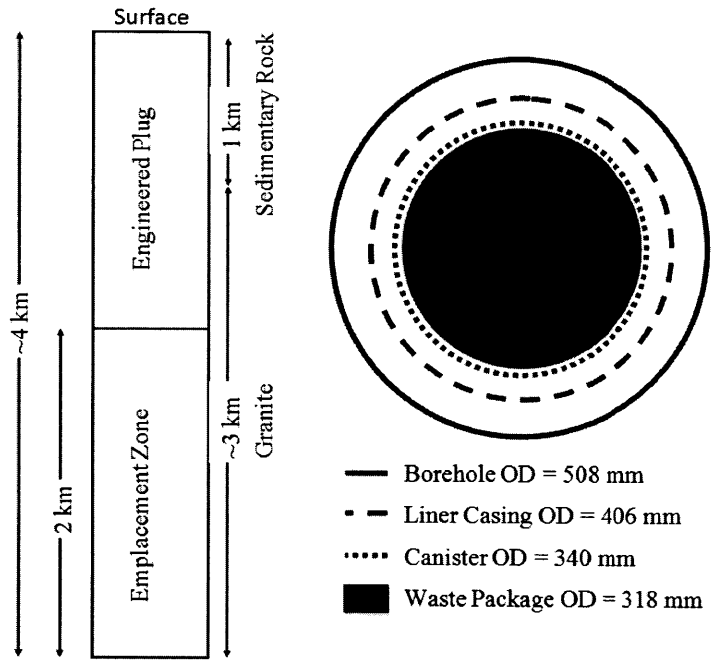

Figure 2.1: Cross Section of Borehole Reference Design and Plan View of Hoag Canister (not to scale)

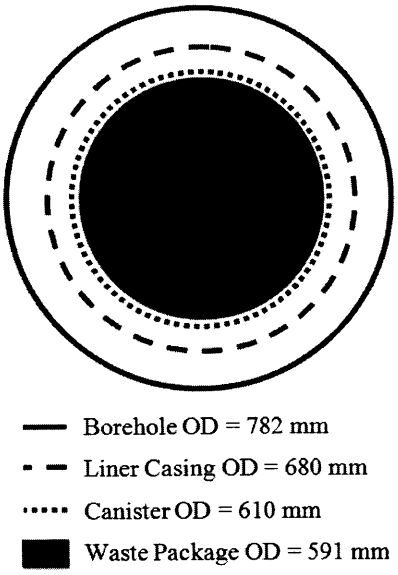

Figure 2.2: Cross Section of DOE Canister (not to scale)

Table 2.3: Dimensions of Canister Designs

	Borehole	Liner Casing	Canister	Waste Package
Reference Outer Diameter	---	406 mm	340 mm	318 mm
Reference Inner Diameter	508 mm	387 mm	318 mm	--
DOE Outer Diameter	---	680 mm	610 mm	591 mm
DOE Inner Diameter	782 mm	661 mm	591 mm	--

2.5 Borehole Attributes that Govern Nuclide Transport

Radioactive waste would be sealed in boreholes when the borehole environment is dry because the lack of aqueous electrolyte in a borehole is a major beneficial environmental feature of the granite borehole. However, it is possible that after some time period, the borehole fills with water. This is not likely, however, it must be assumed to occur to assess the upper bound on risk to the public. In the remainder of this thesis, the assumption that the borehole fills with water is called the design basis failure scenario.

In the design basis failure scenario, the canister and waste form are assumed to immediately fail. The protections against this occurring are discussed in Chapters 4 and 5. Therefore, the water in this scenario is assumed to become contaminated with soluble nuclide species (this process is discussed in Chapter 5). Contaminated water can travel vertically and horizontally. Both types of movement are defined by different borehole rock properties.

Horizontal transport is based on diffusion of the contaminated water through the rock surrounding the borehole. The properties that govern this process include permeability, porosity, rock water content, and rock density. These properties are described in sections 2.5.1 through 2.5.3

Vertical transport of nuclides is defined by water density gradients. As the nuclides decay, the decay power heats the water and therefore decreases the density. If there were no resisting mechanism, this contaminated water could rise to the surface. The resisting mechanisms in this situation cause an increase in the density of water as depth increases to offset the density decrease from the decay heat. Borehole properties such as salinity, down-hole pressure, and geothermal gradient are the natural mechanisms that affect the water density and affect vertical transport of nuclides.

Borehole attributes that do not directly affect nuclide-contaminated water transport are discussed in section 2.6. All borehole attributes mentioned are summarized in table 2.4.

2.5.1 Porosity and Permeability

Porosity is the volume of all the open spaces in the intact rock. Permeability is the rate at which fluid flows through interconnected pathways in a porous material. Porosity, and more specifically, permeability are key inputs into Darcy's Law, which governs movement through a

porous media, therefore, accurate measurements of these values are vital to understand the transport mechanisms of radionuclides.

The target value is less than one percent by volume for porosity and less than one microdarcy for permeability.[50] Lower values for permeability are desirable to ensure low water movement velocity. Lower values are more desirable for porosity because diffusion of a chemical through water in a porous media is directly related to the porosity of the material. This is quantified below.[51]

$$D_{eff} = \frac{D}{R} \quad [2\text{-}1]$$

$$R = 1 + K\frac{\rho_d}{n} \quad [2\text{-}2]$$

where:

D_{eff} = molecular diffusion coefficient of a chemical in a porous media, m^2/s
D = molecular diffusion coefficient in pure water, m^2/s
R = retardation factor, unitless
K = retention factor specific to the nuclide, m^3/kg
ρ_d = bulk density, kg/m^3
n = porosity, unitless

Therefore, as porosity decreases, the retardation factor is increased and therefore, the molecular diffusion coefficient is decreased. This diffusion coefficient plays two roles. First, it determines how much of the nuclide is captured in the host rock and therefore, if D_{eff} decreases, the maximum concentration of nuclides in water will decrease. Second, the distance from the borehole at which the maximum concentration occurs decreases as D_{eff} decreases. This is noteworthy because it means that the maximum concentration will occur closer to the well if D_{eff} decreases; this keeps the sphere of influence of the waste as small as possible.

The mechanism for transport of water through permeable rock is assumed to be through the faults and fractures of the bedrock.[52] Faults have been found at these depths and the transport of water through cracks would be much greater than the capillary transport through intact rock.[53] At large depths, the lithostatic pressure compresses the cracks; therefore, the permeability of a core sample must be measured under pressure to prevent a false-high reading.[54]

2.5.2 Rock Density

As shown in Equation [2-2], a higher rock bulk density is better because the retardation factor increases as the density increases. This decreases the effective molecular diffusion coefficient; therefore, concentration of nuclides in water and distance of maximum contamination decrease when the rock density increases.

2.5.3 Radial Transport Summary

The preceding rock properties are the governing parameters as contaminants travel radially through the host rock. If values for permeability and porosity are close to those specified in table 2.4 and the pressure gradient is close to lithostatic, it can be shown that the transport radially through permeable rock can be reduced to a 1 km radius over a million years.[55] This means that the risk of contamination at depths accessible to humans is bounded by vertical nuclide transport. The properties that affect vertical transport are described in sections 2.5.4 through 2.5.7. Both the vertical and horizontal transport mechanisms are summarized in figure 2.3.

2.5.4 Salinity

Salinity is the dissolved salt content in the borehole water produced by the leaching of the host rock. Sodium and chloride leaching increases with temperature and depth.[56] Therefore, the decay heat increases the already significant salinity gradient at 4 km. Therefore, the process

would lead to positive feedback; as the temperature increases from decay heat, the density decreases, but the salinity also increases, which produces an increased density as a counter balance.

Experimental data show that water in deep boreholes has at least a 10% salinity,[57] which decreases to fresh water levels at depths close to the surface. This salinity is produced by a down-hole rock salinity of greater than 40 grams of salt per kg of rock at 3 km.[58] This salinity gradient produces a corresponding 10% density gradient. This density gradient is large enough to compensate for the density decrease from the decay heat (approximately 6.7%).[59] From a nuclide transport perspective, higher salinity values are more desirable because they maximize the ability to compensate for heat produced in the borehole. However, from a corrosion perspective, minimizing salinity is ideal. Because this section is focused on nuclide transport, the ideal goal for salinity in table 2.4 reflects the ideal values in reference to nuclide transport and not corrosion.

2.5.5 Down-hole Pressure

Like salinity, the down-hole pressure slightly increases the density of the water in the borehole as depth increases. Without any pressure buildup from gas formation, the down-hole pressure will be close to hydrostatic pressure (the pressure exerted by the weight of a column of water above a point). This density gradient is about 1.2% at 3 km[60] and, like the salinity density gradient, can aid in the offset of the decay heat temperature density gradient.

One source predicts that the pressure gradient in granite basement rock is 0.03 Gigapascals per km.[61] Another specifies that the pressure at 2-5 km in granite is 0.1-0.2 GPa, which is roughly the same as the previous estimation.[62] Both of these values are slightly above the hydrostatic

pressure gradient (~11 MPa/km). Pressure slightly greater than hydrostatic pressure is desirable (but not necessary) to maximize the ability to compensate for the decay heat density gradient. However, if one balances near and far-field hydrostatic columns to obtain a net buoyant force, the pressure effect in a uniform rock stratum will largely cancel, and in any event be much lower than temperature induced buoyancy differentials.

2.5.6 Geothermal Gradient

In addition to the decay heat from the waste, there is also an increase in heat from the geothermal gradient. It is desirable to minimize this temperature gradient by the selection of repository rock conditions so that it does not exacerbate the problem of the "chimney effect" of contaminated water. One study that specifically focused on crystalline basement rock gave the mean thermal gradient value in granite basement rock as 2°C/100m (20°C/km).[63] However, data from geothermal exploration in New Mexico indicates a maximum temperature gradient between 55°C/km and 89°C/km.[64] The average thermal gradient in the area is 25°C/km,[65] which is used as the expected gradient for the present thesis. This particular borehole is exposed to a great deal of geothermal activity, and is therefore a conservative estimate for a borehole sited specifically to limit the geothermal gradient. The ideal borehole would likely be sited with a geothermal gradient below this average. Site selection is made easier by the present research in vertical geothermal gradients from the prospective of siting Enhanced Geothermal Systems (EGS) drilled into hot dry rock.[66] The less attractive sites for EGS would be ideal for waste disposal.

2.5.7 Vertical Transport Summary

Decay heat and geothermal gradient increase the temperature at emplacement depths in a borehole. This decreases the density of any contaminated water. However, natural protective

features such as salinity and down-hole pressure counteract this by increasing the density of water at emplacement depths. Analyses have shown that these protective features significantly delay and dilute any contaminants arriving at hypothetical human receptors, even if a water supply well is located directly above the disposal borehole.[67] However, this process will likely be analyzed further in future borehole performance assessments. Figure 2.3 summarizes the various transport mechanisms of contaminated water in a borehole environment.

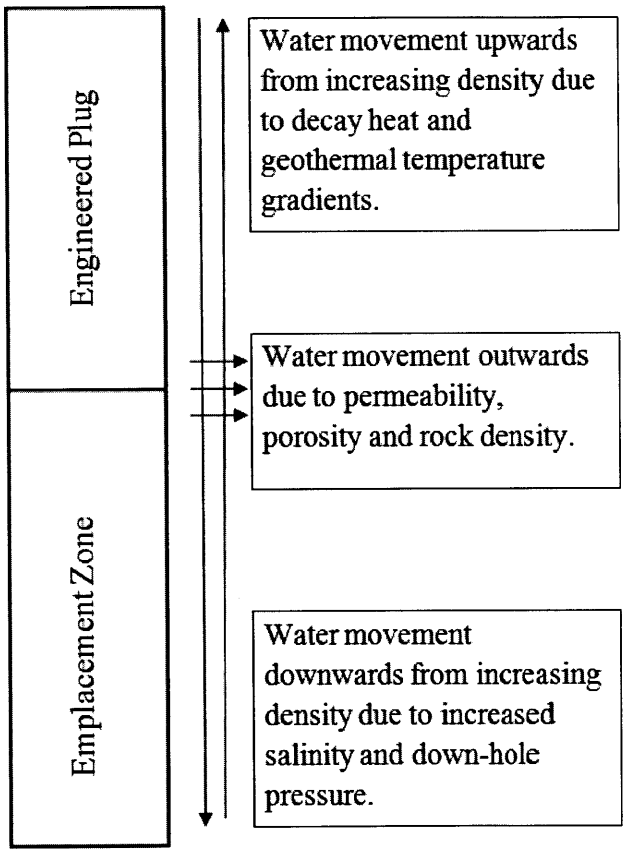

Figure 2.3: Mechanisms for Transport of Nuclide-Contaminated Water

2.6 Other Attributes of the Borehole Environment

This section focuses on the borehole attributes that do not directly affect nuclide transport. These properties include pH, thermal conductivity, heat capacity, and reduction potential and are described in this section. These parameters do not necessarily affect borehole siting to the extent of the parameters that govern nuclide transport. However, they are included in table 2.4 for coherency.

2.6.1 Down-hole pH

Very basic or acidic values for pH increase the corrosion rate of the canister and affect the solubility of radionuclides.[68] Therefore, the ideal down-hole pH would be between 6 and 9.[69] Whenever possible, it is desirable to decrease corrosion rates so that the canister stays intact for as long as possible. However, in the transport analysis, the liner and canister are expect to fail immediately upon waste emplacement. Therefore, ensuring a lower corrosion rate for the waste canister is an additional conservatism.

2.6.2 Thermal Conductivity and Heat Capacity

The thermal conductivity of a material characterizes its ability to transfer heat. In the deep borehole scenario, limiting the temperature gradients is desirable to minimize the density gradients. Therefore, the ideal thermal conductivity for deep bore holes would be very large. Heat capacity is the amount of heat required to change the temperature of a substance. Ideally, this would be as high as possible so that the decay heat changes the temperature of the granite by as little as possible. However, the thermal properties are restricted to prospective host rock properties, which fall within a fairly narrow range. It can be noted here that salt (an alternative borehole environment) has a higher thermal conductivity than granite.

2.6.4 Reduction Potential

The reduction potential (E_h) of the borehole environment is the measure of the tendency for species in borehole water to acquire electrons. Borehole environments tend to have a negative potential, which is one of the conditions responsible for the reducing environment (other conditions that contribute are the oxygen poor environment and the prevalence of nitrogen and hydrogen).[70] This reducing environment causes solubility to be limited and sorption onto host rock to increase.[71] This relationship is described further in Chapters 4 and 5. At Yucca Mountain Nuclear Waste Repository, the conditions are oxidizing, which increases corrosion rates and mobility of the radionuclides. Therefore, the negative potential is one advantage of a deep borehole repository that was not present in the Yucca Mountain Repository.

2.7 Chapter Summary

This chapter describes the environment and waste form associated with disposal of DNW. To understand the waste form, it is necessary to understand how and why the defense waste was created. The resulting nuclide composition of the bounding DNW is found in table 2.1. These nuclides are immobilized in borosilicate glass, which is the waste form described in section 2.3. The composition of waste formers in the borosilicate glass is described in table 2.2.

The environmental model includes the repository geometry as well as the borehole attributes. The diameter specifications of the Hoag canister and are shown in figure 2.1 and listed in table 2.3. The DOE canister considered in this thesis is shown in figure 2.2 and described in table 2.3. The borehole attributes are separated into 3 categories; properties that define vertical nuclide transport, properties that define radial nuclide transport, and other borehole attributes. These are described in sections 2.5 and 2.6. The borehole properties that define vertical nuclide transport

(salinity, down-hole pressure, and geothermal gradient) demand the most attention because vertical transport is the pathway by which nuclides could reach levels accessible by humans. A summary of the borehole attributes mentioned as well as the ideal specifications associated with each property and the value for granite are given in table 2.4.

Table 2.4: Summary of Parameters and Values for Granite

Environmental Attribute	Ideal Specifications	Granite Value used in Analyses	Reference
Permeability	$<1 \times 10^{-6}$ Darcy	10^{-5} Darcy	[72]
Porosity	<1% by volume	0.5%	[73]
Granite Density, ρ	As large as possible	2600 kg/m³	[74]
Granite Thermal Conductivity, k	As large as possible	2.6 W/m/^{0}C	[75]
Granite Heat Capacity, C_p	As large as possible	790 J/kg/^{0}C	[76]
Granite Thermal Diffusivity, $\propto = \frac{k}{\rho * C_p}$		39.9 m²/y	
Average Geologic Gradient	As low as possible	25^{0}C/km	[77]
Average Temperature at Borehole Bottom, T		135^{0}C	
Salinity	As large as possible	100g/kg	[78]
Major Borehole Brine Constituents		20 mol/kg Calcium, 100 mol/kg Chloride, 60 mol/kg Sodium	[79]
Average pH	>6, <9	7 to 9	[80]
Reduction Potential, E_h	< 0 mV	-200 to -300 mV	[81]
Down-hole Pressure in Rock	Close to hydrostatic	26 MPa/km	[82]
Hydrostatic Water Pressure		10.8 MPa/km	[83]

Once the environmental and waste form models are defined, it is possible to begin other analyses on the feasibility of borehole disposal of U.S. weapons waste.

3 Thermal Analysis

3.1 Chapter Introduction

One of the principal constraints on the feasibility of deep borehole disposal is the maximum temperature attained by the rock surrounding the waste during the post-emplacement period. The objective of the thermal analysis is to find the maximum temperature change between the far field granite and the granite directly surrounding the borehole filled with emplaced waste. It is also valuable to find the time at which this maximum temperature occurs. Temperature changes in the waste form, waste canister, liner, and gaps are also found.

3.2 Temperature Difference in Granite

The simplest way of modeling the thermal performance of a borehole repository is to treat the string of canisters as an infinite line source in an infinite, homogeneous granite slab. This was the method employed in this analysis because it has been shown, by Jonathan S. Gibbs in his MIT Master's thesis,[84] to adequately match the temperature changes in host rock surrounding pressurized and boiling water reactor spent fuel canisters calculated using two and three dimensional analyses in the Solidworks Simulation code for the first 20 years after emplacement.[85] Gibbs' two dimensional analysis involves finding the temperature changes over time in a 30 m by 100 m slab with the thickness the same as the length of the reactor fuel assembly studied, with adiabatic boundary conditions on all slab faces, with the exception of the heat flux onto the borehole wall. The three dimensional analysis involves finding the temperature changes in a 1/10 scale slab of the repository and includes vertical diffusion of heat through the repository. Although these analyses were conducted for pressurized water reactor

and boiling water reactor assemblies, the heat transfer processes would be the same as those for DNW.

The infinite line source approximation bounds the two and three dimensional analysis for the first 6 years and is within 2% for the first 20 years after emplacement. In all models, the maximum temperature occurs within the first 20 years;[86] therefore, the infinite line source approximation is an adequate model for the maximum temperature changes to the granite surrounding emplaced waste. The general solution for the radial temperature profile resulting from an infinite line source in an infinite, homogeneous medium is given in equation [3-1].[87] Host rock and waste properties are given in table 2.4.

$$\Delta T(r,t) = \frac{1}{4\pi k}\int_0^t q'(\theta) * e^{-\frac{r^2}{4\alpha(t-\theta)}}\frac{d\theta}{t-\theta} \qquad [3\text{-}1]$$

where:

$\Delta T(r,t)$ = Change between borehole wall and far field temperatures, ^{0}C
t = Time after Emplacement, years
θ = Integration Variable
$d\theta$ = Integration Increment size
k = Granite Thermal Conductivity, W/m/^{o}C
α = Granite Thermal Diffusivity, m^2/year
r = Radius of Borehole, m
$q'(\theta)$ = Decay Heat Function, W/m

Using equation [3-1] involves several inherent assumptions. First, mean waste package thermal properties inside the hole are assumed similar to those of the surrounding host rock. One dimensional conduction is also assumed and the typical 15 - 30°C/km vertical geothermal gradient is ignored.

3.2.1 Decay Heat Model

Ideally, a simple decay heat function, $q'(\theta)$, could be used that allows equation [3-1] to be solved analytically. In reality, the decay function is dependent on the decay mechanisms of all of the nuclides in the waste. To find an acceptable predictive function for the decay heat, the actual decay heat must be found. In order to find the decay heat that incorporates all of the nuclide decay mechanisms, ORIGEN, a program within the SCALE 6.0 software package, was used.[88] First, the curies/m^3 values for each nuclide in the bounding DNW (bounding Waste Treatment Plant waste in Appendix A) were input into the ORIGEN graphical user interface in the composition tab. Then, 40 time increments (the maximum number of increments allowed) were created, starting at 0.3 years (after 2001, year specified for the bounding DNW composition) and increasing by no more than a factor of 1.3 to 3340 years. ORIGEN produced the total decay heat from the waste in Watts/m^3 at each of the time steps. This data was multiplied by the cross sectional area of the canister waste form (0.0794 m^2 for the Hoag canister and 0.274 for the DOE canister) to get decay heat in Watts/m. Then, the cooling time was subtracted from each time output to find time after emplacement. The resulting time steps and corresponding linear decay heat can be found in Appendix A.

Next, it is necessary to find a simple equation for the decay heat so that equation [3-1] can be solved. The decay heat was predicted to decay roughly proportionately to the decay of the dominant nuclides as in equation [3-2]. The dominant nuclides in the waste are Cs-137 and Sr-90 and their short-lived daughters, Ba-137 and Y-90. The cesium and strontium have half lives of approximately 30 years and their daughters have relatively negligible half lives, therefore, the best fit decay constant will likely be close to 30 years.

$$q'(t) = q'(t_c) * e^{-\lambda t} \quad [3\text{-}2]$$

where:

$q'(t)$ = Decay Heat Function, W/m
$q'(t_c)$ = Decay Heat at Time of Emplacement, W/m
λ = Decay Constant of Bounding Nuclide(s), $years^{-1}$
t = Time After Emplacement, years

The decay constant in equation [3-2] was varied to find the best fit to the decay heat data from ORIGEN. Figure 3.1 shows that that equation [3-2] with the best fit decay constant fits the data from ORIGEN very well for the first 200 years after emplacement. The best fit decay constant corresponds to a nuclide half life of 29.63 years and fits the ORIGEN data for the Waste Treatment Plant bounding DNW with an R^2 value of 0.99996 for the first 200 years.

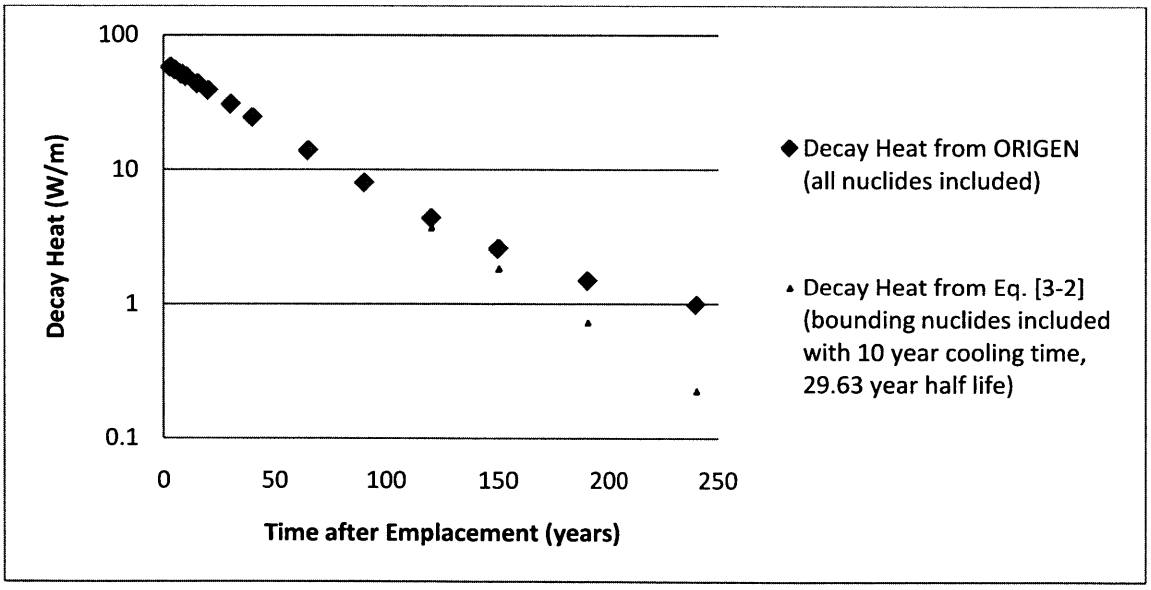

Figure 3.1: Best Fit Decay Heat vs. Time for ORIGEN Data and Equation [3-2]

Understanding the decay heat associated with the bounding DNW is important in this analysis because this waste produces the largest possible temperature difference in the granite. Therefore,

the dominant nuclide half life of 29.63 was fit to the bounding Waste Treatment Plant DNW listed in Appendix A. However, this nuclide half life also fits the non-bounding data fairly well for the first 200 years. The differences in the waste composition of the various DNW are described in section 2.2.3 and Appendix A. Table 3.1 shows each of the wastes described in Appendix A and the R^2 value for each data set and equation [3.2] with a nuclide half life of 29.63 years.

Table 3.1: Correlation Coefficients for Non-Bounding DNW and Equation [3.2]

DNW Type	R^2 Value for the First 200 Years
Waste Treatment Plant Bounding Waste [89]	0.99996
Waste Treatment Plant Average Waste [90]	0.9999
Defense Waste Processing Facility Batch 1 A [91]	0.9902
Defense Waste Processing Facility Batch 1 B [92]	0.9995
Defense Waste Processing Facility Batch 2-3C [93]	0.99995
Defense Waste Processing Facility Batch 4-10 [94]	0.9934

3.2.2 Analytical Approximation of Temperature Changes in Granite from Defense Waste

Once a decay heat function is determined, it is possible to numerically solve for the temperature changes in the granite. This is accomplished by using the midpoint method Riemann sum approximation found in equation [3-3].

$$\Delta T(r,t) = \frac{1}{4\pi k}\sum_{0}^{t} q'(t_c) * e^{-\lambda\theta} * e^{-\frac{r^2}{4\alpha(t-\theta)}} * \frac{d\theta}{t-\theta} \qquad [3\text{-}3]$$

where:

$\Delta T(r,t)$ = Maximum change between borehole wall and far field temperatures, ^{0}C
T = Time after Emplacement, years
t_c = Cooling Time, years
θ = Integration Variable
dθ = Integration Increment size
k = Granite Thermal Conductivity, W/m/^{0}C
α = Granite Thermal Diffusivity, m^2/year
r = Radius of Borehole, m
$q'(t_c)$ = Decay Heat at Time of Emplacement, W/m
λ = Decay Constant of Bounding Nuclide, $years^{-1}$

Because DNW was created at over several decades, the time variables in equation [3-3] are not immediately intuitive. Therefore, figure 3.2 is a timeline for DNW. The zero axis of Figure 3.2 is January 1, 2001 because the estimations of the radiochemical inventory for the bounding DNW are available for this date (refer to Appendix A). The zero axis for the Defense Waste Processing Facility waste described in Appendix A would be 2004, because the nuclide compositions are available for 2004 for waste from Savannah River Site.

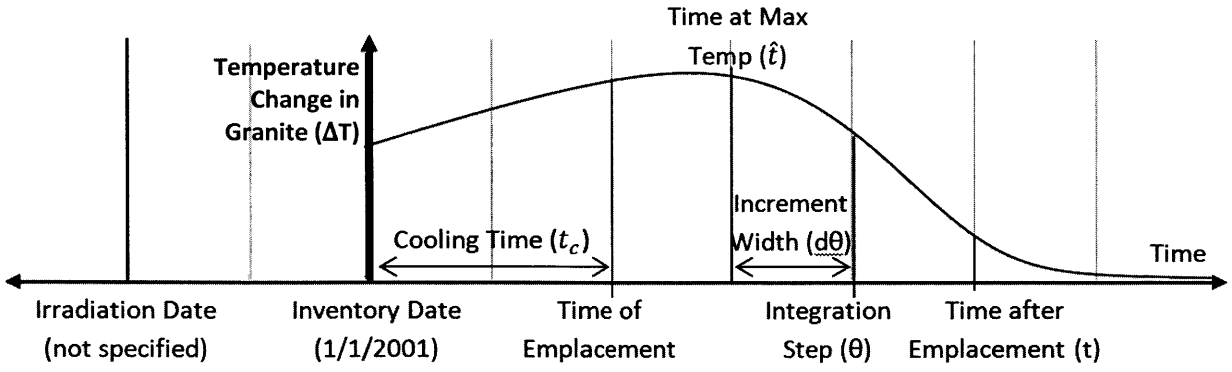

Figure 3.2: Time Variables for Host Rock Temperature Changes for Defense Nuclear Waste

Equation [3-3] was solved for several different combinations of cooling times, granite properties, and canister radius. This was accomplished by creating the MATLAB code included in Appendix B. Because equation [3-3] is a summation, the number of increments to produce accurate results must be found. Through repeated runs of the MATLAB code, it became apparent that the largest temperature changes per increment occurred when the integration step, θ, was close to the time after emplacement, t. In other words, large changes in temperature occur in the last increment of the Riemann sum. In the unaltered midpoint method Riemann sum, the last increment was treated like all of the other increments prior, which produced unacceptable error. Therefore, the last increment is separated into additional increments. Then, the number of main increments and the number of sub-increments in the last main increment were increased by a factor of 10 until the temperature changes converged. Convergence was assumed when the increased number of increments produced a maximum difference in values of less than 2.5%. Using this criterion, the number of main increments and sub-increments that produced adequately accurate data was 10E6 and 10E4, respectively. Before being implemented, the MATLAB code in Appendix B was verified against other studies (Gibbs[95] and Ranade[96]) to ensure accuracy.

Solving equation [3-3] produces a matrix that includes each time step and the host rock temperature change at each time step. However, the most meaningful values are the maximum host rock temperature change and the time step at which this occurs. These values for several different combinations of host rock properties, borehole radii, and cooling times can be found in Table 3.2.

Table 3.2: Maximum Temperature Changes in Granite and Time to Maximum Temperature for Bounding DNW

	Cooling Time (t_c, years)	Linear Decay Heat (q'(t_c), W/m)	Dominant Nuclide Half Life ($t_{1/2}$, years)	Thermal Diffusivity of Host Rock (α, m²/yr)	Borehole Radius (r, m)	Max Temp Change in Granite (ΔT, ° C)	Time at Max Temp Change ($\hat{t}$, years)
1	10	61.735	100	39.919	0.254	17.120	15.927
2	10	61.735	30	39.919	0.254	15.097	5.438
3	10	61.735	29.63	39.919	0.254	15.077	5.384
4	10	61.735	10	39.919	0.254	13.281	2.051
5	10	2.991	29.63	39.919	0.13	0.840	4.731
6	10	400.543	29.63	39.919	0.5	83.320	6.313
7	10	2.991	29.63	79.838	0.13	0.897	4.283
8	10	400.543	29.63	19.960	0.5	76.034	6.905
9	10	206.787	29.63	39.919	0.391	45.714	5.888
10	20	48.781	100	39.919	0.254	13.528	15.927
11	20	48.781	30	39.919	0.254	11.930	5.438
12	20	48.781	10	39.919	0.254	10.494	2.051
13	50	24.311	100	39.919	0.254	6.742	15.770
14	50	24.311	30	39.919	0.254	5.945	5.384
15	50	24.311	10	39.919	0.254	5.230	2.031
16	100	8.022	100	39.919	0.254	2.225	15.927
17	100	8.022	30	39.919	0.254	1.962	5.331
18	100	8.022	10	39.919	0.254	1.726	2.010

The predicted values for cooling time, dominant half life, thermal diffusivity and borehole radius are given in line 3 for the Hoag canister and line 9 for the DOE canister and are shown in grey shading in table 3.2. Thus, the predicted maximum change in temperature in the granite due to DNW is approximately 15.1^{0}C for the Hoag canister and 45.7^{0}C for the DOE canister. When added to the expected nominal temperature at 4 km (120^{0}C, refer to section 2.4), the expected maximum temperature in a borehole is approximately 135.1^{0}C for the Hoag canister and 165.7^{0}C for the DOE canister. The impact of this temperature on prospective canister materials is discussed in Chapter 4.

The maximum temperature changes for the non-bounding DNW were also calculated for both the DOE and Hoag canisters under the expected borehole conditions in table 2.4. These can be found in table 3.3. Note that all of the temperature differences for the non-bounding DNW are less than the corresponding temperature difference for bounding DNW.

Table 3.3: Temperature Changes in Granite for Non-bounding DNW

DNW Type	Temperature Difference (°C)	
	DOE Canister	Hoag Canister
Waste Treatment Plant Bounding Waste	45.714	15.077
Waste Treatment Plant Average Waste	3.2294	1.0328
Defense Waste Processing Facility Batch 1 A	0.1541	0.0493
Defense Waste Processing Facility Batch 1 B	0.6362	0.2034
Defense Waste Processing Facility Batch 2-3C	0.8047	0.2574
Defense Waste Processing Facility Batch 4-10	7.2833	2.3296

3.2.3 Analytical Approximation of Temperature Changes in Granite for Spent Fuel

The temperature change in the granite surrounding a borehole emplaced with spent nuclear fuel (SNF) has been extensively studied.[97] However, it is useful to calculate the temperature change for spent fuel under the various conditions (cooling time, granite properties, canister radius) to compare this with the corresponding temperature change for DNW.

Equation [3-4] is a general form of the decay heat function of SNF.[98] Equation [3-5] is a specific form of the decay heat function for SNF and is used in the MATLAB code in Appendix A. Equation [3-5] corresponds to a fuel burnup of 60MWd/kg.[99] Equation [3-5] is used as an input into equation [3-1] and produces the analytical equation shown in equation [3-6].

$$q'(t) = q'(t_c) * \left(\frac{t_c}{t + t_c}\right)^{3/4} \quad [3\text{-}4]$$

$$q'(t) = \frac{2200}{(t + t_c)^{3/4}} \quad [3\text{-}5]$$

$$\Delta T(r,t) = \frac{1}{4\pi k} \sum_{0}^{t} \frac{2200}{(t + t_c)^{3/4}} * e^{-\frac{r^2}{4\alpha(t-\theta)}} * \frac{d\theta}{t - \theta} \quad [3\text{-}6]$$

where:

$\Delta T(r,t)$ = Maximum change between borehole wall and far field temperatures, ^{0}C
t = Time after Emplacement, years
t_c = Cooling Time, years
θ = Integration Variable
$d\theta$ = Integration Increment size
k = Granite Thermal Conductivity, W/m/^{0}C
α = Granite Thermal Diffusivity, m^2/year
r = Radius of Borehole, m
$q'(t_c)$ = Decay Heat at Time of Emplacement, W/m

Equation [3-5] was used in the MATLAB code in Appendix A to calculate the temperature changes in the granite surrounding the SNF canisters. The number of time increments was the same as for the DNW analysis. The maximum temperature changes and the times to maximum temperature are listed in table 3.4. In future sections, the data in tables 3.2 and 3.4 are called data histories.

Table 3.4: Maximum Temperature Changes in Granite and Time to Maximum Temperature for Spent Nuclear Fuel

	Cooling Time (t_c, years)	Thermal Diffusivity of Host Rock (α, m²/yr)	Borehole Radius (r, m)	Max Temperature Change in Granite (ΔT, ° C)	Time at Max Temp Change ($\hat{t}$, years)
19	10	79.838	0.127	106.052	1.732
20	10	39.919	0.254	84.303	2.265
21	10	19.960	0.508	63.441	3.146
22	40	39.919	0.254	34.905	7.552
23	100	39.919	0.254	19.281	16.907
24	100	79.838	0.127	23.276	14.276

Applicable values in table 3.4 are within 11% of the temperature changes calculated in other studies using similar parameters.[100] The predicted values for cooling time, thermal diffusivity, and borehole radius are given in line 22 and are shaded grey in table 3.4. The explanations for, and sources of, these values are given in table 2.4. Therefore, the predicted maximum change in temperature in the granite due to SNF is approximately 34.9°C. When added to the expected nominal temperature at 4 km (120°C, refer to Section 2.5.6), the expected maximum temperature at the borehole wall is approximately 155°C for SNF.

The expected temperature difference for SNF is greater than that from DNW for the same granite properties and canister dimension. This is also true for other combinations of repository properties analyzed in this study; however, the SNF values only bound the corresponding DNW when the borehole radius is 0.254 m or less. This is shown in figure 3.3. This figure shows the temperature differences in granite over time for SNF and DNW for both canister types.

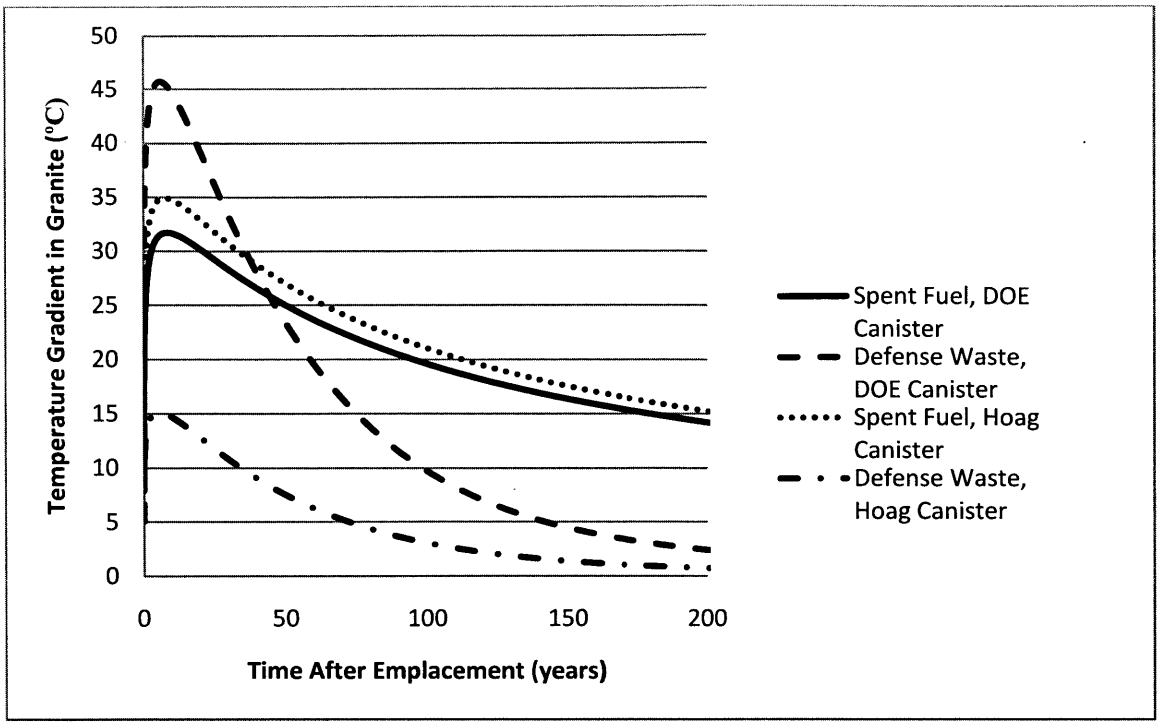

Figure 3.3: Temperature Differences in Granite for the First 200 Years After Emplacement

Note that for the Hoag canister in figure 3.3, the SNF differences bound the DNW differences for all time steps. However, for the DOE canister (which has a larger diameter), the SNF differences are less than the DNW differences. Also note that the spent fuel temperature differences for both the canisters are very similar, and the DNW temperature differences vary significantly. This is because the initial decay heat in the decay heat calculation for DNW (equation [3-2]) increases significantly with increases in radius. The decay heat calculation for SNF (equation [3-5]) does not depend on the borehole radius. Therefore, statements about SNF bounding DNW temperature differences in granite must be made carefully. With that in mind, this generality can be made: for temperature changes in the host rock, SNF can be assumed to bound DNW temperature changes, provided that host rock properties are the same, the cooling time of the

spent fuel and the dominant half life of the DNW is less than 100 years, and the borehole radius is 0.254 m or less.

3.2.4 Model for Temperature Changes in Granite and Time to Maximum Temperature

Once the maximum temperature changes in the granite are calculated, it is useful to find a model that can predict these maximum temperature changes without the need to repeat the analyses. For simplicity, equation [3-1] can be separated into equation [3-7] and [3-8].

$$\Delta T(r,t) = \frac{q'(t_c)}{4\pi k} G(r,\alpha,t) \quad [3\text{-}7]$$

$$G(r,\alpha,t) = \int_{\theta=0}^{t} \left[\frac{q'(\theta)}{q'(t_c)}\right] e^{-\frac{r^2}{4\alpha(t-\theta)}} \frac{d\theta}{t-\theta} \quad [3\text{-}8]$$

where:

$\Delta T(r,t)$ = Maximum change between borehole wall and far field temperatures, □C
t = Time after Emplacement, years
t_c = Cooling Time, years
θ = Integration Variable
dθ = Integration Increment size
k = Granite Thermal Conductivity, W/m/°C
$\propto$ = Granite Thermal Diffusivity, m²/year
r = Radius of Borehole, m
$q'(t_c)$ = Decay Heat at Time of Emplacement, W/m
$q'(\theta)$ = Decay Heat Function (from Equations [3-2] and [3-4]), W/m

The parameter G cannot be solved for explicitly. However, it is not necessary to know the values for G at all time steps; the values of most interest are the maximum values of G and the time at which this occurs. This corresponds to the maximum change in host rock temperature. Therefore, a predictive model for the $\hat{G}$, the peak value of parameter G, must be found. Equation [3-9] is used to find $\hat{G}$ that corresponds to the maximum temperature change in granite.

$$\hat{G} = \Delta T_{max} * \frac{4\pi k}{q'(t_c)} \quad [3\text{-}9]$$

where:

$\hat{G}$ = Peak Host Rock Temperature Factor (maximum value of parameter G), unitless
ΔT_{max} = Maximum Temperature Change in Granite calculated from MATLAB code, °C
t_c = Cooling Time, years
k = Granite Thermal Conductivity, W/m/°C
$q'(t_c)$ = Decay Heat at Time of Emplacement, W/m

After a parametric study, $\hat{G}$ was found to be a function of $\ln\left(\frac{4\alpha t_{\frac{1}{2}}}{r^2}\right)$ for DNW and $\ln\left(\frac{4\alpha t_c}{r^2}\right)$ for SNF. Once the time to maximum temperature, $\hat{t}$, was normalized by the cooling time for the SNF and the dominant half life for DNW, it was also found to be a function of $\ln\left(\frac{4\alpha t_{\frac{1}{2}}}{r^2}\right)$ for DNW and $\ln\left(\frac{4\alpha t_c}{r^2}\right)$ for SNF. It was previously understood that the values for $\hat{G}$ are a function of $\ln\left(\frac{4\alpha t_c}{r^2}\right)$.[101] However, this correlation did not hold for DNW and it is not immediately apparent that replacing t_c by $t_{1/2}$ would produce a better fit. The analysis that leads to this conclusion can be found in Figure 3.4. Basically, in order to find a correlation between t_c and $t_{1/2}$, the equations for calculating decay heat for both SNF and DNW were set equal to each other and rearranged, with several simplifying assumptions.

$$SNF\ Decay\ Function: q_{SNF}'(t) = q'(t_c) * \left(\frac{t_c}{t + t_c}\right)^{3/4}$$ From Equation [3-4]

$$q'(t_c) * \left(\frac{t_c}{t + t_c}\right)^{3/4} \approx q'(t_c) * \left(\frac{1}{1 + \frac{3}{4}\left(\frac{t}{t_c}\right)}\right)$$

$$Set\ \frac{t}{t_c} = x$$

$$q_{SNF}'(t) \approx q'(t_c) * \left(\frac{1}{1 + \frac{3}{4}x}\right)$$

$$DNW\ Decay\ Function: q_{DNW}'(t) = q'(t_c) * e^{-\lambda t}$$ From Equation [3-2]

$$q'(t_c) * e^{-\lambda t} \approx q'(t_c)\left(\frac{1}{1 + \lambda t}\right) = q'(t_c) * \left(\frac{1}{1 + \lambda t_c\left(\frac{t}{t_c}\right)}\right)$$

$$Set\ n = \lambda t_c$$

$$q_{DNW}'(t) \approx q'(t_c) * \left(\frac{1}{1 + nx}\right)$$

$$q_{SNF}'(t) = q_{DNW}'(t)$$

$$q'(t_c) * \left(\frac{1}{1 + \frac{3}{4}x}\right) \approx q'(t_c) * \left(\frac{1}{1 + nx}\right)$$

$$\therefore n = \frac{3}{4}$$

$$n = \lambda t_c = \frac{\ln(2)}{t_{\frac{1}{2}}} * t_c \approx \frac{3}{4}$$

$$t_c \approx t_{\frac{1}{2}} * \frac{3}{4 * \ln(2)} \approx 1.08 * t_{\frac{1}{2}}$$

$$\boldsymbol{hence, t_c \approx t_{\frac{1}{2}}}$$

Figure 3.4: Justification for Replacing t_c by $t_{1/2}$ in Defense Waste Calculations

The assumption that t_c can be replaced by $t_{1/2}$ in DNF calculations leads to the correlations depicted in figure 3.2 and quantified in equations [3-10] and [3-11].

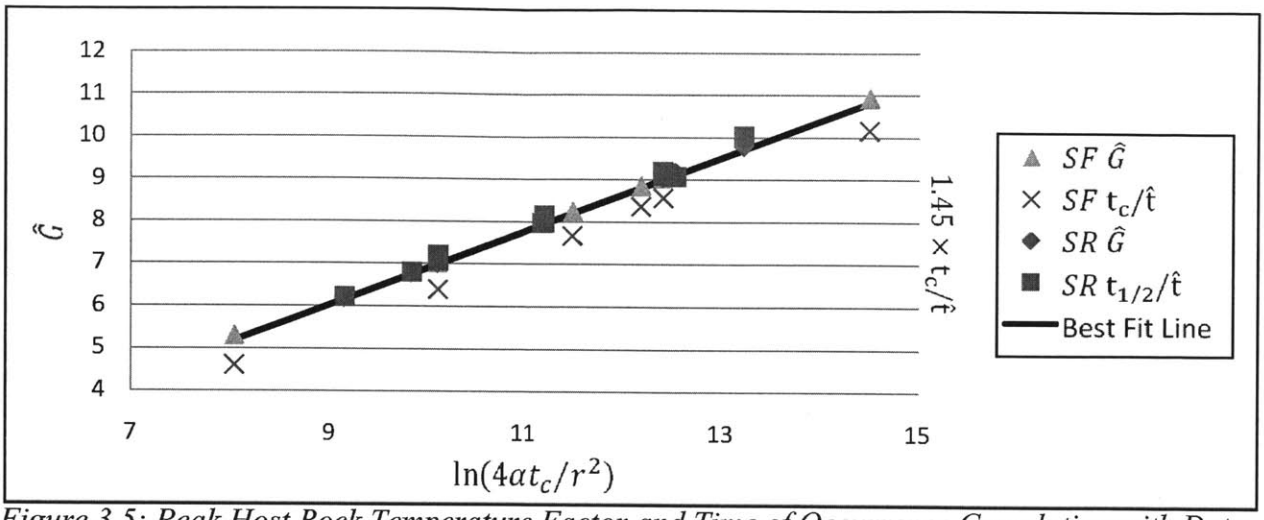

Figure 3.5: Peak Host Rock Temperature Factor and Time of Occurrence Correlation with Data Histories (replace t_c by $t_{1/2}$ for DNW)

As can be seen, from figure 3.5, the behavior of $\hat{G}$ is remarkably linear. Least squares curve fits give equations [3-10] and [3-11]. These equations can be used as simple approximations of the maximum host rock temperature and time to maximum temperature for future analyses.

$$\hat{G} = 0.872 \ln\left(\frac{4\alpha t_c}{r^2}\right) - 1.827 \qquad [3\text{-}10]$$

$$\frac{t_c}{\hat{t}} = 0.601 \ln\left(\frac{4\alpha t_c}{r^2}\right) - 1.260 \qquad [3\text{-}11]$$

where:

$\hat{t}$ = Time to Maximum Temperature Change, °C
t_c = Cooling Time (replace with $t_{1/2}$ for DNW), years
$\propto$ = Granite Thermal Diffusivity, m²/year
r = Radius of Borehole, m

The fit of these equations to the data histories (in tables 3.2 and 3.4) is shown in table 3.5. It is also interesting to note the analytically suggested relation in equation [3-12].

$$\frac{t_c}{\hat{t}} = \frac{\hat{G}}{1.45} \approx \frac{2}{3}\hat{G} \qquad [3\text{-}12]$$

where:

$\hat{t}$ = Time to Maximum Temperature Change, °C
t_c = Cooling Time (replace with $t_{1/2}$ for DNW), years
$\propto$ = Granite Thermal Diffusivity, m²/year
r = Radius of Borehole, m

Equations [3-10], [3-11], [3-12] were created using the following range of variables: 20 m²/year $< \alpha <$ 80 m²/year, 10 years $< t_c <$ 100 years, 10 years $< t_{1/2} <$ 100 years, and 0.13m $<$ r $<$ 0.50m.

Table 3.5: Fit of Equations [3-10] and [3-11] to Data Histories

	Max Difference Equation Fit	Least Squares Chart Fit
Defense Nuclear Waste $\widehat{G}$	±0.86%	$R^2 = 0.9999$
Defense Nuclear Waste $\frac{t_c}{\hat{t}}$	±3.3%	$R^2 = 0.9941$
Spent Nuclear Fuel $\widehat{G}$	±2.3%	$R^2 = 0.9997$
Spent Nuclear Fuel $\frac{t_c}{\hat{t}}$	±11.0%	$R^2 = 0.9977$

The higher uncertainty in peak time is in part due to the very flat profile of the temperature history. The higher uncertainty in the spent fuel is likely due to the fewer number of SNF data histories included in determination of equations [3-10] and [3-11].

Table 3.6 compares the correlation in equation [3-10] to borehole study results developed by others using more elaborate models and computer codes. Agreement is more than adequate considering the correlation's inherent assumptions and the fairly modest need for precision in the applications of equation [3-10].

Table 3.6: Comparison of Correlation with Code Results

Reference	Sizgek[102]	Kuo [103]	Gibb et al. [104]Case No. 4
Method of Calculation	Finite Volume 2D, CFX-4.2	Heating-3 Code	In-house Finite Difference Code
q', W/m	1060	103.7	525
r, m	0.6	0.254	0.3
α, m^2/y	34.3	31.6	34.1
t_c, y	5	10	20
k, W/m/°C	2.5	2.5	2.2
$\Delta\hat{T}$,°C	148	21.2	151
Eq [3-10], $\hat{G}$	4.76	6.79	7.17
Eq [3-7], ΔT, ^{0}C	161	22.4	136

It should be noted that, for a wide range of cases in granitic crystalline basement rock, one can take $\hat{G}$ as approximately 7 for preliminary planning purposes: a generalization also suggested by Kuo.[105]

Typical values of peak temperature rise are quite well tolerated. In general, temperature changes to the environment in borehole repositories are considerably lower than in their shallower mined counterparts as a consequence of the lower linear power due to small hole diameters provided by conventional oil/gas/geothermal well drilling technology. Also, the predicted temperature change in granite due to DNW is bounded by the predicted temperature change for SNF for the conditions outlined in section 3.2.3. Therefore, it is likely that a borehole designed to receive SNF can receive DNW without incurring higher thermal loading.

3.3 Temperature Difference in Waste Package, Canister, Liner, and Gaps

3.3.1 Model Overview

After the temperature at the borehole wall is calculated it is possible to find the temperature differences in the other radial layers of the borehole repository, such as the gaps, liner, and

canister. This leads to the calculation of the waste package centerline temperature. Figure 3.6 shows the dimensions of the gaps, liner casing, and canister for the DOE canister and the Hoag canister. This figure is based on the repository geometries in figures 2.1 and 2.2.

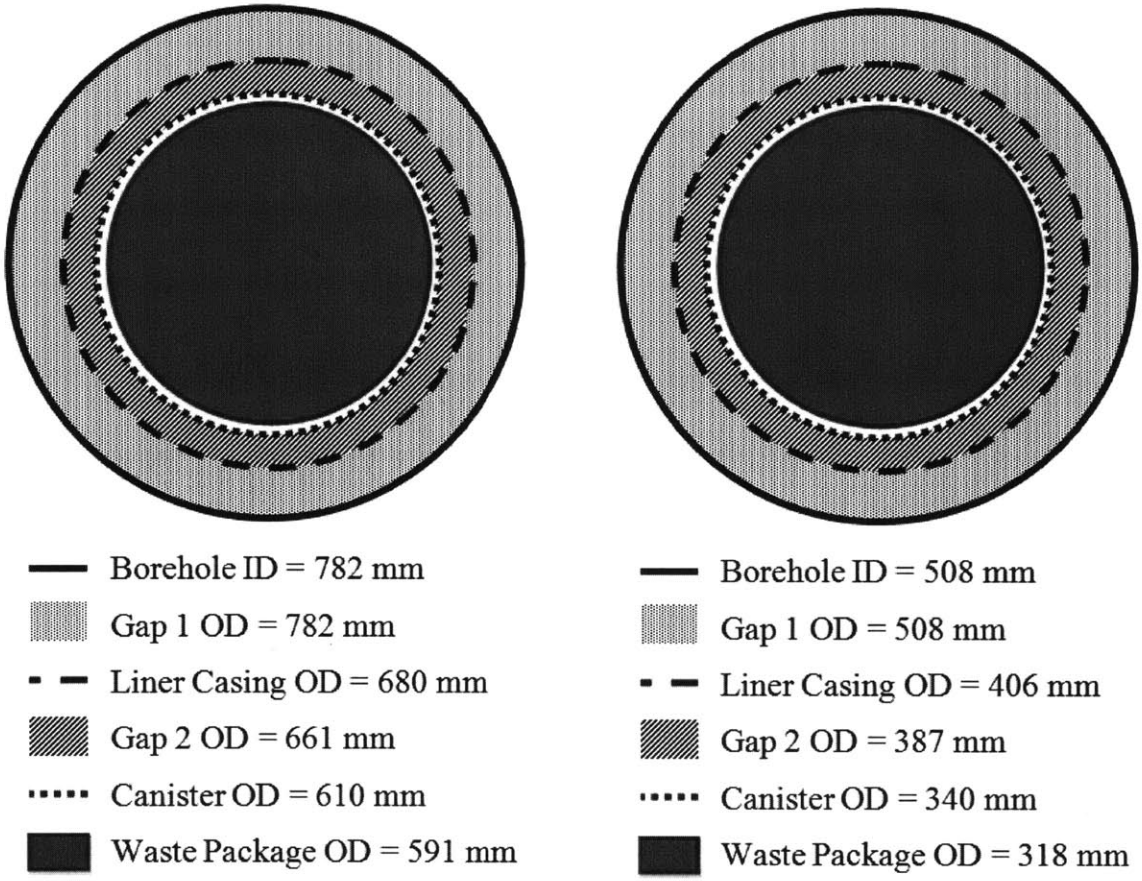

Figure 3.6: DOE Canister (Left) and Reference Canister (Right) Dimensions

Gap 1 is the space between the borehole wall and the liner casing. It is assumed to be filled with cement.[106] Gap 2 is the space between the liner and the canister. This is assumed to be filled with graphite sand. [107] Table 3.7 gives the dimensions and materials of each feature.

Table 3.7: Canister Dimensions and Gap Materials

Feature	Material	Thermal Conductivity		DOE Canister		Hoag Canister	
		Value (W/m/°C)	Ref.	Inner Diameter (m)	Outer Diameter (m)	Inner Diameter (m)	Outer Diameter (m)
Borehole Wall	Granite	2.6	[108]	0.782	---	0.508	---
Gap 1	Cement	1.21 (average)	[109]	0.68	0.782	0.406	0.508
Liner Casing	H40 Steel (Section 2.4)	50.2	[110]	0.661	0.68	0.387	0.406
Gap 2	Graphite Sand	0.37	[111]	0.61	0.661	0.34	0.387
Canister	Copper (Chapter 4)	377.2	[112]	0.591	0.61	0.318	0.34
Waste Form	Borosilicate Glass	1.1	[113]	---	0.591	---	0.318

Equation [3-13] shows the method used to calculate the temperature difference in the gaps, liner, and casing.[114]

$$T_{inner\ wall} = T_{outer\ wall} + \frac{q'(t)\ln\left(\frac{r_{outer}}{r_{inner}}\right)}{2\pi k} \qquad [3\text{-}13]$$

where:

$T_{inner\ wall}$ = Temperature on Inner Surface, °C
$T_{outer\ wall}$ = Temperature on Outer Surface, °C
$q'(t)$ = Linear Decay Power, W/m
r_{outer} = Outer Surface Radius, m
r_{inner} = Inner Surface Radius, m
k = Thermal Conductivity of Repository Feature, W/m/°C

As shown in equation [3-13], the temperature on the inside wall of each feature is greater than the temperature of the outside wall. For each radial feature, the temperature of the outside wall is the same as the temperature of the inside wall of the feature directly outside. Thus, the temperature increases starting with the borehole wall temperature calculated in section 3.2 proceeding inward to the highest temperature at the waste package centerline. Note that radiation is considered negligible.[115]

Equation [3-14] shows an analytical representation of the radial temperature differences based on the decay heat model used in section 3.2.1. It can be used as a simple way to calculate the temperature differences across the repository features when decay heat from ORIGEN is not available. Equation [3-14] fits the temperature differences for the radial repository features of both the DOE and Hoag canisters with an R^2 value of 0.99996 for the first 200 years.

$$T_{inner\ wall} = T_{outer\ wall} + \frac{q'(t_c) * e^{-\lambda t} * \ln\left(\frac{r_{outer}}{r_{inner}}\right)}{2\pi k} \qquad [3\text{-}14]$$

where:

$T_{inner\ wall}$ = Temperature on Inner Surface, °C
$T_{outer\ wall}$ = Temperature on Outer Surface, °C
r_{outer} = Outer Surface Radius, m
r_{inner} = Inner Surface Radius, m
k = Thermal Conductivity of Repository Feature, W/m/°C
$q'(t_c)$ = Decay Heat at Time of Emplacement, W/m
λ = Decay Constant of Bounding Nuclide(s), $years^{-1}$
t = Time After Emplacement, years

Equation [3-15] is the equation for the maximum centerline temperature of the waste form.[116] The decay heat model from section 3.2.1 can also be applied to this equation (with a R^2 value for

0.99996). Tabulated values for the temperatures in the waste form, canister, liner, and gaps can be found in Appendix B.

$$T_{centerline} = T_{waste\ form\ wall} + \frac{q'(t)}{4\pi k} \quad [3\text{-}15]$$

where:

$T_{centerline}$ = Centerline Temperature of the Waste Form, °C
$T_{waste\ form\ wall}$ = Temperature on Outer Surface of Waste Form, °C
$q'(t)$ = Linear Decay Power, W/m
k = Thermal Conductivity of Waste Form, W/m/°C

3.3.2 Temperature Difference Results for Repository Features

Table 3.8 shows the results for the maximum temperature difference calculations for the waste form, canister, liner, and gaps. The temperatures given represent the temperature at the inner wall of each radial feature.

Table 3.8: Maximum Temperatures in Repository Features

Feature	Material	Max Temp for DOE Canister (°C)	Max Temp for Hoag Canister (°C)
Borehole Wall	Granite	165.71	135.08
Gap 1	Cement	169.51	136.90
Liner Casing	H40 Steel	169.53	136.91
Gap 2	Graphite Sand	176.67	140.35
Canister	Copper	176.67	140.35
Waste Form	Borosilicate Glass	191.63 (Centerline Temperature)	144.82 (Centerline Temperature)
R^2 Value for fit with Eqs. [3-14] and [3-15]		0.99996	0.99996

Table 3.8 shows that the maximum centerline temperature for the waste form is approximately 192^{0}C for the DOE canister and 145^{0}C for the Hoag canister containing DNW. Gibbs suggests comparing this centerline temperature to the transportation canister peak fuel centerline thermal limit of 380^{0}C.[117] It should be noted that the leaching of the borosilicate waste form increases with temperature.[118] The implications of this are described in Chapter 5.

3.4 Chapter Summary

One of the principal constraints on the feasibility of deep borehole disposal is the maximum temperature attained by the rock surrounding the waste during the post-emplacement period. The objective of the thermal analysis was to find the maximum temperature change between the far field granite and the granite directly surrounding the borehole filled with emplaced waste. This is done by first creating a model for the decay heat function and implementing the model in the temperature difference equation for an infinite line source in a homogeneous granite slab. It is also valuable to find the time at which this maximum temperature occurs. Temperature changes in the waste form, waste canister, liner, and gaps are also found.

The decay heat from ORIGEN was found to fit very well with an exponential decay function multiplied by the initial linear decay heat at the time of emplacement (equation [3.2]). The decay constant that fits the bounding DNW the best corresponds to a dominant nuclide half life of 29.63 years. This is shown in figure 3.1. This decay constant also fits the non-bounding DNW well. The correlation coefficients for the decay heat model for the first 200 years are given in Table 3.1.

The analytical approximation of temperature difference in granite is shown in equation [3-3]. This equation was solved for the bounding DNW at the borehole environmental conditions described in table 2.4. The resulting temperature difference for the Hoag canister is 15.1^{0}C and 45.7^{0}C for the DOE Canister. When added to the expected geothermal difference, the resulting maximum temperature at the bottom of the borehole is 135.1^{0}C (Hoag Canister) and 165.7^{0}C (DOE Canister) for the bounding DNW at expected environmental conditions. This was found to occur 5.4 years and 5.9 years after emplacement for the Hoag Canister and the DOE Canister, respectively.

The expected borehole conditions (radius, thermal diffusivity of basement rock, and dominant half life) were varied to understand the dependence of the resulting maximum temperature difference on these conditions. The same was done for spent fuel in a borehole repository. This data was correlated to form simple analytic equations that can be used to calculate the maximum temperature difference and time to maximum temperature for both DNW and spent fuel. These are given in equations [3-10] and [3-11]. These equations were compared with theory and temperature differences given in other references.

The method used to calculate the temperature difference in the waste package, canister, liner, and gaps is given in equations [3-13] and [3-15]. Equation [3-14] allows the decay heat model from section 3.2 to be used to calculate the temperature differences in the gaps. The centerline temperature for the borosilicate glass waste form is approximately 192^{0}C for the DOE Canister and 145^{0}C for the Hoag Canister. The temperature differences for each of the repository features (waste form, canister, liner casing, and gaps) are given in table 3.6.

4 Waste Canister Corrosion Analysis

4.1 Chapter Introduction

Prospective canister materials including copper, tantalum, titanium, aluminum, iron, chromium, nickel, and their alloys were evaluated for suitability in the borehole environment through a literature review and a stability analysis using Pourbaix diagrams. The ideal waste canister should be corrosion resistant in a borehole environment to prevent the release of nuclides. A robust canister is especially important for vitrified waste because the borosilicate glass used to vitrify defense waste dissolves much faster than spent fuel in geologic environments.[119] The stable form of the metal of the ideal canister should also be insoluble at the temperatures and conditions predicted in a borehole environment. Copper is the canister material chosen for repositories in several other countries;[120] however other metal options are included in this analysis.

Material properties other than corrosion, such as toughness, strength, and ductility are not considered in this analysis. This is because once a metal or alloy is chosen, small changes in composition can be made if the mechanical properties are not adequate. Also, the most suitable metal could be plated onto a stronger or lower cost alloy if the suitable metal does not exhibit desired properties. Therefore, mechanical properties of the waste canister is outside the scope of this analysis, but should be examined in future work. Instead, the following sections provide some of the benefits and disadvantages of using various canister materials and a comparison of the corrosion susceptibility of each canister material using Pourbaix diagrams.

4.2 Pourbaix Diagram Methodology

In continuing a conservative analysis of the borehole repository design basis failure scenario, the borehole is assumed to fill with water. This is not likely, however, it must be assumed to occur to assess the upper bound of the risk to the public. If a borehole fills with water, canister and waste form degradation could occur. The degradation of the canister is defined by the corrosion mechanisms specific to the outer canister metal or alloy.

The HSC 6.0 Chemistry Software Package[121] was used to create the Pourbaix diagrams for each canister material considered (copper, tantalum, titanium, aluminum, iron, chromium, nickel). This program is able to produce suitable Pourbaix diagrams for a wide variety of aqueous systems because it has an extensive database of thermodynamic and equilibrium constants for most elements. Standard Pourbaix diagrams published in literature would not be suitable because of the concentrated brine in the borehole environment; therefore, HSC 6.0 was used to create appropriate diagrams. These diagrams show the specific conditions of potential and pH under which a metal either can react (or not) to form oxides or complex ions.[122]

It should be noted that Pourbaix diagrams are for an element rather than for an alloy. There is a distinct possibility that the corrosion resistance of an alloy may be different than the Pourbaix diagram for the alloy's main element. Therefore, the Pourbaix diagrams in this chapter can only be applied to pure metals; additional research is necessary to determine the stable form of each alloy at borehole conditions. Also, Pourbaix diagrams describe thermodynamic material behavior; further research is required to understand the kinetics of these behaviors. Localized chemistry conditions due to pits, crevices, and radiolysis may exist which could lead to localized corrosion such as pitting and stress corrosion cracking. Such conditions are not analyzed directly with Pourbaix diagrams.

The user-specified inputs necessary to create each Pourbaix diagram are the main element, other elements from the environmental data, and temperature. The species mode input in the HSC 6.0 Chemistry software package is specified as condensed and aqueous ions. To ensure conservative analyses, the temperature, pressure, and chemical composition at the bottom of the hole is used because it is the most severe (thermally, mechanically, and chemically). The expected temperature at the bottom of the borehole was found by adding the maximum temperature change at the borehole wall (found in section 3.2) to the average geothermal gradient and a predicted ambient temperature (assumed to be 20°C). The average thermal gradient considered in this thesis is 25°C/km,[123] even though the ideal borehole would likely be sited with a geothermal gradient below the average. The geothermal gradient in the borehole environment is explained further in section 2.5.6. The environmental attributes used as inputs in the HSC 6.0 software are summarized in table 4.1. Borehole attributes including average pH and reduction potential are specified to show the borehole environment range in the resulting diagrams and are also listed in table 4.1 A more complete listing of borehole environmental attributes can be found in table 2.4.

Table 4.1: Attributes of Deep Borehole Environment used in the HSC 6.0 Chemistry Software

Environmental Attribute	Value	Reference
Maximum Temperature Change from Defense Wastes	15.1°C	Section 3.2
Average Geologic Gradient	25°C/km	[124]
Expected Temperature at Borehole Bottom (Hoag Canister)	135°C	Section 3.2
Major Borehole Brine Constituents	20 mol/kg Calcium, 100 mol/kg Chloride, 60 mol/kg Sodium	[125]
Average pH	7 to 9	[126]
Electric Potential	-200 to -300 mV	[127]

Borehole repositories will likely contain heavy metal ions (discussion in the Chapter 5) as well as possibly significant levels of geology-specific constituents such as silica, magnesium, iron, etc.[128] However, these are not included in the Pourbaix diagrams because the concentrations are usually small compared to the sodium, chloride, and calcium concentrations. The temperature associated with the Hoag canister is used in this analysis because the material of this canister can be specified. The DOE canister employed at the Defense Waste Processing Facility is already designed, so the material has already been specified.

The following sections first outline the results of the literature review of the specified material and corresponding alloys and then comment on the stable form of the pure metal using the Pourbaix diagram.

4.3 Copper and Copper Alloy Suitability

The Swedish repository canister is a long-lived, 50 mm-thick copper waste package with an iron insert.[129] The copper canister's predicted performance is based on native copper experience; because the copper has been stable in the reducing environment of the granite for long geologic periods,[130] it can be assumed that it will continue to be stable.[131] The Finnish repository design also implements a copper outer canister for corrosion prevention.[132] Copper is also desirable for many countries because it is one of the only metals that remains stable as a metal (as opposed to forming an oxide) at normal geologic repository temperatures.[133]

Pure metals tend to be less susceptible to stress corrosion cracking than alloys.[134] This could be because pure metals tend to be weaker and usually cannot maintain the stress necessary to cause stress corrosion cracking or because there is no electrochemical difference among constituents. As long as applied strain is limited, the limited supply of oxygen will minimize the susceptibility of copper to environmental cracking.

Therefore, general corrosion is the most significant concern in a pure metal canister. The failure mechanism of copper is a function of the oxygen availability, the temperature, the salinity of the solution, and the reduction potential.[135] The long-term corrosion rates of many copper-based alloys in reducing geologic environments are also sufficiently low: less than 20 μm/yr at 200 °C.[136] At this rate, it would take approximately 2500 years to corrode through the Hoag canister. This adds conservatism to the analyses because, in the nuclide dissolution analysis in Chapter 5, the canister is assumed to immediately fail. Any time that the canister isolates the waste from the borehole environment allows the waste to decay, thereby reducing temperature, which reduces waste form leaching (discussed further in Chapter 5).[137] Another benefit of a pure copper canister is that the stable form is a metal at the expected borehole conditions. Figure 4.1

is the Pourbaix diagram that illustrates this. The shaded box in figure 4.1 bounds the expected borehole conditions outlined in table 4.1.

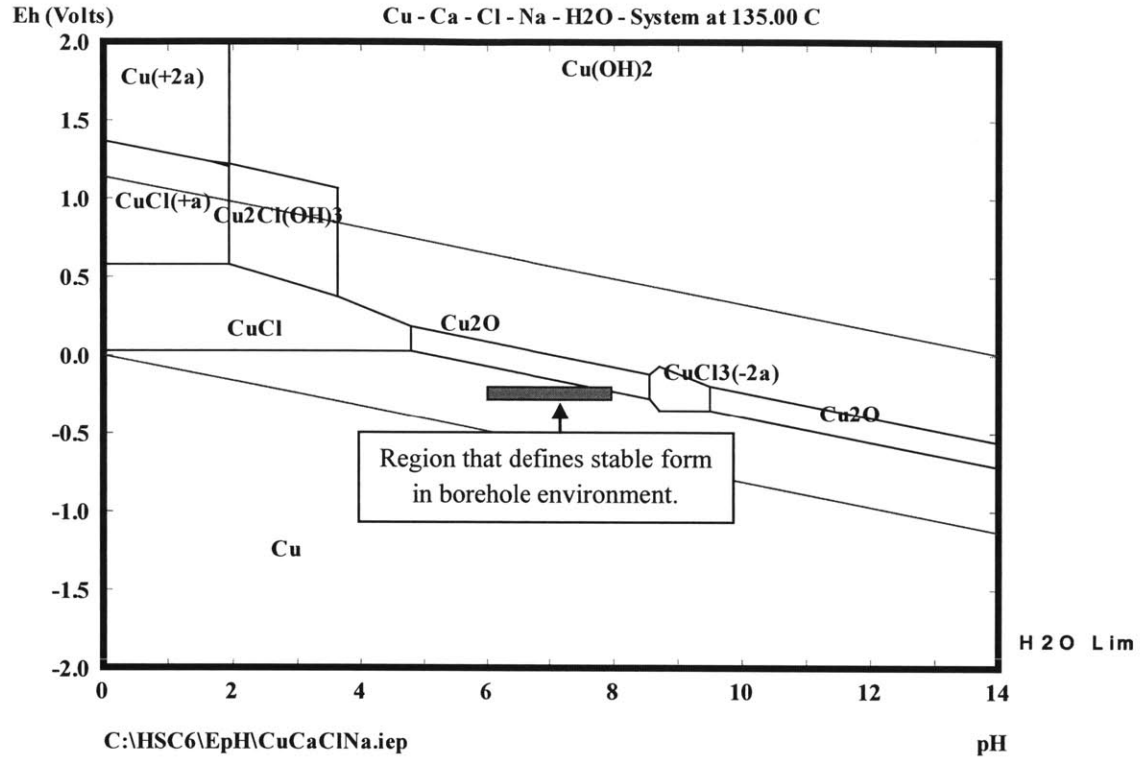

Figure 4.1: Pourbaix Diagram for Copper in a Borehole Environment at 135 °C (shaded area bounds the expected borehole conditions outlined in table 4.1)

One concern for copper alloys is denickelification, which decreases the strength of a copper-nickel alloy through the selective leaching to nickel from an alloy matrix.[138] This process occurs in copper-nickel alloys in waters when subjected to temperatures greater than 150°C, which could occur in a borehole environment (although the temperature calculated in this thesis are lower for the Hoag canister). Pure copper has also been induced to crack in slow strain tests.[139] There has also been research that questions the thermodynamic immunity of copper at elevated temperatures;[140] however, this is not reflected in the Pourbaix diagram.

Because these issues can be avoided (by excluding nickel and limiting strain and temperature), pure copper is found to be the most attractive DNW canister material choice. The main reasons for this are the overall corrosion resistance in a borehole environment and the fact that copper has immunity (forms a stable metal) in predicted borehole conditions.

4.4 Chromium and High-Chromium Stainless Steel Suitability

During the literature search, only limited information was available on pure chromium corrosion. This may be because pure chromium is very brittle and not generally used as a construction material in its pure form. However, extensive information is available on high-chromium stainless steels because of their wide applicability and corrosion resistance. For this reason, high chromium stainless steels are the focus of this section.

High-chromium stainless steel alloys (above 23% chromium) appear to significantly improve corrosion resistance in 250^{0}C oxygen-free brine.[141] One study also found that the passive oxide region broadens with increasing chromium concentration in carbon and stainless steels and nickel alloys in geothermal brines.[142] Another source shows that high-chromium steel alloys form a stable oxide and have negligible general corrosion (and only a few shallow pits) after long-term exposure in a 1800 feet deep, chloride brine borehole environment with a temperature of 260^{0}C.[143] These facts indicate that high chromium stainless steels have a resistance to general corrosion in borehole environments. Pure chromium exhibits a very large passive region. This is illustrated by figure 4.2 because oxides are the stable form over most of the pH and potential values. The shaded rectangle shows the predicted ranges of borehole conditions.

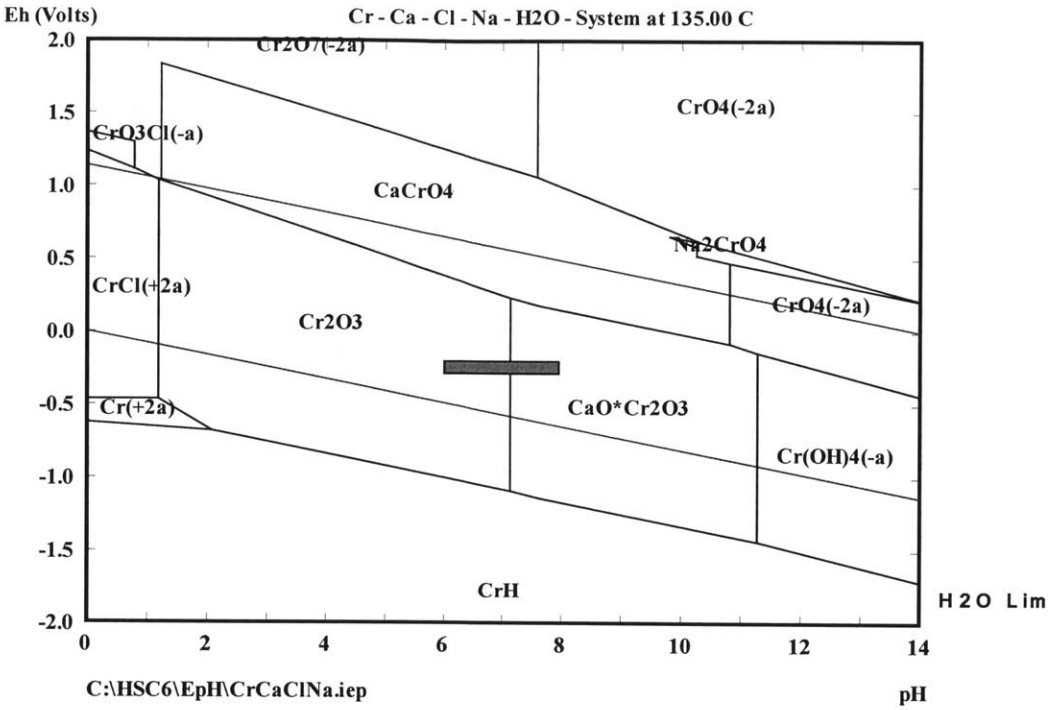

Figure 4.2: Pourbaix Diagram for Chromium in a Borehole Environment at 135 ℃ (shaded area bounds the expected borehole conditions outlined in table 4.1)

Chromium is expected to form passive oxides (Cr_2O_3 or $CaO * Cr_2O_3$) in the predicted borehole environment. The passive property of chromium illustrated in figure 4.2 is conferred on chromium-iron alloys, provided that more than 12% chromium is added to the iron.[144] This agrees with the high-chromium stainless steel corrosion resistance found in the literature review. However, this resistance relies on an oxide film, which can be damaged or broken down, which could in turn result in cracking or corrosion. It should be noted that the current design for the DOE canister employed at the Defense Waste Processing Facility specifies 304L Austenitic stainless steel as the material. This steel has a significant chromium content.

Another drawback of high-chromium stainless steels is the fact that alloys containing both carbon and chromium can be susceptible to sensitization during welding or high-temperature

uses. This refers to the formation of chromium carbide at grain boundaries. Sensitization increases the susceptibility of the alloy to intergranular stress corrosion cracking.[145]

High chromium stainless steels have excellent corrosion resistance in a borehole environment. However, they may be susceptible to oxide film degradation or sensitization. Despite this, high-chromium stainless steels could be a good alternative for DNW canisters.

4.5 Other Metal and Alloy Suitability

Several metals were analyzed but found to be less desirable than pure copper and high-chromium stainless steel for borehole repository canisters. However, the literature review and Pourbaix diagram for each of these materials are included to give examples of less disirable attributes.

4.5.1 Tantalum and Tantalum Alloys

In general, tantalum is the most corrosion resistant metal.[146] This is because it instantly passivates and becomes insoluble. This is reflected in the Pourbaix diagram in figure 4.3. The shaded rectangle indicates the conditions predicted in a borehole environment. However, tantalum very expensive (refer to table 4.4) and therefore not practical for defense waste canisters. Tantalum is also less desirable than copper because tantalum relies on an oxide film for passivation. Oxide films can be damaged or broken down, which could result in cracking or corrosion.

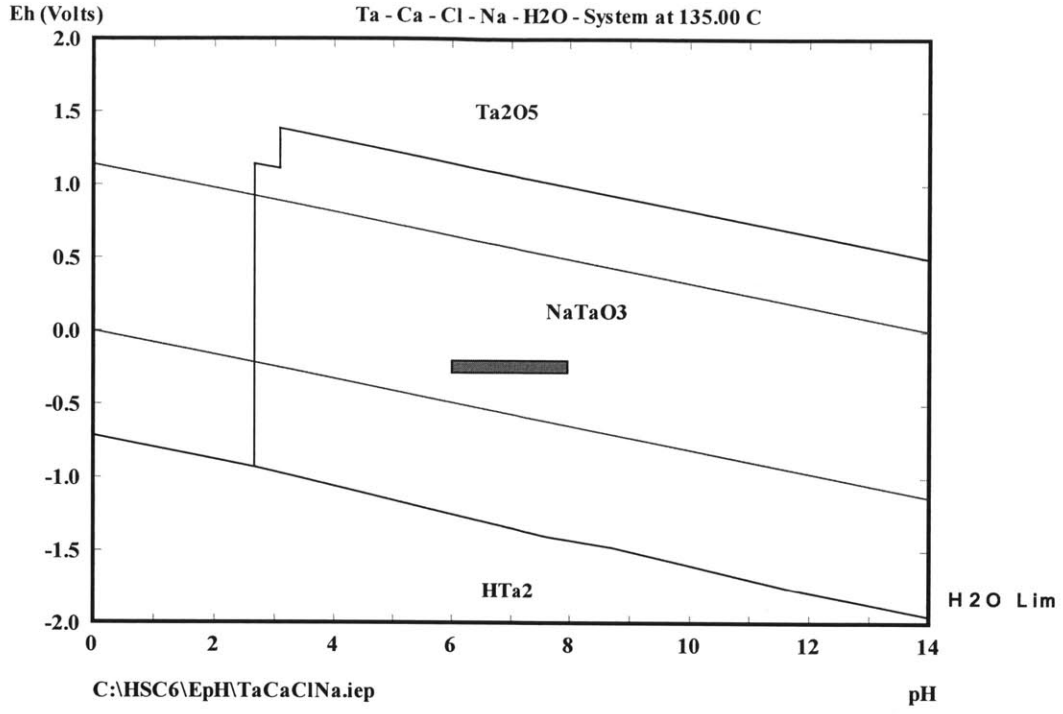

Figure 4.3: Pourbaix Diagram for Tantalum in a Borehole Environment at 135 °C (shaded area bounds the expected borehole conditions outlined in table 4.1)

4.5.2 Titanium and Titanium Alloys

Titanium alloys are under study as candidate materials for the nuclear waste containers in Canada, Japan, and Germany.[147] The titanium alloys were selected as a potential alternative because of their excellent performance in more aggressive brine solutions.[148] Titanium alloys were found to sufficiently withstand 250°C oxygen-free brine.[149] Testing showed that as the temperature and the chloride concentration increased, the repassivation potential of titanium decreased to values well below the corrosion potential.[150] This would allow for passive protection of the canister, and is reflected in the Pourbaix diagram in figure 4.4. The shaded rectangle indicates the conditions predicted in a borehole environment.

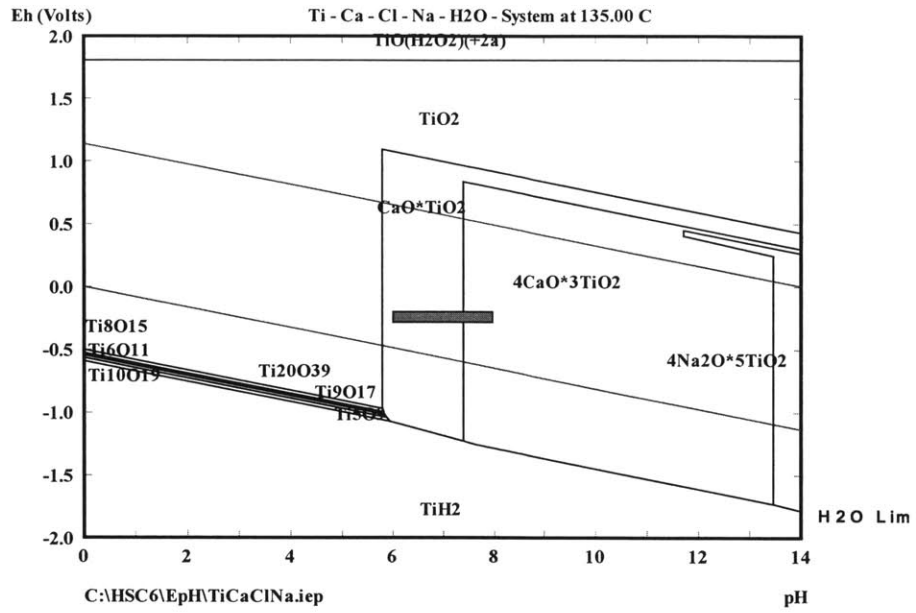

Figure 4.4: Pourbaix Diagram for Titanium in a Borehole Environment at 135 ℃ (shaded area bounds the expected borehole conditions outlined in table 4.1)

The stable form of titanium is $CaO * TiO_2$. Although literature suggests that titanium is passive (forms an insoluble oxide) in borehole conditions, there is very little information about the behavior of $CaO * TiO_2$ specifically. One study found that $CaO * TiO_2$ exhibited corrosion resistance,[151] but the environment in the study was very different than the predicted borehole environment. This mixed oxide could have protective characteristics, but additional analysis is required before this could be assured.

Titanium is also undesirable because it is subject to crevice corrosion in chloride solutions at temperatures above 70° C.[152] Also, although extreme temperatures are not expected, pitting and crevice corrosion problems usually limit titanium service temperature to below 250°C.[153] Above 250°C titanium is not vastly superior to stainless steels in reducing brine.[154] Titanium may undergo environmentally assisted cracking under reducing conditions because of the formation

of hydrides, which will likely be present in a borehole environment.[155] Cost could also be prohibitive for titanium.

4.5.3 Aluminum and Aluminum Alloys

At the conditions expected in a borehole environment (indicated by the shaded rectangle in figure 4.5), aluminum does not form a stable oxide; instead it forms an aluminum hydroxide called diaspore ($AlO(OH)$). Natural diaspore has been shown to dissolve at temperatures between 130° and 300° in a weak alkaline solution.[156] This is not indicative of borehole environments, but it suggests that aluminum will not form a passive oxide film in borehole conditions. Therefore, aluminum is not protected via passivation. This implies that aluminum will be susceptible to general corrosion. For example, Aluminum Alloys 1100 and 6061 were tested at high-chloride concentrations (10,000 parts per million) and both metals exhibited severe general corrosion and pitting, with the pits covering large areas.[157] Generally, aluminum alloys tend to be susceptible to pitting in alkaline chloride solutions.[158] Aluminum is also susceptible to stress corrosion, galvanic, and metal ion attack in geologic environments.[159]

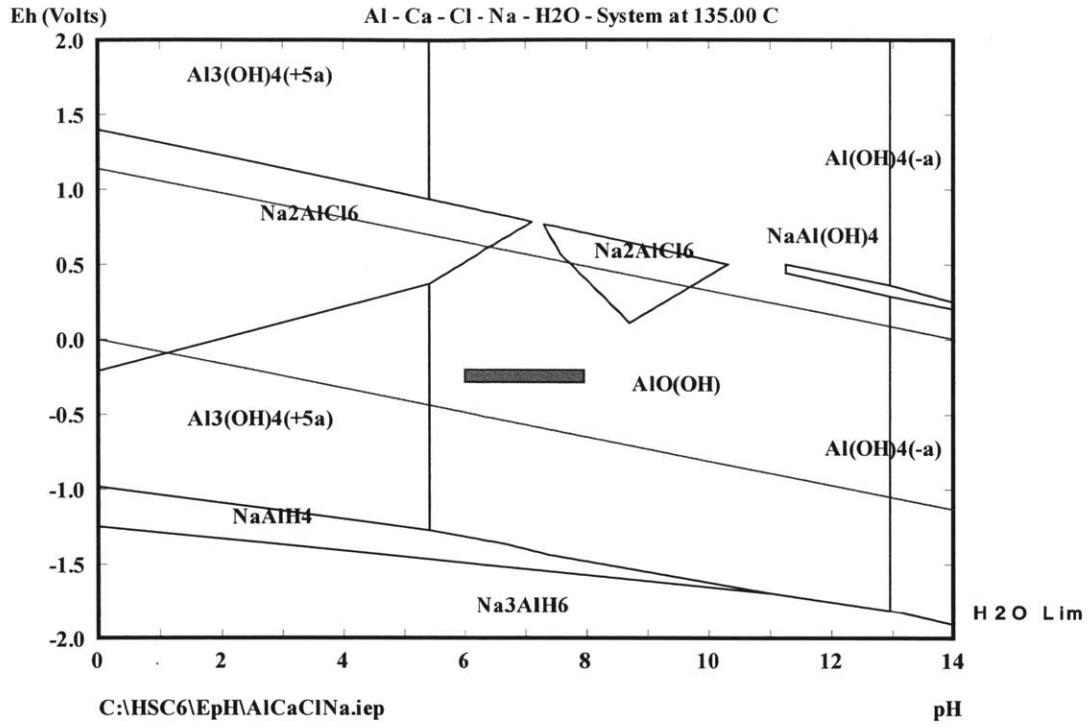

Figure 4.5: Pourbaix Diagram for Aluminum in a Borehole Environment at 135 °C (shaded area bounds the expected borehole conditions outlined in table 4.1)

4.5.4 Iron and Carbon and Stainless Steels

It is not feasible to analyze all iron and steel alloys because the performance of steel alloys is highly dependent on concentrations of other metals. Therefore, some stainless steels are mentioned as appropriate materials in the chromium and high-chromium stainless steels section because the high chromium concentration makes them more corrosion-resistant than steels with high concentrations of other metals.

Pure iron forms a stable oxide in the expected borehole conditions (indicated by the shaded grey rectangle in the Pourbaix diagram in figure 4.6). However, it should be noted that iron and steel alloys may have a very different Pourbaix diagram because of the additional interactions between the borehole environment and alloy additives. Nonetheless, pitting in the oxide film has

been recorded in stainless and carbon steels in chloride solutions.[160] Austenitic stainless steels are also susceptible to stress corrosion cracking in chloride solutions.[161] In addition to chloride-induced corrosion, hydrogen embrittlement and hydrogen blistering of steels is possible in granitic environments.[162]

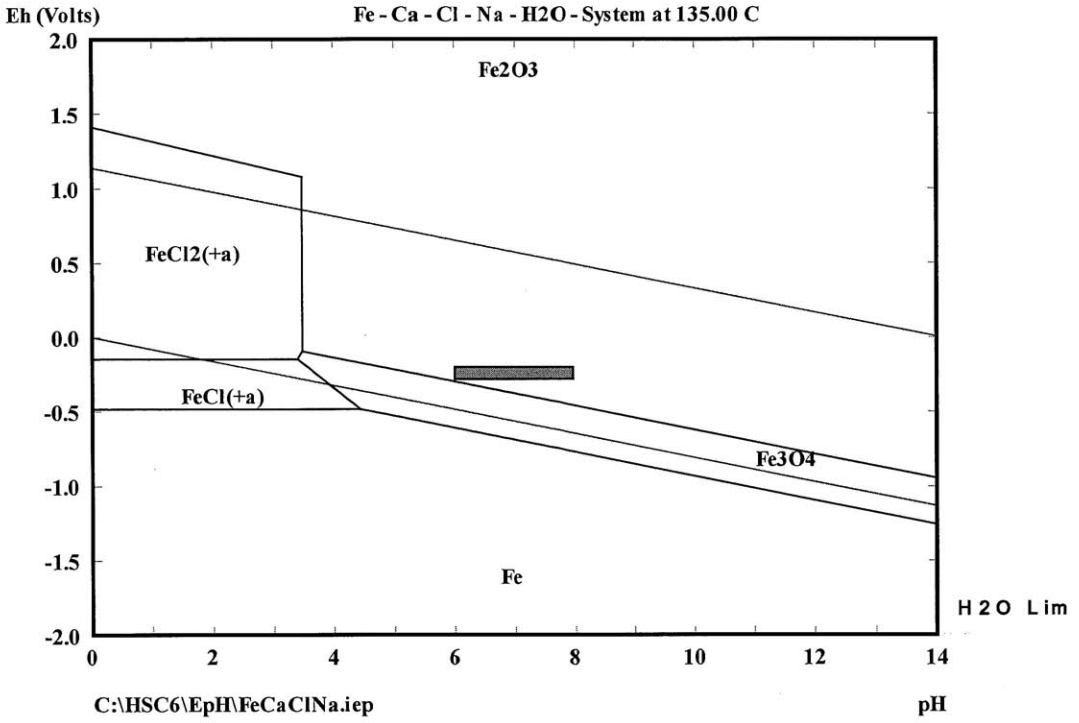

Figure 4.6: Pourbaix Diagram for Iron in a Borehole Environment at 135 °C (shaded area bounds the expected borehole conditions outlined in table 4.1)

4.5.5 Nickel and Nickel Alloys

Nickel forms a passive oxide in the predicted borehole conditions (indicated by the shaded rectangle in figure 4.7). However, pitting is a prevalent problem for nickel and nickel alloys in chloride solutions. For example, Alloy C-4, a nickel-chromium-molybdenum alloy, showed minor pitting at 100 parts per million chloride and definite pitting corrosion at higher tested chloride concentrations.[163] As the temperature is increased, some high nickel alloys become

susceptible to stress corrosion cracking and localized attack.[164] Many copper-nickel alloys exhibit a tendency to crevice corrode in chloride brines[165]. As mentioned previously, denickelification occurs in copper-nickel alloys in waters at temperatures greater than 150°C,[166] which could occur in a borehole environment through geothermal temperature changes and radionuclide decay.

Despite problems with pitting, many nickel based alloys have been shown to be very resistant to hot salt stress corrosion cracking.[167] Pure nickel has been shown to have a low corrosion rate in cool, high-chloride brines.[168] Also, a few of the nickel super alloys (Hastelloy C-276 and Inconel 625) are virtually immune to damage by hot brines.[169] Like steels, nickel performance in a borehole environment is highly dependent on the precise composition of the chosen alloy. However, it was not chosen as an attractive canister material because of the pitting susceptibility.

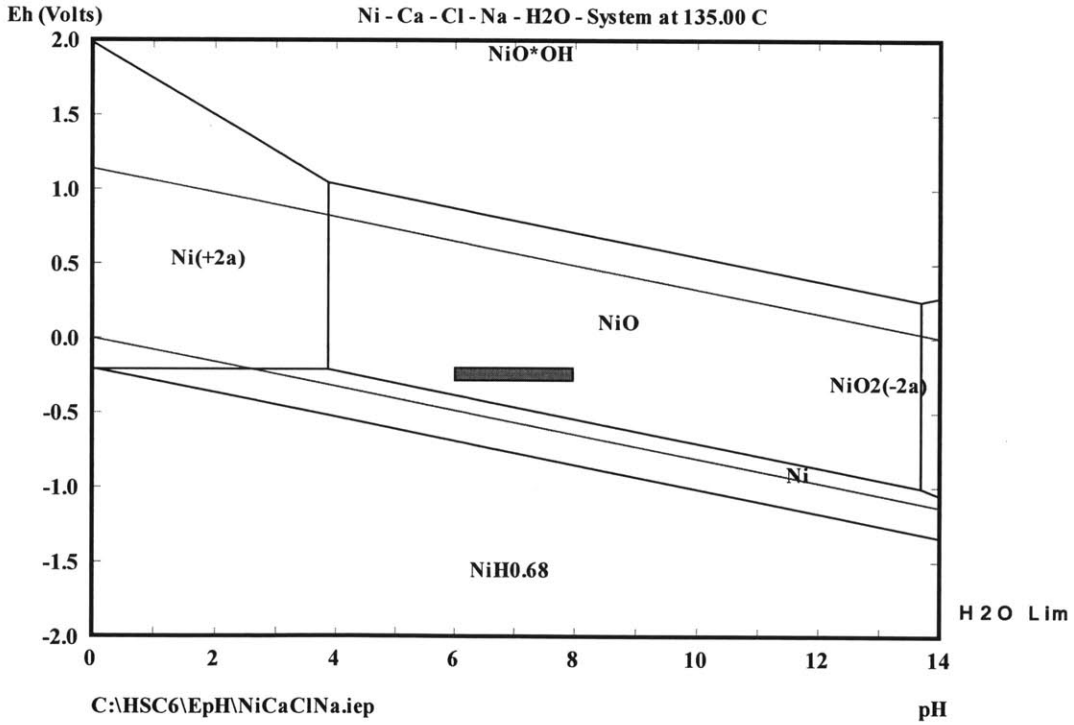

Figure 4.7: Pourbaix Diagram for Nickel in a Borehole Environment at 135 °C (shaded area bounds the expected borehole conditions outlined in table 4.1)

4.6 Chapter Summary

The stable form of each metal, the corrosion susceptibility, and the cost are all to be considered when determining the ideal canister material for DNW. Table 4.2 summarizes the stable form of each canister material in predicted borehole environments. Table 4.3 gives the relative prices of the pure metals considered.

Table 4.2: Summary of Stable Canister Material Forms from Pourbaix Diagrams

Metal	Stable Form at Predicted Borehole Environment
Copper	Cu
Tantalum	$NaTaO_3$
Aluminum	$AlO(OH)$
Chromium	$CaO * Cr_2O_3$
Iron	Fe_2O_3
Nickel	NiO
Titanium	$4CaO * 3TiO_2$

The relative metal prices in table 4.3 are based on the price of carbon steel in May 2011. Carbon steel was included because it provided a more realistic price for iron. It should be noted that these relative prices are merely guides; accurate metal prices can only be found by contacting a supplier. In addition, the cost of fabrication into the form of a canister must be taken into account. In general, package fabrication costs would be greater than canister material costs; thereby making material cost less important.

Table 4.3: Relative Metal Prices

Metal	Relative Price for High Grade Metal according to the May 2011 London Metal Exchange Prices[170]
Copper	9.7
Tantalum	120
Aluminum	2.8
Chromium	6.3
Iron Ore (Carbon Steel)	0.11 (1)
Nickel	1.3
Titanium	43

Because of the thermodynamic properties (the stable form), overall corrosion resistance, and reasonable cost, pure copper was shown to be the best borehole outer canister material. Copper remained as a metal in the Pourbaix diagram in figure 4.1. Therefore, it exhibits immunity in a borehole environment. Copper is more expensive than several other metals, but the price is still reasonable; especially if copper is only used as protective plating on another, lower cost material. Finally, the literature review shows that copper is very resistant to all types of corrosion in borehole environments. Conditions under which corrosion is possible (nickel content and high strain) can be limited or controlled.

High-chromium stainless steels could also be a good option for borehole canisters because they have also been shown to be highly corrosion-resistant in environments very similar to predicted borehole environments. In experiments represented in the literature, high-chromium stainless steels have been shown to passivate and remain stable in borehole environments. This is supported by the passive oxide formation in the Pourbaix diagrams for chromium and iron. High-chromium stainless steels are less expensive than copper as well as many other materials.

Canister materials can only be specified by the repository owner for certain situations considered in this thesis. The material of prospective Waste Treatment Plant canisters (both the DOE canister and the Hoag canister options described in figures 2.1 and 2.2) can be specified because the DNW has not yet been vitrified into any containers (because the plant is still under construction). However, the material of the DOE canister for the Defense Waste Processing Facility cannot be specified by the future repository owner because the waste is already being vitrified into the current design and material for the DOE canister. Future analysis is necessary to understand the behavior of the specific material for the DOE canister (304L Austenitic stainless steel) in a borehole environment. Nonetheless, if the Hoag canister was employed at the Defense Waste Processing Facility, the canister material could be specified because using the Hoag canister would already require that the waste be transferred from the DOE canister (used to vitrify the waste) into a new canister.

In summary, based on the Pourbaix diagrams and a literature review, pure copper is the most attractive canister material for US defense wastes. High-chromium stainless steels could also be an attractive option as a DNW canister material.

5 Waste Form Dissolution Analysis

5.1 Chapter Introduction

The DNW is the waste from the aqueous separation of weapons-grade plutonium and other isotopes for weapons production.[171] This waste was generated and is owned by the DOE.[172] The waste is currently being vitrified in borosilicate glass at Savannah River Site[173] and is slated to be vitrified at Hanford Site upon completion of the Waste Treatment Plant.[174] Details on the generation and composition of the vitrified waste can be found in Section 2.1.

In continuing the analysis of the unlikely design basis failure scenario, the waste-filled borehole is assumed to fill with water (even though the waste would be sealed in the borehole when the borehole is dry). Therefore, canister and waste form degradation could occur. In the case of DNW, the waste form is aqueous defense waste vitrified in borosilicate glass. The canister material will protect the waste form from initial degradation, but to keep the analysis very conservative, the canister is assumed to fail immediately after emplacement. Therefore, the waste form is assumed to begin to alter immediately upon emplacement; even though the canister and possible lack of electrolyte in the borehole environment will likely delay this degradation significantly.

To understand the degradation behavior of the waste form, a literature review and chemical analysis were performed. The literature review outlines the experimental research conducted on waste form behavior in conditions similar to the borehole environment in table 4.1. The chemical analysis is twofold; the first portion is the determination of the stable nuclide form of each nuclide in the waste using Pourbaix diagrams and the second portion is the calculation of the maximum soluble concentration of each nuclide species.

5.2 Borosilicate Glass Suitability in Borehole Environment

Vitrification of defense waste is a technology where waste materials are dissolved in molten glass and cooled to become an integral part of the glass matrix.[175] This process is employed to immobilize the waste so that it can be stored in future repositories.[176] Details on how the vitrification process occurs as well as the history and composition of the waste are in section 2.4. The U.S., Japan,[177] France, and the United Kingdom[178] use borosilicate glass for radioactive waste vitrification.

The conservative assumption that the borehole fills with water initiates the glass dissolution, which has been observed to occur in four stages. The first stage only lasts a few minutes and is associated with a rapid release of alkali elements and boron and results in the formation of a hydrated layer at the water-glass interface.[179] Second, the loss of soluble elements slows down and is controlled by the dissolution of silicon.[180] At this stage a layer is formed consisting of mostly insoluble components (including fission products and actinides).[181] It was found that the glass constituents leached congruently, but other elements leach at a slower rate and remain trapped in the layer.[182] The third phase occurs when the water is enriched with elements from the soluble glass elements.[183] This slows down the glass dissolution significantly. Finally, the slower dissolution rate stabilizes.[184] The dominant dissolution mechanisms of these phases are glass network hydrolysis and diffusion controlled ion-exchange.[185]

The glass dissolution rate specific to a borehole environment is not well-understood. This is because glass dissolution is highly dependent on leachant composition, pH, flow rate, reduction potential, temperature, and glass composition.[186] Because of this variability, it would require extensive research to assign accurate dissolution rates to DNF in a borehole environment.

However, qualitative conclusions can be gained from the literature to show benefits and drawbacks of employing a borehole repository for waste vitrified in borosilicate glass.

It has been well-documented that borosilicate glass dissolution occurs faster as temperature increases.[187] It has also been shown that the solubility and diffusion coefficient of glass increases with temperature.[188] These are drawbacks because boreholes may have higher temperatures than a geologic repository like Yucca Mountain Nuclear Waste Repository because of the geothermal gradient of ~25°C/km implicit in borehole repositories (described in section 2.5). Another study found that stress corrosion cracking occurred in a glass waste form because of the interaction of polar hydroxide groups with stressed borosilicate glass surfaces exposed to water.[189] The stresses in the glass were found to be internal stresses developed during cooling; therefore, stress could be present in the waste form regardless of the canister design.[190] In theory, cracking in the waste form would increase the effective surface area available for leaching by groundwater and could decrease the lifetime of the waste form. However, one study found that micro-cracking in glasses cooled at rates similar to those currently used for DNW does not significantly affect the leachability of the glass.[191] It should also be noted that internal stresses, if present, are based on waste form production and therefore independent of the type of repository.

In addition to waste form alteration from exposure to water and high temperatures, there are also several inherent disadvantages of borosilicate glass. Even though defense waste undergoes an extensive sampling and control procedure prior to storage,[192] crystallization or devitirification can occur.[193] This process creates interphase boundaries that are often structurally and energetically favorable for localized and accelerated corrosion.[194] Also, glasses are generally more soluble in groundwater than crystalline forms of similar chemistry.[195]

One promising effect of the borehole environment on borosilicate glass is the inverse relationship between granite content and glass leaching. This study found that, in general, exposure to granite reduced the leaching of glass matrix components (but not necessarily the radionuclides vitrified in the matrix).[196] Granite would likely leach into any groundwater that comes in contact with the waste form; this could combat the increase in dissolution from increases in temperature.

5.3 Waste Form Chemical Analysis

5.3.1 Stable Element Form Model Overview and Assumptions

To understand the behavior of nuclides in a borehole environment, Pourbaix diagrams were created for several nuclides that contribute the most radioactivity in Curies/m³ to the bounding waste form. These diagrams were used to find the stable nuclide form at the borehole environment summarized in table 4.1.

The HSC 6.0 Chemistry Software Package[197] was used to create the Pourbaix diagrams for the 10 elements that contribute most to the waste form heat loading. These diagrams show the specific conditions of potential and pH under which an element can react to form oxides or complex ions.[198] It is important to note that Pourbaix diagrams are for an element rather than for a specific isotope. Figure 5.1 is the Pourbaix diagram for plutonium and will be used as an example. In this figure, the grey shaded area represents the predicted borehole environment and falls on the section labeled PuO_2OH. Therefore, the stable form of plutonium in the borehole environment described in table 4.1 is PuO_2OH.

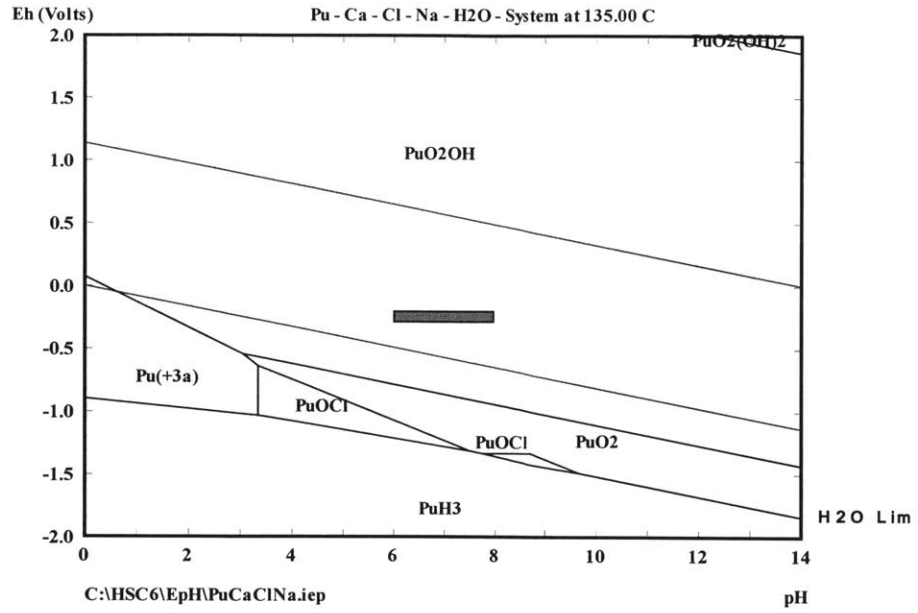

Figure 5.1: Pourbaix Diagram for Plutonium in Borehole Environment (shaded area bounds the expected borehole conditions outlined in table 4.1)

The Pourbaix diagrams for the 9 additional nuclides can be found in Appendix C. The stable nuclide forms are summarized in table 5.1.

5.3.2 Maximum Soluble Concentration Model Overview and Assumptions

Once the stable element form is found, the reaction for that form and the corresponding solubility products can be used to calculate the maximum concentration of the soluble ion species. Instructions for this process are outlined for plutonium below, but the same steps are applied for the other nuclides. The steps below are carried out in the sample calculation for the maximum soluble concentration of plutonium in figure 5.2.

First, find the stable nuclide form (in this case, PuO_2OH) in the Common Thermodynamic Database Project (CTDP).[199] This will give the form of the ion or species (PuO_2OH is solid) and

a predicted reaction for it. Check the forms of each of the species in the predicted reaction. In the 10 nuclides examined, this predicted reaction contains at least one aqueous ion. In this analysis, if a species was aqueous, it was assumed to be soluble to the extent described by the solubility product. If a species in the predicted reaction was solid, it is assumed to be insoluble and the activity in the solubility product equation was assumed to be identity (i.e. 1.0). However, regardless of the form (solid or aqueous) of the stable nuclide species, the solubility product for that species was used to define the reaction.

Next, look up the log of solubility product for the ion or species at the two highest temperatures given in the database. For most of the nuclides analyzed, these temperatures were at 75°C and 100°C. Check the plot of the log of the solubility product (log(K)) to ensure that the behavior is linear at the temperatures given in the database. If the log(K) values are linear (or close to linear) at temperatures less than 100°C, it is assumed that this linear behavior of the log(K) can be continued to 135°C. Then use the slope method of linear interpolation to find the solubility product for 135°C from the values given in the Common Thermodynamic Database.

Use the definition of the solubility product (shown in Figure 5.2) to set up an equation to solve for the concentration of the soluble ion in the predicted reaction. The activity of solid species and water are both assumed to be 1. If hydrogen gas is in the reaction, the concentration of H^+ can be replaced with $10^{-\mathrm{pH}}$ based on the definition of pH. For the purposes of this analysis, the pH was assumed to be 7 because it is in the middle of the predicted range of pH values given in table 4.1. Changes in this pH could significantly change the maximum soluble concentration. Therefore, it would be useful to conduct a parametric study of the maximum soluble concentration in future analyses.

Finally, the maximum concentration of soluble ion can be calculated for each nuclide (provided that there was only one soluble ion in the predicted reaction). This concentration is the maximum concentration of the soluble species that could occur in the borehole if the species-water system were allowed to reach equilibrium. In reality, other nuclides would be leaching as well. This would affect the actual concentration of nuclides.

The application of these steps from plutonium can be found in figure 5.2

Predicted Reaction from Common Thermodynamic Database:

$$\boldsymbol{PuO_2{}^+(aq) + H_2O(aq) \leftrightarrow PuO_2OH(s) + H^+(g)}$$

Solubility Products from Common Thermodynamic Database:

$$logK(75^0C) = -4.08929$$

$$logK(100^0C) = -3.72575$$

Linear Interpolation to Find Solubility Product at 135□C:

$$\frac{-4.08929 - logK(135^0C)}{75^0C - 135^0C} = \frac{-3.72575 - logK(135^0C)}{100^0C - 135^0C}$$

$$logK(135^0C) = -3.2168$$

Definition of Solubility Product:

$aA + bB \leftrightarrow CC + dD$, where A, B, C, and D are activities of reaction species.

$$K = \frac{[C]^c[D]^d}{[A]^a[B]^b}$$

Calculation of Maximum Soluble Concentration from Solubility Product:

$$K = \frac{[PuO_2OH][H^+]}{[PuO_2{}^+][H_2O]} = \frac{1 * [10^{-pH}]}{[PuO_2{}^+] * 1} = \frac{1 * [10^{-7}]}{[PuO_2{}^+] * 1} = 10^{-3.2168}$$

$$[PuO_2{}^+] = 10^{-3.783} = \boldsymbol{1.647 * 10^{-4}\ gram\ moles\ per\ liter\ (M)}$$

Figure 5.2: Maximum Concentration of Soluble Species of Plutonium Calculation

The steps in figure 5.2 outline the ideal progression for calculating the maximum soluble concentration. However, there are several nuclides for which the actual procedure deviates from this. For example, the stable form found in the Pourbaix diagram for Yttrium was not listed in the CTDP, therefore the temperature-adjusted Gibbs free energy of the reaction was used to find the solubility product (refer to Section C.10). After the solubility product was calculated, the procedure is the same as the example in figure 5.2. Also, it was not possible to calculate the maximum nuclide concentration for several nuclides. This is because there were too many soluble ions in the reaction given in CTDP for the stable form. Therefore, there were too many unknown values to calculate the maximum nuclide concentration using the solubility product. The predicted reaction and Pourbaix diagrams for these nuclides were included to show the stable forms.

5.3.3 Waste Form Chemical Analysis Results

Table 5.1 summarizes the stable form and the maximum concentration of soluble species for each element. A complete listing of the Pourbaix diagrams and calculations for each of the 10 highest heat producing elements can be found in Appendix C. If the soluble concentration was less than 10^{-12} molar, the concentration was specified as $<10^{-12}$M in table 5.1. This is because the accuracy is very low as such small concentrations. Note that throughout this thesis, molarity (M) is defined as moles of nuclide or metal per liter of solution in the borehole.

Table 5.1: Concentration of Soluble Nuclide Species in Borehole Environment at 135°C

Nuclide	Stable Form at Environment In Table 4.1	Potential Resulting Soluble Species	Maximum Concentration of Soluble Species
Americium	$Am(OH)_3$	Am^{3+}	$4.340 * 10^{-12} M$
Antimony	Sb_4O_5 *or* $Ca_3(SbO_4)_2$	$4SbO_2^-$ or $Ca_3(SbO_4)_2$	$< 10^{-12}$M or $2.422 * 10^{-10} M$
Cadmium	$CdOHCl$	CdOHCl *and* Cd^{2+}	Calculation not possible
Cesium	Cs^+	Cs^+	2.5258 M
Europium	$Eu(OH)_3$	$Eu(OH)_3$ and Eu^{3+}	Calculation not possible
Iodine	HIO	HIO *and* IO^-	Calculation not possible
Nickel	NiO	NiO_2^{-2}	$< 10^{-12}$M
Plutonium	PuO_2OH	PuO_2^+	$1.647 * 10^{-4} M$
Strontium	$SrCl^+$	$SrCl^+$ *and* Sr^{2+}	Calculation not possible
Technetium	Tc	TcO_4^-	$< 10^{-12}$M
Yttrium	$Y(OH)_3$	Y^{3+}	Calculation not possible

This analysis shows that, of the nuclides analyzed, cesium has the largest concentration of soluble species in the borehole environment. Ideally, the concentration of soluble species would be smaller, however, the half life of the most prevalent cesium isotope in defense waste is relatively small (half life of Cs-137 is approximately 30.2 years). This indicates that most of the cesium would decay before the canister would be breached.

The literature suggests that, of the nuclides in DNW, iodine and technetium (I-129 and Tc-99) represent the largest risk to humans because they are long lived and very mobile in geologic systems.[200] This analysis found that the technetium maximum soluble concentration was

negligible (on the order of 10^{-28} $\frac{moles}{liters\ of\ solution\ in\ borehole}$, see Appendix C). This analysis was not able to find the maximum soluble concentration of iodine because there were too many ions with unknown concentrations in the stable form equation (refer to section C.6). However, in the literature, I-129 is considered one of the limiting species for borehole disposal.[201] Therefore, experimental research is required to understand the solubility of iodine in a borehole environment before final conclusions can be drawn on the risk associated with a borosilicate glass waste form emplaced in a borehole repository.

It should be noted that the borehole has a reducing environment, where the Yucca Mountain Repository had an oxidizing environment. This reducing environment limits solubility and increases sorption of nuclides onto granite.[202] Therefore, the maximum concentrations of soluble nuclides would likely be smaller in a borehole repository than in a repository like Yucca Mountain.

5.4 Chapter Summary

In continuing a conservative risk assessment of a borehole repository, the canister is assumed to fail. No credit is taken for engineered barriers or material choice. Therefore, the dissolution of the glass matrix and the nuclides in the waste must be understood.

The borosilicate glass used as the waste form has been shown to leach faster and have higher diffusion rate at higher temperatures.[203] This implies that alteration will occur faster in boreholes than it would in a geologic repository. Also, stress corrosion cracking has been shown to occur due to internal stresses from cooling.[204] It is unclear if this will be a problem in defense waste. Devitrification can also occur and create interphase boundaries that are more susceptible to

corrosion.[205] Finally, waste form leaching was shown to decrease as granite content in the water increases.[206] This could offset some of the leaching increase due to temperature.

To understand the leaching of the nuclides, Pourbaix diagrams were created for several nuclides in defense waste. The diagrams were used to determine the stable form of the nuclide. The Common Thermodynamic Database was used to determine the reaction associated with the stable form. Then, the solubility product was used to find the maximum concentration in the borehole environment of any possible resulting soluble nuclide ions. The maximum concentration would only be the actual concentration in the borehole if the system were allowed to reach equilibrium; time is not considered in the calculation. Also, the calculation did not account for other environmental elements in the water surrounding the borehole (other than the calcium, sodium, and chloride implicit in the Pourbaix diagrams). In reality, all the elements will be leaching concurrently and this will affect the actual concentration of each element.

Cesium ion was found to have the highest concentration in the borehole environment. However, the relatively low half life (~30 years) of the most abundant cesium isotope suggests that the cesium would decay before the canister is breached. The maximum soluble concentration of technetium, one of the nuclides with high mobility in other geologic systems,[207] was negligible. However, this analysis not able to find the maximum soluble concentration of iodine, Therefore, experimental research is required to better understand the solubility of iodine in a borehole environment before final conclusions can be drawn on the risk associated with a borosilicate glass waste form emplaced in a borehole repository. Note that I-129 is one of the limiting radionuclides assumed for spent fuel disposal in boreholes in analyses at Sandia National Laboratories and MIT.

This chapter explored the processes by which the defense nuclear waste form alters in the borehole environment. Additional research is required to understand dissolution in a borehole environment of nuclides' reactions that were not analyzed in this thesis. Experimental data would also allow for the calculation of the maximum soluble concentrations of the nuclides with too many unknown ion concentrations in the stable form equation. Nonetheless, based on this analysis, boreholes are an acceptable repository for defense nuclear waste because of the low maximum soluble nuclide concentrations in table 5.1.

6 Cost Analysis

6.1 Chapter Introduction

Part of analyzing the feasibility of borehole disposal of vitrified defense waste is understanding the time and costs associated with disposal activities. For this reason, V-DeepBoRe-II (a modification of the original version developed by Jonathan S. Gibbs)[208] was created to calculate the drilling and emplacement costs of vitrified DNW disposal in a vertical borehole. These costs were added to the vitrification and package fabrication costs to get a total cost for disposal of vitrified DNW in a borehole. V-DeepBoRe-II was also utilized to create a data set that was used to create diameter-dependent cost equations. These equations were used to extrapolate predicted costs to encompass the borehole disposal of the canisters currently employed at the Defense Waste Processing Facility and the canisters designed for the Waste Treatment Plant.

6.2 Description of Cost Model

6.2.1 Overview of V-DeepBoRe

In his MIT Nuclear Engineer thesis, Jonathan S. Gibbs created a cost model called V-DeepBoRe, a Monte Carlo simulation based cost model for borehole construction and waste package emplacement.[209] Written in MATLAB, this model calculates the required time and cost of drilling, completing, emplacing waste, and sealing a borehole repository. Gibbs focused his work on the concept of drilling several lateral holes out of one vertical borehole. This allows for spreading of the sunk costs of the vertical shaft over more waste canisters. Also, horizontal emplacement offers the significant advantages of allowing increased emplacement lengths without crushing of the waste package.[210] The hot brine balloon affect described in section 2.5 is

also less prevalent in a horizontal emplacement zone because there is less of a vertical chimney effect. The lateral emplacement concept is illustrated in figure 6.1.

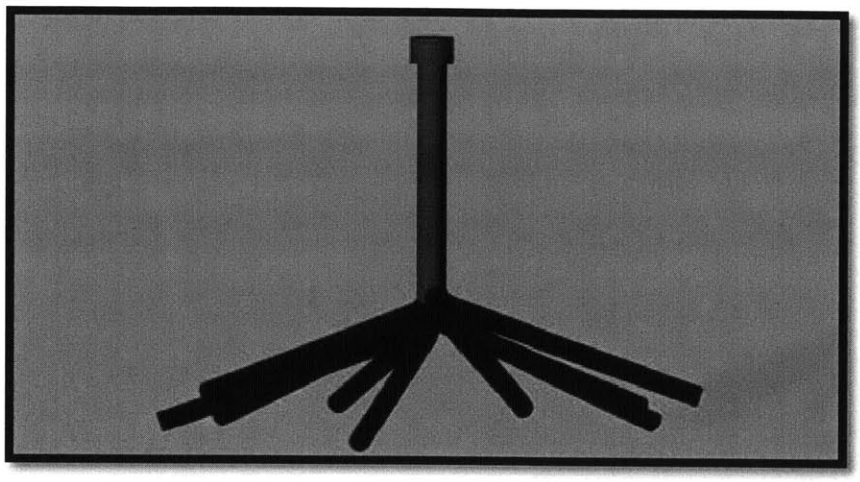

Figure 6.1: Gibbs' 3-D Representation of Multidirectional Borehole with 10 Lateral Holes from a Central Vertical Shaft (from Gibbs)

In the drilling and emplacement cost modules, V-DeepBoRe considers number of lateral holes, waste package diameter, declination angle, material and labor costs, drill bit life, and percentages of vitrified waste, pressurized water reactor fuel assemblies and boiling water reactor fuel assemblies. In his thesis, Gibbs used the code to calculate the cost per kilogram of heavy metal (kgHM) for drilling and emplacing vitrified waste and SNF in a borehole with 10-12 laterals. However, in the present thesis, the decay heat analysis only considers a vertical borehole. Therefore, V-DeepBoRe was altered to consider only vertical borehole cost. The present thesis also considers only vitrified waste, so V-DeepBoRe was changed to reflect the change in waste composition. The resulting code is V-DeepBoRe-II. V-DeepBoRe in its original form can be found in Gibbs' Appendix A[211] and V-DeepBoRe-II can be found in Appendix D of the present thesis.

6.2.2 Comparison of V-DeepBoRe and V-DeepBoRe-II

Several key parameters in the V-DeepBoRe-II code remain unchanged from the parameters used in V-DeepBoRe. These parameters include required depth of surface string, canister length, backhaul speed, casing speed, cementing speed, phase delay, cement cure time, borehole plugging time, drill bit replacement cost, cement material cost, casing material cost, emplacement billing rates, plugging cost, and borehole closeout costs. Many of these parameters are justified by expert input, and several represent reasonable estimates by Gibbs. The value, source, and specific use of each of these parameters are described by Jonathan Gibbs in his thesis in table 2.1.[212]

Other V-DeepBoRe parameters must be changed to account for the differences in assumptions between this and Gibb's thesis. These parameters are listed in table 6.1 along with the corresponding source and value used for each in V-DeepBore-II. The name of each of the variables used in the V-DeepBoRe code is given in parentheses in the 'Parameter' column.

Table 6.1: Specific V-DeepBoRe-II Parameters and Explanations

Parameter	**V-DeepBoRe-II Value**	**Reference**	**Use in V-DeepBoRe-II**
Fraction of Vitrified Waste (vit_frac)	1.0	Chapter 2	All DNW is assumed to be vitrified. Disposal of fuel assemblies in boreholes is outside the scope of this thesis.
Mass Loading in Vitrified Waste (vit_load)	0.45	[213]	Lower waste loading of DNW is likely; however, 45% is the waste loading associated with bounding waste in table 2.1.

Table 6.1 continued.

Parameter (continued)	**V-DeepBoRe-II Value**	**Reference**	**Use in V-DeepBoRe-II**
Length of Emplacement Zone (emplacementlength)	2000 m	Figure 2.1	Gibbs analyzed several borehole configurations. This thesis only looks at one. Future research may be in order to analyze other configurations for DNW boreholes.
Length of Sedimentary Overburden (overburden)	1000 m	Figure 2.1	
Number of Lateral Emplacements per Main Shaft (no_laterals)	1	Figure 2.1	Gibbs analyzed a borehole configuration with several lateral kickoff holes from the main borehole shaft. However, this thesis only analyzes 1 vertical borehole. Table 6.5 gives the specific combinations of input matrices, functions, and scripts that can be used for borehole repository combinations other than the one analyzed in this thesis.
Angle of Emplacement (declination)	90□ from horizontal	Figure 2.1	
Other lateral kickoff parameters (lateraloffset, turnradius, kickoffarc)	0	Figure 2.1	

Table 6.1 continued.

Parameter (continued)	V-DeepBoRe-II Value	Reference	Use in V-DeepBoRe-II
Combination of Casing and Drill Bit Diameters or Pipe Schedule (pipeschedule)	[1 2 3]	Figure 2.1	This casing combination corresponds to outer diameters of 20 in, 18 in, 16 in for the three-tiered casing strategy. This drilling setup is deemed feasible by Hoag;[214] however, it is not listed in the allowable combinations of pipe diameters in Gibbs' thesis[215] (pipecombos). Nonetheless, this pipe schedule is used because, of the casing diameters in V-DeepBoRe, this pipe schedule is the only three-tiered pipe schedule that allows emplacement of the Hoag canister. Future research is necessary to expand the casing diameters in V-DeepBoRe and to determine if there is a technical reason that this pipe schedule is not listed in Gibb's allowable combinations.
Overall Billing Rate	$4852/hour	[216]	Bates found that overall, the drilling billing rates lie in the range of $3,469/hr to $6,257/hr for normal emplacement operations[217]. An average value of three estimates was specified as $4,852/hr. This value was used in V-DeepBoRe-II.

The values in Table 6.1 were input into the scripts of V-DeepBoRe-II. These scripts, as well as the scripts for V-DeepBoRe are outlined in section 6.4 and copied in Appendix D. Table 6.2 further summarizes the differences between V-DeepBoRe and V-DeepBoRe-II.

Table 6.2: Differences Between V-DeepBoRe and V-DeepBoRe-II

V-DeepBoRe	**V-DeepBoRe-II**
Borehole with 10-12 Lateral Kickoffs	1 Vertical Borehole
80% by mass light water reactor fuel rods, 20% vitrified waste	All waste mass is vitrified waste
Analyzes several borehole geometries (called "tradespaces" in V-DeepBoRe)	Analyzes one borehole geometry (figure 2.1)
400 canister string emplacement strategy	Drop-in emplacement strategy
Cost is calculated as total cost and $/kg of heavy metal. Note that in V-DeepBoRe, a calculated mass of vitrified waste is added to the mass of heavy metal from SNF in wastemass.m. In reality, this is not a good indication of mass because the radioactive and toxic elements in vitrified waste are different than those in spent fuel. Future work is necessary to develop a better method for comparing disposal costs between spent fuel and vitrified waste.	Cost is calculated as total cost and $/kg vitrified waste. From this, $/kg waste oxide, and $/kg of heavy metal were calculated based on the loadings specified in Appendix A.

6.2.3 Emplacement Strategy

In addition to the specific variables listed in table 6.1, the emplacement cost portion of V-DeepBoRe was significantly altered to create V-DeepBoRe-II. Gibbs' emplacement portion of V-DeepBoRe implicitly assumes that all 400 canisters would be connected and lowered as a single 2 km drill string.[218] This results in small loading times for the borehole. However, physically speaking, connecting all 400 canisters outside of the borehole would be very difficult. Therefore, finding another emplacement strategy was necessary.

In his MIT thesis, Ethan Bates evaluates a simple, rapid, "passive" procedure for emplacement of canisters in a deep borehole: free-fall release into a water-flooded borehole.[219] The project

involved both analytic modeling and scaled experiments on a laboratory mockup.[220] Experiments showed good agreement and validated the model.[221] Based on these predictions and a structural analysis, there seems to be little risk of damage to a proposed canister in this emplacement method.[222] The primary economic benefit of the drop-in method is that it does not require the original rig to be present during emplacement.[223] The time and equipment for the lowering and retrieval stages are essentially eliminated from the emplacement process, leaving only the loading period. An added benefit is that, with the drop-in method, drilling of the next borehole can begin while canisters are emplaced in the first borehole, greatly expediting repository construction.[224] V-DeepBoRe-II reflects Bates' drop-in emplacement method.

To change the emplacement strategy, the emplacement portion of drill_bit_life.m was removed and replaced with equations [6-1], [6-2]. and [6-3]. It was then saved as drill_bit_life_II.m (see Appendix D). The cost of emplacement ($700,000 according to Bates) accounts for an increased radiation worker billing rate ($10,500/hour).[225] Equation [6-1] calculates the total cost for borehole drilling and emplacement; the cost in units of $/kg of vitrified waste is calculated from the total cost at the end of the script. The time of emplacement from Bates (10 minutes/canister) was implemented in equation [6.2].

$$Cost_{After\ Emplaced} = Cost_{Before\ Emplaced} + \$700{,}000 \quad [6\text{-}1]$$

$$Time_{After\ Emplaced} = Time_{Before\ Emplaced} + \frac{10\frac{minutes}{canister} * 400\ canisters}{60\frac{minutes}{hour} * 24\frac{hours}{day}} \quad [6\text{-}2]$$

$$Depth_{After\ Emplaced} = Depth_{Before\ Emplaced} \quad [6\text{-}3]$$

Future research is necessary to understand the structural impacts of the drop-in method on vitrified DNW. Bates calculated that at the bottom of the borehole, his spent-fuel-filled canister is predicted to be moving at a maximum of speed 2.6 m/s, which could easily be mitigated with an engineered bumper or other energy absorber.[226] Bates conducted a dimensional analysis for the canisters in the present thesis as well. The terminal velocity of the Hoag canister was 1.63 m/s in borehole conditions at the 4 km borehole depth. The terminal velocity of the DOE canister was 1.28 m/s under the same conditions. Details of his analysis are included in Appendix D. The maximum speed of the vitrified waste canisters is smaller than that of the canister used by Bates; however, a structural analysis on vitrified waste should be completed to ensure that the glass waste form is not damaged. If reducing the velocity is necessary to ensure undamaged vitrified waste, Bates outlines and quantifies methods of adding form and friction losses that are feasible to lower the speed even further.[227]

6.3 Results of Cost Analysis

Once completed, V-DeepBoRe-II was used to find the cost and time of drilling and emplacement for a vitrified DNW-filled borehole. Because V-DeepBoRe-II uses a Monte Carlo simulation for drill bit failures, the average and standard deviations for the cost and time of drilling and emplacement of 100,000 trials was found and included in table 6.3.

Table 6.3: Average Drilling and Emplacement Cost and Time for Vitrified Waste

	Average Value for 10^5 Realizations	Standard Deviation	Maximum Value (with 99.9% confidence)
Cost ($/kg of vitrified DNW)	41.18	1.300	45.05
Time (days/canister)	0.2078	$9.193 * 10^{-3}$	0.2354

The plotted V-DeepBoRe-II output for one example trial is shown in figure 6.2. For the first two graphs in figure 6.2, the vertical axis is "Total Pathlength, Hole Depth (m)." Therefore, when the graphed line goes from 0 to approximately -4000 m, the corresponding time and cost refer to those of drilling the hole. When the graphed line goes from approximately -4000 m to 0, the time and costs correspond to those associated with emplacing waste and plugging the hole.

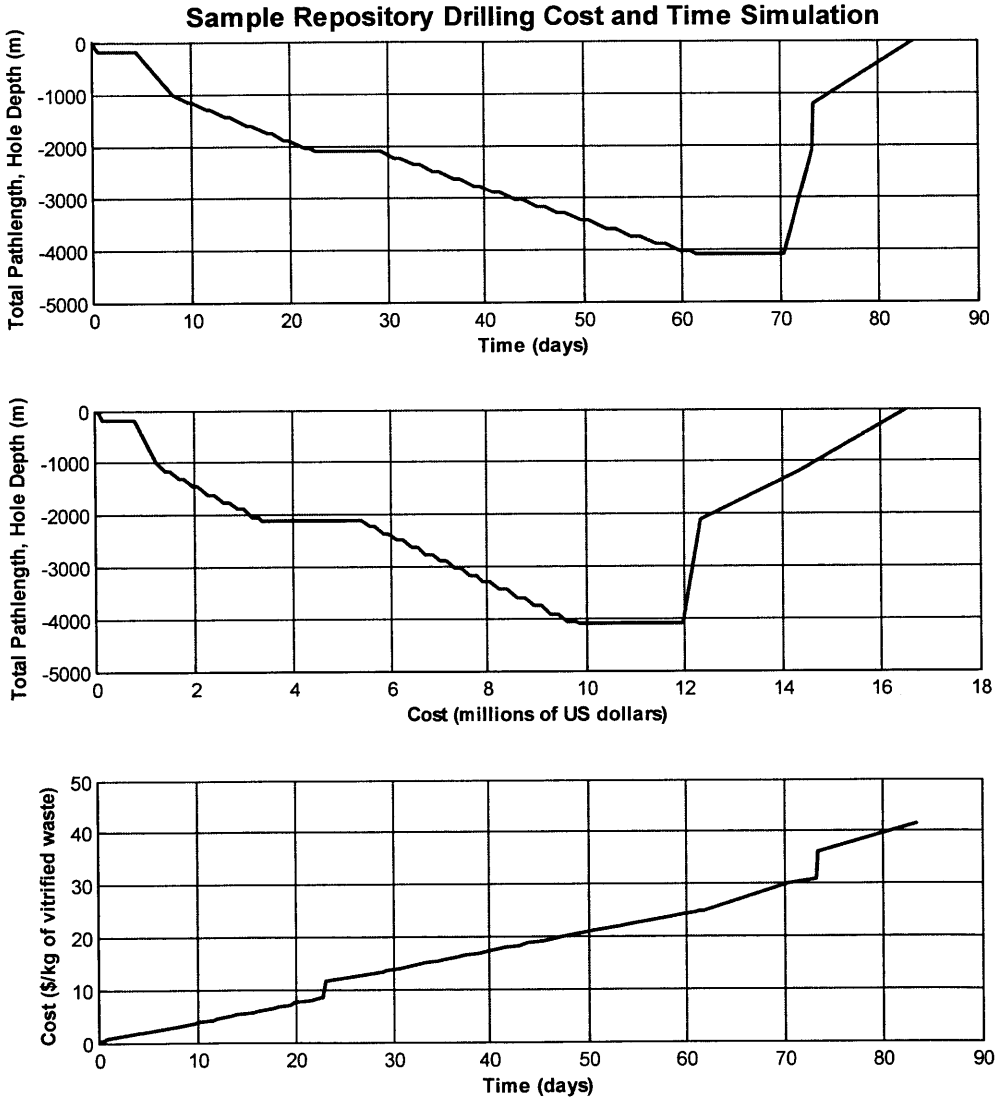

Figure 6.2: Sample Output of 1 Realization from V-DeepBoRe-II

Package and canister fabrication costs are not considered in the values listed in Table 6.3. However, the DNW is vitrified and allowed to set in canisters at the Waste Treatment Plant and the Defense Waste Processing Facility. Therefore, the canisters could be considered part of the vitrification costs and not part of the disposal costs. Nonetheless, one source specifies a value of $\$300{,}000/m^3$ of high level waste unit (assumed to be the volume of vitrified waste) for vitrification and package fabrication costs for the Yucca Mountain Nuclear Repository,.[228] These costs are expected to be similar for a borehole repository because the vitrification and packaging processes would not change considerably. The canister material could be different, but this should be a small percentage of the total vitrification cost. Therefore, using the value for vitrification and package fabrication and the bounding DNW specified in Chapter 2, the vitrification and package fabrication costs are predicted to be approximately $107 /kg vitrified waste. This amount is added to the maximum drilling and emplacement costs of the borehole repository.

Additional research and development would also add significantly to the total cost of a borehole repository. These costs are not included in tables 6.3 or 6.4. Table 6.4 gives a comparison of total predicted costs of the Yucca Mountain Nuclear Waste Repository and a borehole repository. The costs listed in Table 6.4 do not include transportation costs, but do include vitrification, package fabrication, drilling, borehole completing, and emplacement costs. All costs in table 6.4 are rounded to the next dollar.

Table 6.4: Total Cost Comparison for Vitrified Waste in Borehole and Geologic Repository

	Predicted Yucca Mountain Repository Cost	**Predicted Borehole Repository Cost**
Disposal Costs (Drilling and Emplacement only)	$332 /kg of vitrified waste[229]	$46 /kg of vitrified waste
Total Conditioning and Disposal Costs (Vitrification, Package Fabrication, Drilling, and Emplacement)	$440 /kg vitrified waste	$153 /kg of vitrified waste

The values for the predicted Yucca Mountain Repository disposal costs were given in the literature in units of $/kg of heavy metal (HM) equivalent. [230] A kg of HM equivalent in defined by this source as the amount [in kg] of Yucca Mountain capacity used by HLW of a given composition originating from 1 kg HM. For the waste considered in this thesis, the repository capacity used by HLW is the volume of vitrified waste. Therefore, in table 6.4, the Yucca Mountain Repository costs are given in $/kg of vitrified waste. It should be noted that the values in table 6.4 are approximate costs in 2010 U.S. dollars.

As shown in table 6.4, vitrified DNW disposed of in a borehole repository is less expensive than disposal at Yucca Mountain. However, comparing the costs of disposing vitrified DNW and spent fuel is more difficult. Gibbs calculated $47/kg HM as the maximum disposal cost of spent fuel in a borehole. Therefore, the costs for disposing spent fuel in units of $/kg HM is approximately equal to the cost of disposing of DNW in units of $/kg of vitrified waste. However, the actual waste oxides (waste product) to be disposed of are only 45% of the vitrified waste by mass and the metal mass of the waste oxides only constitutes approximately 20% of vitrified waste. Spent fuel on the other hand, is all considered waste product. Therefore, one must be careful about units when comparing costs of disposal of spent fuel and vitrified waste in

any repository. Table 6.5 summarizes the differences in cost units between spent fuel and vitrified waste disposal.

Table 6.5: Cost Unit Comparison for Disposal of DNW

	Vitrified Waste	**Waste Oxide**	**Heavy Metal Content in Waste Oxide**
Percentage of Total Canister Mass	100%	45%	20.1% (refer to Appendix D)
Borehole Drilling and Emplacement Cost	\$46 / kg of vitrified waste	\$101 / kg of waste oxide	\$225 / kg HM
Total Borehole Cost	\$153 / kg of vitrified waste	\$338 / kg of waste oxide	\$757 / kg HM

The values in table 6.5 were calculating with a simple unit analysis, assuming the density of the vitrified waste was 2810 kg/m^3.[231] The calculation of the heavy metal content in the waste oxides can be found in Appendix D.

6.4 Implementing V-DeepBoRe and V-DeepBoRe-II in Future Research

6.4.1 Running V-DeepBoRe and V-DeepBoRe-II

Because the costs of only one canister configuration, repository geometry, and waste form were calculated in this thesis, it is important to offer a guide to calculating costs for other borehole disposal scenarios. Because Gibbs is the creator of V-DeepBoRe, and V-DeepBoRe-II is based heavily on this code, it would helpful for the user to first read Appendix A of Jonathan Gibbs' MIT Nuclear Engineer thesis. In his appendix, the organization of the scripts used in V-DeepBoRe is described.[232] The organization of V-DeepBoRe-II is exactly the same; however, the names of some of the scripts have been changed slightly for differentiation between the two

models. It is also possible to combine scripts from V-DeepBoRe and V-DeepBoRe-II to analyze different repository combinations. Table 6.6 gives four combinations of borehole repositories and the appropriate scripts associated with each combination.

Table 6.6: V-DeepBoRe and V-DeepBoRe-II Scripts for Borehole Repository Combinations

<table>
<tr><th></th><th>Vertical Borehole
Vitrified DNW</th><th>Vertical Borehole
Spent Fuel and Vitrified DNW</th><th>Borehole with Laterals
Vitrified DNW</th><th>Borehole with Laterals
Spent Fuel and Vitrified DNW</th></tr>
<tr><td rowspan="4">Save in 'Current Folder' Specified in MATLAB</td><td>Input Matrices: in.mat</td><td>Input Matrices: in.mat, radii.mat, hexarray.mat, squarepacking.mat, pipes.mat</td><td>Input Matrices: in.mat</td><td>Input Matrices: in.mat, radii.mat, hexarray.mat, squarepacking.mat, pipes.mat</td></tr>
<tr><td>vit_wastemass</td><td>wastemass</td><td>vit_wastemass</td><td>wastemass</td></tr>
<tr><td colspan="2">drill_bit_life_II</td><td colspan="2">drill_bit_life
Note to user: edit emplacement costs to reflect method described in Section 6.2.3.</td></tr>
<tr><td colspan="4"></td></tr>
<tr><td>Run Script</td><td colspan="4">drilling_costs_II</td></tr>
<tr><td>Output</td><td colspan="4">Tracker Matrix</td></tr>
</table>

The following scripts are considered part of V-DeepBoRe-II and are therefore included in Appendix D: in.mat, vit_wastemass.m, drill_bit_life_II.m, and drilling_costs_II.m. Both wastemass.m and drill_bit_life.m are part of V-DeepBoRe and are included in Appendix A of Gibbs' thesis.

6.4.2 Diameter Dependence of Costs from V-DeepBoRe-II

Currently, the Waste Treatment Plant canister is designed to have 0.61 m diameter.[233] Procured Defense Waste Processing Facility canisters have outer diameters between 0.607m and 0.613 m,[234] but for the design purposes, 0.61 m is assumed to be the outer diameter of the canister.[235]

Although the diameter of the Hoag canister in this thesis has an outer diameter of 0.34 m (an artifact of prior application of this canister to borehole disposal of light water reactor fuel assemblies),[236] it would be cost efficient if the current DOE canisters could be emplaced in a borehole without repackaging. Unfortunately, the maximum drill bit size in V-DeepBoRe is 0.508 m (20 inches).[237] Therefore, linear interpolation was used to extrapolate cost dependence to larger diameters. Although the cost correlates very well with the drill bit diameters in V-DeepBoRe-II, it is unclear if the same relationship will continue to larger diameters. Additional research is necessary to expand the available diameters in V-DeepBoRe and V-DeepBoRe-II. However, assuming that the cost dependence on diameter remains linear to larger diameters, equations [6-4] and [6-5] can be used to extrapolate costs for disposal and emplacement of vitrified waste.

$$Cost\left(\frac{\$}{kg\ vitrified\ DNW}\right) = 31.789 * ID_{Liner\ Casing}(m) + 30.771 \qquad [6\text{-}4]$$

$$with\ R^2 = 0.9959$$

$$Cost\left(\frac{\$}{kg\ vitrified\ DNW}\right) = 27.716 * ID_{Liner\ Casing}(m) + 30.098 \qquad [6.5]$$

$$with\ R^2 = 0.9992$$

The difference between equations [6-4] and [6-5] is the drill bit progression. V-DeepBoRe and V-DeepBoRe-II specify that the borehole diameter decreases twice over the entire depth of the borehole. Therefore, each borehole analyzed has 3 drill bit sizes. The first and the third drill bit size correspond to the borehole outer diameter and the liner casing outer diameter in figure 2.1, respectively. Gibbs specifies 69 "Allowable Combinations of Pipe Diameter." These provide

several inches between drill bit sizes. Equation 6.4 was fit to the pipe combinations that Gibbs specified. For uniformity, only pipe combinations with comparable spaces between drill bit sizes were used. Hoag's design does not require as much space between the drill bit sizes. Equation [6-5] is fit to pipe combinations with successive drill bit sizes. Note that there is still space between each drill bit size, but not as much as Gibbs' pipe combinations. Refer to Appendix D for the fitted data for both equations. Note that each data point used for equations [6-4] and [6-5] was the drilling and emplacement cost for each particular pipe schedule resulting from 10,000 trials. Increasing the number of trials could produce equations with a slightly better fit. However, because of the high R^2 values of equations [6-4] and [6-5], 10,000 trials were considered sufficient.

Table 6.7 gives the resulting extrapolated drilling and emplacement costs for the DOE canister diameter. The inner diameter of the final casing of the DOE canister was assumed to be 0.68 m because the canister is assumed to fill no more than 90% of the final casing diameter. The two values are essentially the same considering the likely uncertainty in governing parameters.

Table 6.7: Extrapolated Drilling and Emplacement Cost for Current WTP and DWPF Canisters

	Extrapolated Drilling and Emplacement Cost for DOE Canisters
Equation [6.4]	52.32 $/kg vitrified DNW
Equation [6.5]	49.56 $/kg vitrified DNW

Additional research is necessary to ensure that cost does indeed increase linearly with diameter instead of a higher power. Obviously, there is a point where the state of the art of drilling technology does not allow increasing the borehole diameter any larger. However, boreholes with

diameters larger than 0.508 m have been drilled. For example, a 640 m deep borehole with a 0.71 m (28 inch) diameter was drilled to rescue 33 miners in San José Mine in Chile.[238] The values in table 6.7 are given for illustrative purposes and are dependent on the assumption that a borehole that can accommodate the DOE canister can be drilled using current state of the art technology.

6.5 Chapter Summary

V-DeepBoRe was modified to create V-DeepBoRe-II to calculate the drilling and emplacement costs of vitrified DNW disposal in a vertical borehole. The drilling and emplacement costs of the vitrified waste described in Chapter 2 with the repository geometry described in figure 2.1 are not expected to exceed $46/kg of vitrified DNW. These costs were added to the vitrification and package fabrication costs for vitrified waste to get a total cost for disposal of vitrified DNW in a borehole. This brings the total disposal cost of the vitrified waste analyzed in this thesis to $153/kg of vitrified DNW. These costs are summarized in Tables 6.3 and 6.4 and do not include transportation. V-DeepBoRe-II was also used to create a data set that was used to create diameter-dependent cost equations. These equations were used to predict costs of the borehole disposal of the canisters currently employed at the Defense Waste Processing Facility and the ones designed for the Waste Treatment Plant. The drilling and emplacement costs of waste vitrified in these containers are not expected to exceed $53/kg of vitrified waste.

V-DeepBoRe-II allows for the drop-in method of emplacement but does not allow for a lateral-emplacement strategy. Therefore, the drill_bit_life.m script of V-DeepBoRe should be changed to reflect the more feasible drop-in emplacement method if lateral emplacement is desired. Then, V-DeepBoRe could be used for spent fuel and vitrified waste disposal with lateral

emplacement. Additional research should be conducted to find a more appropriate way of comparing the costs of waste of spent fuel and vitrified waste. Increased drill bit sizes should also be added to V-DeepBoRe and V-DeepBoRe-II so that the cost of disposing of larger canisters can be calculated more accurately.

7 Conclusions and Future Work

7.1 Summary of Methodology and Results

The methodology and results from the analyses in each chapter of this thesis are included in this section. Recommended future work and conclusions are in sections 7.2 and 7.3, respectively.

7.1.1 Environmental Conditions and Repository Geometry

To begin this feasibility study, it was first necessary to define the environment and waste form associated with borehole disposal of DNW. The DNW considered in this thesis was created by dissolving spent nuclear fuel rods and targets in acid and separating out the plutonium and uranium for U.S. weapons production. The waste form of DNW is characterized by the nuclide compositions for the 6 DNW data sets described in tables A.1 and A.2, vitrified in the borosilicate glass composition described in table 2.2. The 6 DNW data sets correspond to the bounding and average DNW from the Waste Treatment Plant at Hanford Site and the 4 compositions of DNW from the Defense Waste Processing Facility at Savannah River Site. The bounding waste for a borehole repository was found to be the bounding DNW from the Waste Treatment Plant because it has highest gamma dose, fissile material content, and decay heat of all the vitrified DNW.

The environmental model includes the repository geometry as well as the borehole attributes. Two borehole canisters are considered in this thesis. The diameter specifications of the first canister are based on those in Ian Hoag's MIT Thesis and are shown in figure 2.1 and listed in table 2.3. The second canister considered is the DOE canister currently used to vitrify waste, which is shown in figure 2.2 and described in table 2.3. The borehole attributes are separated into 3 categories; properties that define vertical nuclide transport, properties that define radial nuclide

transport, and other borehole attributes. These are described in sections 2.5 and 2.6. The borehole properties that define vertical nuclide transport (salinity, down-hole pressure, and geothermal gradient) demand the most attention because vertical transport is the pathway by which nuclides could reach levels accessible by humans in an unlikely failure scenario. A summary of the borehole attributes mentioned as well as the ideal specifications associated with each property and the value for granite are given in table 2.4.

7.1.2 Thermal Analysis

One of the principal constraints on the feasibility of deep borehole disposal is the maximum temperature attained by the rock surrounding the waste during the post-emplacement period. The objective of the thermal analysis was to find the maximum temperature change between the far field granite and the granite directly surrounding the borehole filled with emplaced waste. This was done by first creating a model for the decay heat function and implementing the model in the temperature difference equation for an infinite line source in a homogeneous granite slab. It is also valuable to find the time at which this maximum temperature occurs. Temperature changes in the waste string, waste package canister, liner, and gaps are also found.

The decay heat values from ORIGEN were found to fit very well with the exponential decay function shown in equation [7-1].

$$q'(t) = q'(t_c) * e^{-\lambda t} \quad \textbf{[7-1]}$$

where:

$q'(t)$ = Decay Heat Function, W/m
$q'(t_c)$ = Decay Heat at Time of Emplacement, W/m
λ = Decay Constant of Bounding Nuclide(s), $years^{-1}$
t = Time After Emplacement, years

The decay constant that fits the bounding DNW the best corresponds to a dominant nuclide half life of 29.63 years (R^2 = 0.99996 for the first 200 years). This is shown in figure 3.1. This decay constant also fits the non-bounding DNW well (R^2 = 0.9902 to 0.99995 for the first 200 years).

The analytical approximation of temperature change in granite is shown in equation [3-3]. This equation was solved for the bounding DNW at the borehole environmental conditions described in table 2.4. The resulting temperature difference in the granite is 15.1^{0}C for the Hoag canister and 45.7^{0}C for the DOE Canister for the bounding DNW. When added to the expected geothermal gradient, the resulting maximum temperature at the bottom of the borehole at the borehole wall is 135.1^{0}C (Hoag Canister) and 165.7^{0}C (DOE Canister) for the bounding DNW at expected environmental conditions. This was found to occur 5.4 years and 5.9 years after emplacement for the Hoag Canister and the DOE Canister, respectively.

The expected borehole conditions (radius, thermal diffusivity of basement rock, and dominant half life) were varied to understand the dependence of the resulting maximum temperature difference on these conditions. The same was done for spent fuel in a borehole repository. This data was correlated using simple analytic equations that can be used to calculate the maximum temperature differences and times to maximum temperature for both DNW and spent fuel.

These are given in equations [7-1] and [7-2]. These equations were compared with theory and temperature differences given in other references, and were found to be in good agreement.

$$\hat{G} = 0.872 \ln\left(\frac{4\alpha t_c}{r^2}\right) - 1.827 \quad [7\text{-}1]$$

$$\frac{t_c}{\hat{t}} = 0.601 \ln\left(\frac{4\alpha t_c}{r^2}\right) - 1.260 \quad [7\text{-}2]$$

$$\hat{G} = \Delta T_{max} * \frac{4\pi k}{q'(t_c)} \quad [7\text{-}3]$$

where:

$\hat{t}$ = Time to Maximum Temperature Change, years
t_c = Cooling Time (replace with $t_{1/2}$ for DNW), years
$\propto$ = Granite Thermal Diffusivity, m²/year
r = Radius of Borehole, m
$\hat{G}$ = Peak Host Rock Temperature Factor (maximum value of parameter G), unitless
ΔT_{max} = Maximum Temperature Change in Granite calculated from MATLAB code, °C
k = Granite Thermal Conductivity, W/m/°C
$q'(t_c)$ = Decay Heat at Time of Emplacement, W/m

The method used to calculate the temperature rise in the waste form, canister, liner, and gaps is given in equations [3-12] and [3-14]. Equation [3-13] allows the decay heat model from section 3.2 to be used to calculate the temperature differences in the gaps. The centerline temperature for the borosilicate glass waste package is approximately 192°C for the DOE Canister and 145°C for the Hoag Canister. The temperature differences for each of the repository features (waste form, canister, liner casing, and gaps) is illustrated in figure 7.1.

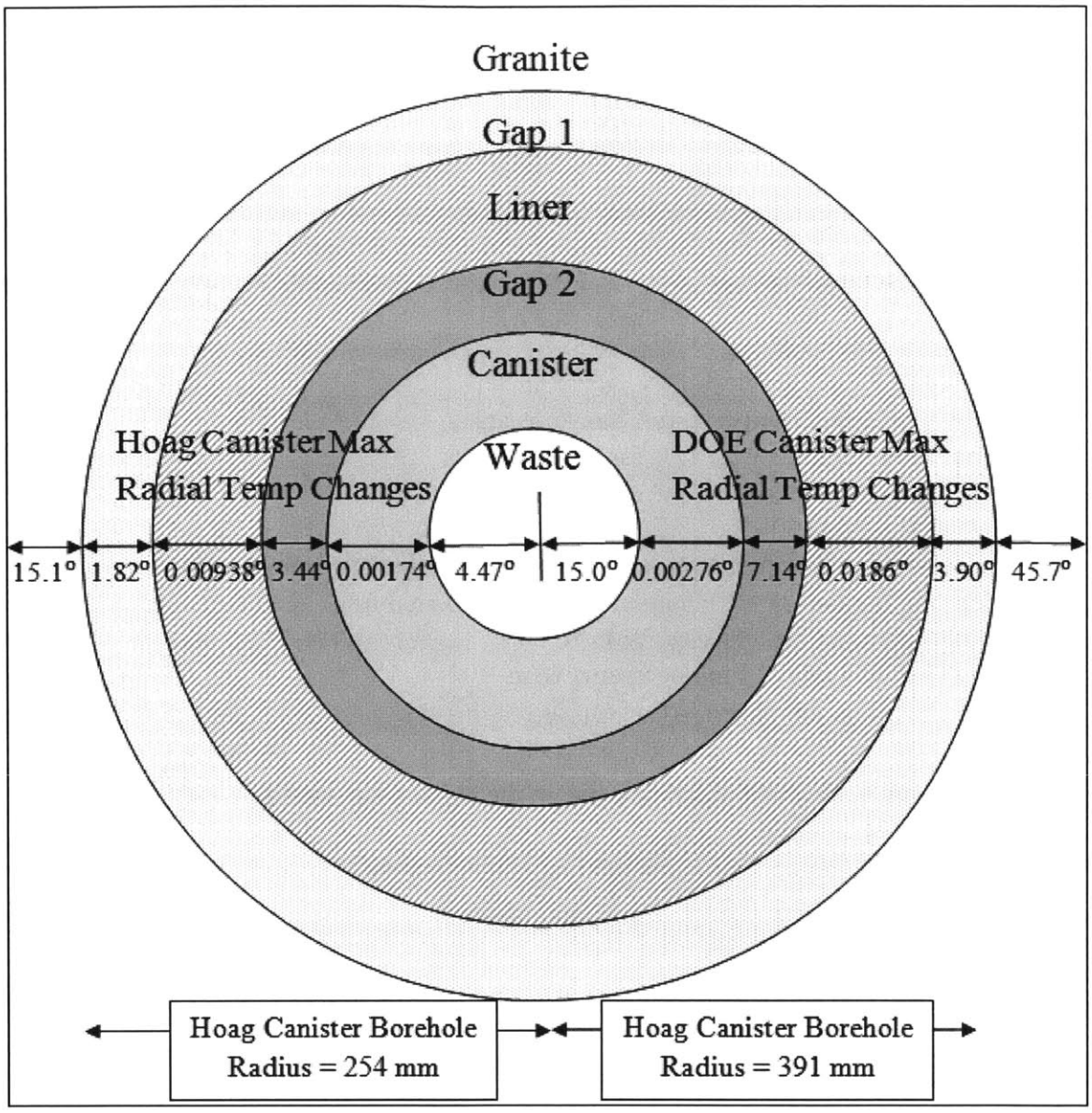

Figure 7.1: Radial Temperature (in °C) Changes in Borehole (not drawn to scale)

The maximum temperature at the outer diameter of each element can be found in table 3.8. All thermal analysis calculations and codes can be found in Appendix B.

7.1.3 Waste Canister Corrosion Analysis

Prospective canister materials including copper, tantalum, titanium, aluminum, iron, chromium, nickel, and their alloys were evaluated for suitability in the borehole environment through a literature review and a stability analysis using Pourbaix diagrams. The ideal waste canister should be corrosion resistant in a borehole environment to prevent the release of nuclides. The stable form of the metal of the ideal canister should also be insoluble at the temperatures and conditions predicted in a borehole environment.

The stable form of each metal, the corrosion susceptibility, and the cost were all considered when determining the ideal canister material for DNW. Table 4.2 summarizes the stable form of each canister material in predicted borehole environments. Table 4.3 gives the relative prices of the pure metals considered.

Because of the thermodynamic properties (the stable form), overall corrosion resistance, and reasonable cost, pure copper was shown to be the best borehole outer canister material. Copper remained as a metal in the Pourbaix diagram shown in figure 7.2; therefore, it exhibits immunity in a borehole environment.

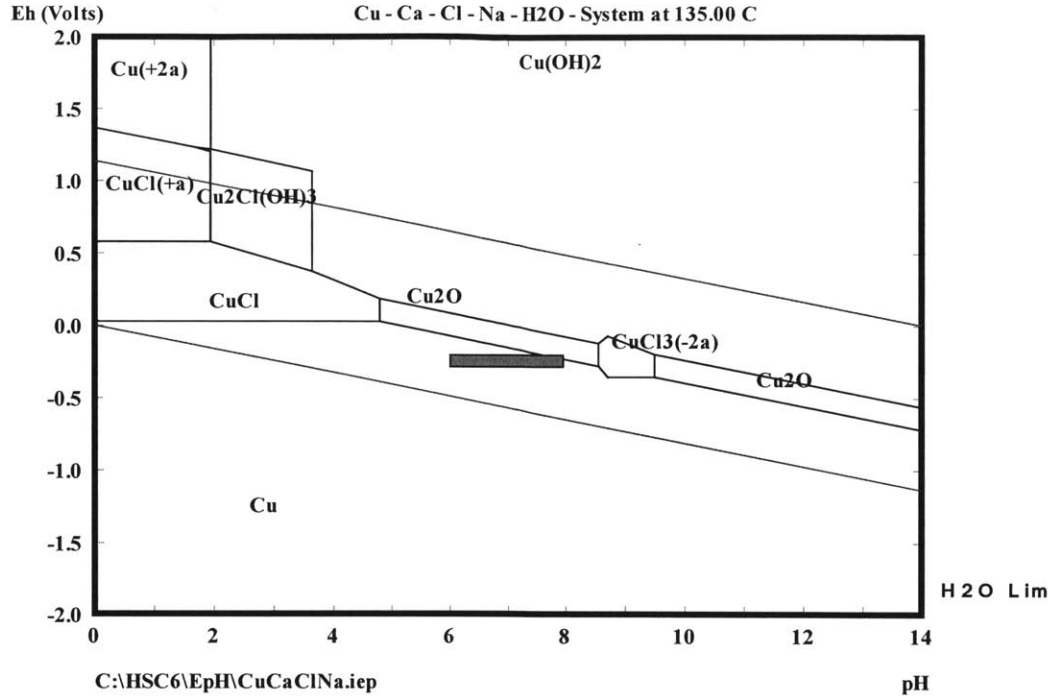

Figure 7.1: Pourbaix Diagram from Copper in Borehole Environment
(shaded area bounds the expected borehole conditions outlined in table 4.1)

Copper is more expensive than several other metals, but the price is still reasonable; especially if copper is only used as protective plating on another, lower cost material. Finally, the literature review shows that copper is very resistant to all types of corrosion in borehole environments. Conditions at which corrosion is possible (nickel content and high strain) can be limited or controlled.

High-chromium stainless steel could also be a good option for borehole canisters because it has also been shown to be highly corrosion-resistant in environments very similar to predicted borehole environments. In experimental literature, high-chromium stainless steels have been shown to passivate and remain stable in borehole environments. This is supported by the passive

oxide formation in the Pourbaix diagrams for chromium and iron. High-chromium stainless steels are less expensive than copper as well as many other materials.

7.1.4 Waste Form Dissolution Analysis

To conduct a conservative analysis, the boreholes are assumed to fill with water. If a borehole fills with water, canister and waste form degradation could occur. The canister material will protect the waste form from initial degradation, but to keep the analysis very conservative, the canister is assumed to fail immediately after emplacement. Therefore, the waste form is assumed to begin to alter immediately upon emplacement; even though the canister and lack of electrolyte (water) in the borehole environment will likely delay this degradation significantly.

To understand the degradation behavior of the waste form, a literature review and chemical analysis were performed. The literature review outlines the experimental research conducted on waste form behavior in conditions similar to the borehole environment in table 4.1. The chemical analysis is twofold; the first portion is the determination of the stable nuclide form of 11 nuclides in the waste using Pourbaix diagrams and the second portion is the calculation of the maximum soluble concentration of each nuclide species.

In the waste form literature review, it was found that the borosilicate glass used as the waste form has been shown to leach faster and have higher diffusion rates at higher temperatures.[239] This implies that alteration will occur faster in boreholes than it would in a geologic repository. Also, stress corrosion cracking has been shown to occur due to internal stresses from cooling.[240] It is unclear if this will be a problem in defense waste. Devitrification can also occur and create interphase boundaries that are more susceptible to corrosion.[241] Finally, waste form leaching

was shown to decrease as granite content in the water increases.[242] This could aid in offsetting the increased leaching due to the higher temperatures.

To understand the leaching of the nuclides, Pourbaix diagrams were created for several nuclides in defense waste. The diagrams were used to determine the stable form of the nuclide and can be found in Appendix C. The Common Thermodynamic Database was used to determine the reaction associated with the stable form. Then, the solubility product was used to find the maximum concentration in the borehole environment of any possible resulting soluble nuclide ions. The maximum concentration would only be the actual concentration in the borehole if the system were allowed to reach equilibrium; time is not considered in the calculation. Also, the calculation did not account for elements in the water surrounding the borehole (other than the calcium, sodium, and chloride implicit in the Pourbaix diagrams). In reality, all the nuclides and glass formers will be leaching concurrently and this will affect the actual concentration of each element.

Cesium ion was found to have the highest concentration in the borehole environment. However, the relatively short half life of the most abundant cesium isotope suggests that the cesium would decay before the canister is breached. This analysis found that the maximum soluble concentration for technetium was negligible (on the order of 10^{-28} M, see Appendix C). However, this analysis was not able to find the maximum soluble concentration of iodine because there were too many ions with unknown concentrations in the stable form equation (refer to section C.6). The maximum soluble concentrations of each nuclide considered can be found in table 5.1.

7.1.5 Cost Analysis

Part of analyzing the feasibility of borehole disposal of vitrified defense waste is understanding the time and costs associated with disposal activities. For this reason, V-DeepBoRe-II was created (based on Jonathan Gibbs' V-DeepBoRe) to calculate the drilling and emplacement costs of vitrified DNW disposal in a vertical borehole. These costs were added to the vitrification and package fabrication costs for vitrified waste to get a total cost for disposal of vitrified DNW in a borehole. V-DeepBoRe-II was also utilized to create a data set that was used to create the diameter-dependent cost equations shown in equations [7-5] and [7-6]. These equations were used to extrapolate the predicted costs of the borehole disposal of the canisters currently employed at the Defense Waste Processing Facility and the ones designed for the Waste Treatment Plant.

$$Cost\left(\frac{\$}{kg\ vitrified\ DNW}\right) = 31.789 * ID_{Liner\ Casing}(m) + 30.771 \quad [7\text{-}5]$$

$$Cost\left(\frac{\$}{kg\ vitrified\ DNW}\right) = 27.716 * ID_{Liner\ Casing}(m) + 30.098 \quad [7\text{-}6]$$

The drilling and emplacement costs of the vitrified waste described in Chapter 2 with the repository geometry described in figure 2.1 are not expected to exceed $46/kg of vitrified DNW for the Hoag canister. These costs were added to the vitrification and package fabrication costs for vitrified waste to get a total cost for disposal of vitrified DNW in a borehole. This brings the total disposal cost of DNW to $153/kg of vitrified DNW for the Hoag canister. These costs are summarized in Tables 6.3 and 6.4 and do not include transportation. Equations [7-5] and [7-6] were used to predict costs of the borehole disposal of waste in the DOE canister described in table 2.3. The drilling and emplacement costs of waste vitrified in DOE containers are not expected to exceed $53/kg of vitrified DNW.

7.2 Future Work

Useful future work became apparent in each of the analyses involved in this thesis. Future work involving the environment and waste composition include analyzing additional defense waste types (naval fuel, transuranic waste, low-level waste, by-product material, etc.) as well as analyzing other waste forms (ceramics or grout, for example). It would also be useful to further quantify the natural resistance of the borehole environment to the rise of a contaminated hot brine "balloon." Experiments on the canister-liner combination in a borehole environment are required to ensure that that galvanic corrosion does not occur.

Analyzing the thermal properties of additional borehole configurations would be beneficial. For example, it would be useful to look at specific types of cement, grout, or fill in the gaps between the canister and liner and the liner and borehole. Knowing the optimal configuration from thermal loading, retrievability, and cost perspectives would save time in future analyses. The Hoag canister analyzed in this thesis has a length of 5 m. This was based on the assumption that these canisters would be used for spent fuel assemblies.[243] Therefore, the optimal vitrified waste reference canister may have a different length based on structural stability or cost. A future optimization study would be useful to find the ideal reference canister length.

Material properties other than corrosion, such as toughness, strength, and ductility were not considered in the corrosion analysis. This is because once a metal or alloy is chosen, small changes in composition can be made if the mechanical properties are not adequate. Also, the most suitable metal could be plated onto a stronger or lower cost alloy if the suitable metal does not exhibit desired properties. Therefore, mechanical properties of the specific waste canister design should be examined in future work. It would also be valuable to analyze the affect of

other borehole brine constituents (silica, magnesium, iron, etc.) on the canister. Radiation damage of canisters in a borehole environment (for example: that resulting from water radiolysis) should also be understood.

Additional research and experiments must be conducted to understand and quantify the leaching behavior over time of borosilicate glass and nuclides in a borehole environment vice a geologic repository environment. A parametric study is also required to understand the sensitivity of nuclide solubility on pH, salinity and other borehole properties. It would also be beneficial to analyze possible protective features for the waste form in the borehole (different fill material in the borehole gaps, additional liners, etc.). Also, research on the feasibility of removing the waste from one canister and putting it into another, smaller diameter, canister would be necessary if drilling a borehole large enough to allow for the DOE canister was technically unfeasible or too expensive (however, it was found in Chapter 6 that the DOE canister could be emplaced at a cost only slightly greater than that of the Hoag Canister). Experimental research is required to understand the solubility of iodine in a borehole environment before final conclusions can be drawn about the risk associated with a borosilicate glass waste form emplaced in a borehole repository. However, other work suggests that I-129 is the limiting radionuclide for spent light water reactor fuel disposal.

Additional work should be performed to find a more appropriate way of normalizing spent fuel and vitrified waste that allows definition of a comparable equivalent mass. Increased drill bit sizes should also be added to V-DeepBoRe and V-DeepBoRe-II so that the cost of disposing of larger canisters can be calculated. Also, the structural impacts of the drop-in emplacement method must be evaluated specifically for DOE canisters.

7.3 Conclusions

Boreholes drilled several kilometers into crystalline basement rock remain a contender for the disposal of high-level nuclear waste whether intact fuel assemblies or defense wastes. Although additional research is required before in-depth design work can begin, this thesis found that a borehole repository is an economically and technically feasible permanent repository for DOE-owned defense nuclear waste. This feasibility is based on environmental, thermal, corrosion, dissolution, and cost studies. In many of these analyses, a borehole repository for defense waste was found to be a more attractive disposal option than the canceled Yucca Mountain Nuclear Waste Repository.

Appendix A: Defense Waste Compositions

There are 55 clearly identified and distinctly different waste types that will be processed at the Waste Treatment Plant, 17 of which will be processed at the Defense Waste Processing Facility.[244] There are 6 compositions of DNW analyzed in this thesis, The first 2 compositions are for the bounding and average waste at the Waste Treatment Plant.[245] The other 4 are the "batches" of waste to be processed at Defense Waste Processing Facility.[246] These were the batches used to create the Yucca Mountain Total Systems Performance Assessment;[247] therefore, they are considered adequate to describe the bounding wastes at the Defense Waste Processing Facility, even though they may not describe each of the 17 high-level waste types present at Savannah River Site. Table A.1 gives the Waste Treatment Plant DNW nuclide compositions and Table A.2 gives the Defense Waste Processing Facility DNW nuclide compositions. Table A.3 gives the assumed glass former compositions used in this thesis. Although the glass former composition will not be the same for every DNW in this thesis, the waste loading (mass percent of metal oxides) is assumed to remain 45% for each DNW and the glass former composition is assumed to be quite similar for each waste. Table A.4 gives the table that determines the total metal content within the metal oxides.

Table A.1: Waste Treatment Plant DNW Nuclide Composition

Isotope	Radionuclide	Average WTP DNW (Curies/m³)	Bounding WTP DNW (Curies/m³)
227	Ac	1.545E-02	1.218E-04
241	Am	1.723E+01	3.966E+02
243	Am	1.783E-03	8.403E-02
14	C	0.000E+00	1.042E-01
242	Cm	1.723E-02	3.580E-01
243	Cm	1.545E-03	5.227E-02
244	Cm	3.506E-02	1.168E+00

Table A.1 continued.

Isotope	Radionuclide	Average WTP DNW (Curies/m³)	Bounding WTP DNW (Curies/m³)
60	Co	9.638E-01	1.790E+01
134	Cs	2.175E+00	2.303E+02
137	Cs	5.443E+03	9.328E+04
152	Eu	1.937E-01	6.160E+00
154	Eu	1.173E+01	2.134E+02
155	Eu	9.222E+00	2.756E+02
129	I	5.704E-03	0.000E+00
137	mBa	5.158E+03	8.824E+04
113	mCd	1.913E+00	3.521E+01
93	mNb	4.611E-01	3.000E+00
59	Ni	1.628E-01	4.168E-01
63	Ni	1.521E+01	4.588E+01
237	Np	1.676E-02	2.101E-01
231	Pa	3.233E-02	3.563E-04
238	Pu	5.800E-01	2.067E+00
239	Pu	8.212E+00	1.790E+01
240	Pu	1.462E+00	5.403E+00
241	Pu	1.486E+01	1.588E+02
242	Pu	1.188E-04	8.328E-04
226	Ra	1.070E-05	1.092E-05
228	Ra	7.487E-03	4.840E-05
106	Ru	1.212E-01	6.008E+00
125	Sb	2.959E+00	1.588E+02
79	Se	1.450E-02	7.689E-02
151	Sm	4.171E+02	3.269E+03
126	Sn	6.881E-02	4.824E-01
90	Sr	6.002E+03	7.706E+04
99	Tc	3.530E+00	1.941E+01
229	Th	2.377E-04	9.076E-08
232	Th	9.507E-04	1.261E-04
232	U	5.110E-03	4.328E-04
233	U	6.061E-02	1.756E-03
234	U	2.615E-02	1.227E-02
235	U	1.070E-03	4.672E-04
236	U	7.131E-04	9.916E-04
238	U	2.365E-02	8.487E-03
90	Y	6.002E+03	7.706E+04
93	Zr	5.716E-01	4.840E+00

Table A.2: Defense Waste Processing Facility DNW Nuclide Composition

Radionuclide	Batch 1A (Curies/m³)	Batch 1B (Curies/m³)	Batches 2 to 3C (Curies/m³)	Batches 4 to 10D (Curies/m³)
227Ac	7.64E-08	5.58E-08	1.01E-07	8.15E-08
241Am	4.91E+00	5.47E+00	2.62E+01	8.50E+01
243Am	2.78E-02	4.22E-02	4.37E-01	5.11E-09
245Cm	4.16E-04	0.00E+00	3.17E-03	7.31E-03
135Cs	3.86E-04	6.14E-04	8.85E-04	1.48E-01
137Cs	2.06E+01	5.36E+01	1.22E+02	2.03E+04
129I	0.00E+00	8.68E-05	6.21E-06	0.00E+00
237Np	1.03E-02	1.25E-02	1.11E-02	2.58E-02
231Pa	1.92E-07	1.59E-07	3.08E-07	2.49E-07
210Pb	1.37E-08	5.32E-08	9.74E-09	9.26E-09
238Pu	3.24E+01	5.53E+01	2.55E+01	6.54E+02
239Pu	4.98E+00	4.02E+00	6.29E+00	1.34E+01
240Pu	1.33E+00	1.40E+00	2.01E+00	6.34E+00
241Pu	4.30E+00	8.14E+00	6.26E+00	1.14E+02
242Pu	1.17E-03	2.33E-03	3.76E-03	1.37E-02
226Ra	4.90E-08	1.68E-07	4.26E-08	4.64E-08
228Ra	8.23E-13	1.33E-04	2.96E-05	1.08E-03
79Se	8.07E-03	6.98E-02	5.13E-02	0.00E+00
126Sn	4.77E-03	2.75E-02	3.68E-02	0.00E+00
90Sr	1.91E+02	1.45E+03	1.92E+03	1.68E+04
99Tc	1.62E-01	1.48E-01	1.03E-01	9.30E+00
229Th	1.58E-04	2.04E-04	2.24E-05	9.89E-05
230Th	6.66E-06	1.73E-05	7.39E-06	1.02E-05
232Th	1.07E-12	1.37E-04	3.08E-05	1.12E-03
232U	0.00E+00	0.00E+00	0.00E+00	1.53E-04
233U	1.90E-02	3.59E-02	8.77E-03	3.91E-02
234U	2.28E-02	3.27E-02	3.14E-02	6.91E-02
235U	2.57E-04	2.54E-04	5.39E-04	4.39E-04
236U	6.18E-04	8.69E-04	7.76E-04	1.84E-03
238U	8.07E-03	6.34E-03	2.07E-02	1.96E-02
Total Canisters	495	726	705	3,134

Table A.3: Glass Former Compositions for Waste Treatment Plant DNW

	WTP Average		**WTP Bounding**	
	kg/m³of vitrified DNW	**Average Mass %**	**kg/m³**	**kg/m³of vitrified DNW**
Al2O3	108.62	3.85%	108.22	3.83%
B2O3	166.38	5.91%	166.13	5.88%
Fe2O3	52.17	1.85%	52.00	1.84%
Li2O3	65.60	2.32%	65.21	2.31%
Na2O	288.79	10.25%	288.12	10.20%
SiO2	869.93	30.83%	866.61	30.68%
Total Glass Formers	1551.49	55.00%	1553.78	55.00%
Total Glass Mass	2819.52		2810.92	

Table A.4: Mass Percent of Metal in Metal Oxide in Waste Form

Waste Oxide	Mass of Waste Oxide (kg)	Mass % of Total Waste Form	Molar Mass of metal (g/mol)	Mass % of Metal in Oxide	Mass of Heavy Metal in Oxide (kg)	Mass % of Total Waste Form
AgO	1.82	0.05%	107.868	0.871%	1.585	0.044%
As205	0.88	0.03%	74.922	0.652%	0.574	0.020%
Al2O3	147.26	4.43%	26.982	0.529%	77.938	2.345%
B203	8.35	0.25%	137.327	0.851%	7.108	0.213%
BaO	4.01	0.12%	137.327	0.896%	3.592	0.107%
BeO	0.19	0.01%	9.012	0.360%	0.068	0.004%
Bi203	0.41	0.01%	208.980	0.897%	0.368	0.009%
CaO	17.76	0.53%	40.078	0.715%	12.693	0.379%
Cl	0.18	0.01%	35.453	1.000%	0.180	0.010%
CdO	39.98	1.20%	112.411	0.875%	34.999	1.050%
CeO2	5.23	0.16%	140.115	1.156%	6.044	0.185%
Co203	0.33	0.01%	58.933	0.711%	0.235	0.007%
CuO	1.76	0.05%	63.546	0.799%	1.406	0.040%
Cr2O3	63.87	1.92%	51.996	0.684%	43.700	1.314%
F	2.5	0.08%	63.546	1.000%	2.500	0.080%

Table A.4 continued.

Waste Oxide	Mass of Waste Oxide (kg)	Mass % of Total Waste Form	Molar Mass of metal (g/mol)	Mass % of Metal in Oxide	Mass of Heavy Metal in Oxide (kg)	Mass % of Total Waste Form
Fe2O3	587.81	17.68%	18.998	0.442%	259.727	7.812%
K20	14.97	0.45%	138.906	0.473%	7.077	0.213%
La2O3	21.39	0.64%	6.941	0.224%	4.799	0.144%
Li20	0.24	0.01%	6.941	0.232%	0.056	0.002%
MgO	9.26	0.28%	24.305	0.603%	5.584	0.169%
MoO3	14.78	0.44%	95.940	0.667%	9.851	0.293%
Mn02	8.32	0.25%	54.938	0.632%	5.258	0.158%
Na2O	181.71	5.47%	22.990	0.371%	67.402	2.029%
Nd203	16.8	0.51%	144.240	0.857%	14.404	0.437%
NiO	32.29	0.97%	58.690	0.786%	25.373	0.762%
PbO	1.71	0.05%	207.200	0.928%	1.587	0.046%
P205	3.54	0.11%	30.974	0.436%	1.545	0.048%
Pr2O3	2.77	0.08%	140.908	0.854%	2.367	0.068%
Rb20	0.38	0.01%	85.468	0.457%	0.174	0.005%
Rh203	1.23	0.04%	102.906	0.811%	0.997	0.032%
Ru2O3	8.73	0.26%	101.070	0.808%	7.055	0.210%
Si02	26.67	0.80%	28.086	0.467%	12.467	0.374%
SO3	16.45	0.49%	32.066	0.401%	6.588	0.196%
SrO	2.28	0.07%	87.620	0.846%	1.928	0.059%
Sb203	0.05	0.00%	121.750	0.835%	0.042	0.000%
Se02	2.14	0.06%	78.960	0.333%	0.712	0.020%
Ta2O5	0.05	0.00%	180.948	0.819%	0.041	0.000%
TeO2	0.55	0.02%	127.600	0.800%	0.440	0.016%
ThO2	1.64	0.05%	232.038	0.879%	1.441	0.044%
Ti02	0.67	0.02%	47.880	0.599%	0.402	0.012%
Tl2O3	0.05	0.00%	204.383	0.895%	0.045	0.000%
U3O8	46.65	1.40%	238.029	0.848%	39.559	1.187%
V2O5	0.5	0.01%	50.942	0.560%	0.280	0.006%
ZnO	0.87	0.03%	65.390	0.803%	0.699	0.024%
ZrO2	196.88	5.92%	91.224	0.004%	0.740	0.022%
Total	1495.91	44.98%			**671.629**	**20.100%**

The percents of metal in the metal oxides in Table D.4 were calculated by dividing the molar mass of the metal by the total molar mass of the oxide. This was multiplied by the mass of each

oxide present in the bounding waste and divided by the total mass to get the mass of metal in the waste form. This was used to calculate a cost in $/kg of heavy metal to compare with spent fuel costs. However, the masses of metals do not give a good indication of the waste form because the nuclides in the waste form are oxides, not elemental metals.

Appendix B: Thermal Analysis Calculations

B.1 Decay Heat Model

Refer to Section 3.2.1 for additional explanation for the Decay Heat Model. Tables B.1-B.3 gives the ORIGEN-generated decay heat (in W/m^3) for each time step from all 6 DNW compositions analyzed in this thesis. The next two columns for each DNW composition are the linear decay power in W/m found by multiplying the ORIGEN decay heat by the cross-sectional area of the waste package associated with the DOE Canister and the Hoag Canister, respectively. In spread sheets not included in this Appendix, equation [3-2] was used to generate values corresponding to both waste packages for each of the DNW compositions for each time step. Then, this data was correlated with the corresponding linear decay power in W/m and the R^2 value was recorded in Tables B.1-B.3. Note, only the data for times after emplacement of less than 200 years were correlated with equation [3-2]. These values are highlighted in Tables B.1-B.3.

To use equation [3-2], the value for $q'(t_c)$, Decay Heat at Time of Emplacement (W/m) must be taken for both waste packages from each DNW composition. The nuclide composition for Waste Treatment Plant bounding and average wastes was given for 2001; therefore, a 10 year cooling time would make the time of emplacement the year 2011. This is the most conservative emplacement time, because the sooner the waste is emplaced, the greater the decay heat for each waste. The nuclide composition for the Defense Waste Processing Facility batches was given for the year 2004. Therefore, to maintain consistency, the time of emplacement for these batches was also considered to be 2011. Therefore, the value for $q'(t_c)$ is taken from the row where time = 7 years for DWPF waste and time = 10 years for WTP waste.

Table B.1: Decay Heat for DWPF Batch 1A and 1B for DOE and Hoag Canisters

		DWPF Batch 1A			DWPF Batch 1B		
Time	Time After Emplaced	ORIGEN	DOE Canister	Hoag Canister	ORIGEN	DOE Canister	Hoag Canister
(yrs after 2004)	(yrs after 2011)	(W/m³)	(W/m)	(W/m)	(W/m³)	(W/m)	(W/m)
0.30		2.803	0.769	0.223	12.080	3.314	0.959
0.39		2.800	0.768	0.222	12.060	3.308	0.958
0.50		2.795	0.767	0.222	12.030	3.300	0.955
0.65		2.788	0.765	0.221	11.990	3.289	0.952
0.80		2.782	0.763	0.221	11.960	3.281	0.950
1.00		2.774	0.761	0.220	11.900	3.264	0.945
1.30		2.762	0.758	0.219	11.830	3.245	0.940
1.60		2.749	0.754	0.218	11.750	3.223	0.933
2.00		2.733	0.750	0.217	11.650	3.196	0.925
2.60		2.709	0.743	0.215	11.510	3.157	0.914
3.30		2.681	0.735	0.213	11.340	3.111	0.901
4.20		2.646	0.726	0.210	11.120	3.050	0.883
5.40		2.600	0.713	0.206	10.840	2.974	0.861
7.00	0.00	2.540	0.697	0.202	10.490	2.878	0.833
9.00	2.00	2.468	0.677	0.196	10.060	2.760	0.799
10.00	3.00	2.434	0.668	0.193	9.848	2.702	0.782
13.00	6.00	2.333	0.640	0.185	9.254	2.539	0.735
15.00	8.00	2.270	0.623	0.180	8.880	2.436	0.705
18.00	11.00	2.179	0.598	0.173	8.352	2.291	0.663
20.00	13.00	2.122	0.582	0.169	8.019	2.200	0.637
25.00	18.00	1.988	0.545	0.158	7.252	1.989	0.576
30.00	23.00	1.867	0.512	0.148	6.569	1.802	0.522
40.00	33.00	1.657	0.455	0.132	5.418	1.486	0.430
50.00	43.00	1.482	0.407	0.118	4.501	1.235	0.357
75.01	68.01	1.161	0.318	0.092	2.934	0.805	0.233
100.00	93.00	0.948	0.260	0.075	2.021	0.554	0.161
130.00	123.00	0.777	0.213	0.062	1.393	0.382	0.111
160.00	153.00	0.659	0.181	0.052	1.034	0.284	0.082
200.00	193.00	0.552	0.151	0.044	0.762	0.209	0.061
250.00	243.00	0.462	0.127	0.037	0.576	0.158	0.046
325.00	318.00	0.380	0.104	0.030	0.429	0.118	0.034
420.00	413.00	0.321	0.088	0.025	0.335	0.092	0.027
540.00	533.00	0.281	0.077	0.022	0.276	0.076	0.022

Table B.1 continued.

		DWPF Batch 1A Continued			DWPF Batch 1B Continued		
Time	Time After Emplaced	ORIGEN	DOE Canister	Hoag Canister	ORIGEN	DOE Canister	Hoag Canister
(yrs after 2004)	(yrs after 2011)	(W/m³)	(W/m)	(W/m)	(W/m³)	(W/m)	(W/m)
700.10	693.10	0.253	0.069	0.020	0.238	0.065	0.019
910.10	903.10	0.232	0.064	0.018	0.213	0.058	0.017
1180.0	1173.00	0.215	0.059	0.017	0.194	0.053	0.015
1530.0	1523.00	0.202	0.055	0.016	0.179	0.049	0.014
1980.0	1973.00	0.191	0.052	0.015	0.168	0.046	0.013
2570.0	2563.00	0.182	0.050	0.014	0.159	0.044	0.013
3340.0	3333.00	0.175	0.048	0.014	0.152	0.042	0.012
$R^2$for Eq.[3-2]			**0.9902**			**0.9995**	

Table B.2: Decay Heat for DWPF Batches 2-3C and 4-10 for DOE and Hoag Canisters

		DWPF Batch 2-3C			DWPF Batch 4-10		
Time	Time After Emplaced	ORIGEN	DOE Canister	Hoag Canister	ORIGEN	DOE Canister	Hoag Canister
(yrs after 2004)	(yrs after 2011)	(W/m³)	(W/m)	(W/m)	(W/m³)	(W/m)	(W/m)
0.30		15.350	4.211	1.219	136.800	37.528	10.865
0.39		15.320	4.203	1.217	136.600	37.473	10.849
0.50		15.280	4.192	1.214	136.300	37.390	10.825
0.65		15.230	4.178	1.210	135.900	37.281	10.794
0.80		15.180	4.164	1.206	135.500	37.171	10.762
1.00		15.110	4.145	1.200	135.000	37.034	10.722
1.30		15.010	4.118	1.192	134.200	36.814	10.659
1.60		14.920	4.093	1.185	133.400	36.595	10.595
2.00		14.790	4.057	1.175	132.400	36.321	10.516
2.60		14.590	4.002	1.159	130.800	35.882	10.388
3.30		14.370	3.942	1.141	129.000	35.388	10.246
4.20		14.100	3.868	1.120	126.800	34.784	10.071
5.40		13.730	3.766	1.090	123.900	33.989	9.840
7.00	0.00	13.270	3.640	1.054	120.100	32.946	9.539
9.00	2.00	12.710	3.487	1.009	115.600	31.712	9.181
10.00	3.00	12.440	3.413	0.988	113.400	31.108	9.007
13.00	6.00	11.670	3.201	0.927	107.100	29.380	8.506
15.00	8.00	11.190	3.070	0.889	103.100	28.283	8.188

Table B.2 Continued

		Continued DWPF Batch 2-3C			Continued DWPF Batch 4-10		
Time	Time After Emplaced	ORIGEN	DOE Canister	Hoag Canister	ORIGEN	DOE Canister	Hoag Canister
(yrs after 2004)	(yrs after 2011)	(W/m³)	(W/m)	(W/m)	(W/m³)	(W/m)	(W/m)
18.00	11.00	10.510	2.883	0.835	97.430	26.727	7.738
20.00	13.00	10.080	2.765	0.801	93.870	25.751	7.455
25.00	18.00	9.094	2.495	0.722	85.620	23.488	6.800
30.00	23.00	8.219	2.255	0.653	78.220	21.458	6.212
40.00	33.00	6.754	1.853	0.536	65.610	17.998	5.211
50.00	43.00	5.598	1.536	0.445	55.450	15.211	4.404
75.01	68.01	3.657	1.003	0.290	37.690	10.339	2.993
100.00	93.00	2.564	0.703	0.204	27.030	7.415	2.147
130.00	123.00	1.846	0.506	0.147	19.480	5.344	1.547
160.00	153.00	1.460	0.401	0.116	15.070	4.134	1.197
200.00	193.00	1.187	0.326	0.094	11.660	3.199	0.926
250.00	243.00	1.010	0.277	0.080	9.320	2.557	0.740
325.00	318.00	0.865	0.237	0.069	7.478	2.051	0.594
420.00	413.00	0.752	0.206	0.060	6.296	1.727	0.500
540.00	533.00	0.653	0.179	0.052	5.539	1.519	0.440
700.10	693.10	0.558	0.153	0.044	5.031	1.380	0.400
910.10	903.10	0.471	0.129	0.037	4.676	1.283	0.371
1180.0	1173.00	0.395	0.108	0.031	4.408	1.209	0.350
1530.0	1523.00	0.334	0.092	0.027	4.200	1.152	0.334
1980.0	1973.00	0.290	0.079	0.023	4.053	1.112	0.322
2570.0	2563.00	0.260	0.071	0.021	3.957	1.086	0.314
3340.0	3333.00	0.242	0.066	0.019	3.898	1.069	0.310
$R^2$for Eq.[3-2]			**0.99995**			**0.9934**	

Table B.3: Decay Heat for WTP Bounding and Average DNW for DOE and Hoag Canisters

		WTP Bounding			WTP Average		
Time	Time After Emplaced	ORIGEN	DOE Canister	Hoag Canister	ORIGEN	DOE Canister	Hoag Canister
(yrs after 2004)	(yrs after 2011)	(W/m³)	(W/m)	(W/m)	(W/m³)	(W/m)	(W/m)
0.30		980.700	269.030	77.890	67.060	18.396	5.326
0.39		978.600	268.454	77.723	66.920	18.358	5.315
0.50		975.900	267.713	77.509	66.740	18.308	5.301
0.65		972.300	266.726	77.223	66.500	18.243	5.282
0.80		968.800	265.766	76.945	66.270	18.179	5.263
1.00		964.000	264.449	76.563	65.950	18.092	5.238
1.30		957.000	262.529	76.007	65.480	17.963	5.201
1.60		950.000	260.608	75.451	65.010	17.834	5.163
2.00		940.800	258.085	74.721	64.390	17.664	5.114
2.60		927.300	254.381	73.649	63.480	17.414	5.042
3.30		911.800	250.129	72.418	62.430	17.126	4.958
4.20		892.300	244.780	70.869	61.100	16.761	4.853
5.40		867.000	237.839	68.859	59.390	16.292	4.717
7.00		834.600	228.951	66.286	57.170	15.683	4.541
9.00		795.900	218.335	63.212	54.520	14.956	4.330
10.00	0.00	777.300	213.233	61.735	53.250	14.608	4.229
13.00	3.00	724.100	198.638	57.510	49.600	13.607	3.939
15.00	5.00	690.800	189.503	54.865	47.310	12.978	3.757
18.00	8.00	643.700	176.583	51.124	44.080	12.092	3.501
20.00	10.00	614.200	168.490	48.781	42.050	11.535	3.340
25.00	15.00	546.300	149.864	43.389	37.390	10.257	2.970
30.00	20.00	486.100	133.349	38.607	33.250	9.121	2.641
40.00	30.00	385.400	105.725	30.609	26.340	7.226	2.092
50.00	40.00	306.100	83.971	24.311	20.900	5.733	1.660
75.01	65.01	173.900	47.705	13.812	11.850	3.251	0.941
100.00	90.00	101.000	27.707	8.022	6.877	1.887	0.546
130.00	120.00	55.160	15.132	4.381	3.757	1.031	0.298
160.00	150.00	32.470	8.907	2.579	2.223	0.610	0.177
200.00	190.00	18.770	5.149	1.491	1.307	0.359	0.104
250.00	240.00	12.300	3.374	0.977	0.885	0.243	0.070
325.00	315.00	9.177	2.517	0.729	0.697	0.191	0.055
420.00	410.00	7.654	2.100	0.608	0.618	0.170	0.049
540.00	530.00	6.399	1.755	0.508	0.560	0.154	0.044
700.10	690.10	5.108	1.401	0.406	0.501	0.137	0.040
910.10	900.10	3.850	1.056	0.306	0.443	0.122	0.035

Table B.3 Continued.

		WTP Bounding Continued			WTP Average Continued		
Time	Time After Emplaced	ORIGEN	DOE Canister	Hoag Canister	ORIGEN	DOE Canister	Hoag Canister
(yrs after 2004)	(yrs after 2011)	(W/m^3)	(W/m)	(W/m)	(W/m^3)	(W/m)	(W/m)
1180.00	1170.00	2.744	0.753	0.218	0.392	0.108	0.031
1530.00	1520.00	1.864	0.511	0.148	0.350	0.096	0.028
1980.00	1970.00	1.256	0.345	0.100	0.319	0.088	0.025
2570.00	2560.00	0.895	0.246	0.071	0.298	0.082	0.024
3340.00	3330.00	0.719	0.197	0.057	0.284	0.078	0.023

B.2 Temperature Difference in Granite Calculations

B.2.1 Model Overview

To solve for the temperature changes in granite a MATLAB code was written to solve equation [3-3] with the Riemann Sum method of integration. Various combinations of thermal diffusivity of host rock, dominant nuclear half life, and borehole radius were used as input to the code in Section B.2.2. When the borehole radius is changed, the initial decay power was changed as well. The initial decay power was calculated by multiplying the decay power from ORIGEN, in W/m^3, by the waste form diameter that corresponds to the changed borehole radius. Each trial produces a matrix with the time after emplacement in the first column and the temperature difference in the second. The maximum temperature change and the corresponding time were taken from each matrix and added to Table 3.1.

Section B.2.2 gives the MATLAB code to find the temperature difference in the granite for DNW. Section B.2.3 gives the MATLAB code to calculate the temperature difference in granite

for spent fuel. The combinations of variables in B.2.2 correspond to combination 3 in Table 3.1 and combination 22 in Table 3.2 for B.2.3.

B.2.2 MATLAB Code to Calculate Temperature Difference in Granite for Defense Waste

```
%%%%%%%%%%%%%%%%%%%%%%%%%%%%%%%%%%%%%%%%%%%%%%%%%%%%%%%%%%%%%%%%%%%%%%%
% Code to Calculate Temperature Difference in Granite for DNW
% Frances Dozier
% August 2011
%%%%%%%%%%%%%%%%%%%%%%%%%%%%%%%%%%%%%%%%%%%%%%%%%%%%%%%%%%%%%%%%%%%%%%%

%User Input
k=2.6; %W/m*deg C from Carslaw
p= 2600; %kg/m^3 from Carslaw, Jenson and Driscoll
Cp=790; %J/(kg*K) from Jenson and Driscoll, Hoag, Gibbs
a=k/(p*Cp)*3600*24*365; %m^2/yr
tc= 10; %years
r= 0.254; %m, Reference (Hoag) Canister
q0=61.73519; %W/m, see Section B.1 for Bounding DNW
halflife=29.63; %years, best fit dominant half life for Bounding DNW
lambda=log(2)/halflife; % 1/years

%Increments
time=.01; %Starts Time Counter
B=1; %counter

increments1=1000000; %Refer to chapter 3 for increment justification
increments2=10000;
matrix = zeros(1000,2); %preallocates matrix
dT = zeros(increments1,1);%preallocates matrix
dT2 = zeros (increments2,1); %preallocates matrix

%Equations
while(time<1000)
    t=[time/increments1:time/increments1:time-time/increments1];
    dT=1/(4*pi*k)*q0*exp(-lambda*t).*exp(-r^2./(4.*a.*(time-t))./...
        (time-t)*time/increments1;


    newt=[time-time/increments1:time/increments1/increments2:time-time/...
        increments1/increments2];
    dT2=1/(4*pi*k)*q0*exp(-lambda*newt).*exp(-r^2./(4.*a.*(time-newt)))...
        ./(time-newt)*time/increments1/increments2;

    matrix(B, 1)=time;
    matrix(B, 2)=sum(dT)+sum(dT2);
    time=time*1.01;
    B=B+1;
end
temps=matrix(1:B-1,2);
maxtemp=max(temps);
```

```
timeplace = find(temps==maxtemp);
timemax = matrix(timeplace,1);
maxtemp %Returns the maximum temperature
timemax %Returns time at max temperature
```

B.2.3 MATLAB Code to Calculate Temperature Difference in Granite for Spent Fuel

```
%%%%%%%%%%%%%%%%%%%%%%%%%%%%%%%%%%%%%%%%%%%%%%%%%%%%%%%%%%%%%%%%%%%%%%%%%%%%
% Code to Calculate Temperature Difference in Granite for Spent Fuel
% Frances Dozier
% August 2011
%%%%%%%%%%%%%%%%%%%%%%%%%%%%%%%%%%%%%%%%%%%%%%%%%%%%%%%%%%%%%%%%%%%%%%%%%%%%

%User Input
k=2.6; %W/m*deg C from Carslaw
p= 2600; %kg/m^3 from Carslaw, Jenson and Driscoll
Cp=790; %J/(kg*K) from Jenson and Driscoll, Hoag, Gibbs
a=k/(p*Cp)*3600*24*365; %m^2/yr
tc= 40; %years
r= 0.254; %m, Reference (Hoag) Canister
%q'=(2200/(tc+time)^(3/4)) from Sapiie and Driscoll

%Increments
time=.01; %Starts Time Counter
B=1; %counter

increments1=1000000;%Refer to chapter 3 for increment justification
increments2=10000;
matrix = zeros(1000,2); %preallocates matrix
dT = zeros(increments1,1);%preallocates matrix
dT2 = zeros(increments2,1); %preallocates matrix

%Equations
while(time<1000)
    t=[time/increments1:time/increments1:time-time/increments1];
    dT=1/(4*pi*k).*(2200./(tc+t).^(3/4)).*exp(-r^2./(4.*a.*(time-t))./...
        (time-t)*time/increments1;
       %Bounding Scenerio, tc=10

    newt=[time-time/increments1:time/increments1/increments2:time-time...
        /increments1/increments2];
    dT2=1/(4*pi*k).*(2200./(tc+newt).^(3/4)).*exp(-r^2./(4.*a.*...
        (time-newt))./(time-newt)*time/increments1/increments2;
       %Bounding Scenerio, tc=10

    matrix(B, 1)=time;
    matrix(B, 2)=sum(dT)+sum(dT2);
    time=time*1.01;
    B=B+1;
end
```

```
%Pull out max temp and time at max temp
temps=matrix(1:B-1,2);
maxtemp=max(temps);
timeplace = find(temps==maxtemp);
timemax = matrix(timeplace,1);
maxtemp %Returns the maximum temperature
timemax %Returns time at max temperature
```

B.3 Temperature Difference in Waste Form, Canister, Liner, and Gaps

To calculate the temperature differences in the radial repository elements (waste form, canister, liner, and gaps), equation [3-12] was used with the dimensions listed in Table 3.6. The temperature differences for each feature for each time step are listed in Table B.4 and B.5 for the reference and DOE canisters, respectively. Note that the maximum temperature difference in each feature occurs immediately at the time of emplacement.

Table B.4: Temperature Differences in Features for Bounding DNW in the Reference Canister

Time	Time after emplaced (yrs)	ORIGEN Decay Heat (W/m^3)	Linear Decay Heat (W/m)	Temperature Gradient in Feature (°C)				
				Cement	Steel	Graphite Sand	Canister	Waste Form Centerline
10.000	0.000	777.30	61.74	136.90	136.91	140.35	140.35	144.82
13.000	3.000	724.10	57.51	136.78	136.78	139.99	139.99	144.15
15.000	5.000	690.80	54.87	136.70	136.71	139.76	139.76	143.73
18.000	8.000	643.70	51.12	136.59	136.59	139.44	139.44	143.14
20.000	10.000	614.20	48.78	136.52	136.53	139.24	139.24	142.77
25.000	15.000	546.30	43.39	136.36	136.37	138.78	138.78	141.92
30.000	20.000	486.10	38.61	136.22	136.22	138.37	138.38	141.17
40.000	30.000	385.40	30.61	135.98	135.99	137.69	137.69	139.91
50.000	40.000	306.10	24.31	135.80	135.80	137.15	137.16	138.91
75.010	65.010	173.90	13.81	135.49	135.49	136.26	136.26	137.26
100.000	90.000	101.00	8.02	135.32	135.32	135.76	135.76	136.35
130.000	120.000	55.16	4.38	135.21	135.21	135.45	135.45	135.77
160.000	150.000	32.47	2.58	135.16	135.16	135.30	135.30	135.49
200.000	190.000	18.77	1.49	135.12	135.12	135.21	135.21	135.32
250.000	240.000	12.30	0.98	135.11	135.11	135.16	135.16	135.23
325.000	315.000	9.18	0.73	135.10	135.10	135.14	135.14	135.19
420.000	410.000	7.65	0.61	135.10	135.10	135.13	135.13	135.18
540.000	530.000	6.40	0.51	135.09	135.10	135.12	135.12	135.16
700.100	690.100	5.11	0.41	135.09	135.09	135.11	135.11	135.14
910.100	900.100	3.85	0.31	135.09	135.09	135.11	135.11	135.13
1180.00	1170.00	2.74	0.22	135.09	135.09	135.10	135.10	135.11
1530.00	1520.00	1.86	0.15	135.08	135.08	135.09	135.09	135.10
1980.00	1970.00	1.26	0.10	135.08	135.08	135.09	135.09	135.10
2570.00	2560.00	0.90	0.07	135.08	135.08	135.09	135.09	135.09
R^2 Value with Decay Heat Model				0.99996	0.99996	0.99996	0.99996	0.99996

Table B.5: Temperature Differences in Features for Bounding DNW in the DOE Canister

Time	Time after emplaced (yrs)	ORIGEN Decay Heat (W/m^3)	Linear Decay Heat (W/m)	Temperature Gradient in Feature (°C)				
				Cement	Steel	Graphite Sand	Canister	Waste Form Centerline
10.00	0.000	777.30	206.79	169.51	169.53	176.67	176.67	191.63
13.00	3.000	724.10	192.63	169.25	169.27	175.92	175.92	189.86
15.00	5.000	690.80	183.78	169.09	169.10	175.45	175.45	188.75
18.00	8.000	643.70	171.25	168.86	168.87	174.79	174.79	187.18
20.00	10.000	614.20	163.40	168.71	168.73	174.37	174.37	186.19
25.00	15.000	546.30	145.33	168.38	168.39	173.41	173.42	183.93
30.00	20.000	486.10	129.32	168.09	168.10	172.57	172.57	181.92
40.00	30.000	385.40	102.53	167.59	167.60	171.15	171.15	178.56
50.00	40.000	306.10	81.43	167.21	167.21	170.03	170.03	175.92
75.01	65.010	173.90	46.26	166.56	166.56	168.16	168.16	171.51
100.0	90.000	101.00	26.87	166.20	166.21	167.13	167.13	169.08
130.0	120.000	55.16	14.67	165.98	165.98	166.49	166.49	167.55
160.0	150.000	32.47	8.64	165.87	165.87	166.17	166.17	166.79
200.0	190.000	18.77	4.99	165.80	165.80	165.97	165.97	166.34
250.0	240.000	12.30	3.27	165.77	165.77	165.88	165.88	166.12
325.0	315.000	9.18	2.44	165.75	165.76	165.84	165.84	166.02
420.0	410.000	7.65	2.04	165.75	165.75	165.82	165.82	165.97
540.0	530.000	6.40	1.70	165.74	165.74	165.80	165.80	165.92
700.1	690.100	5.11	1.36	165.73	165.74	165.78	165.78	165.88
910.1	900.100	3.85	1.02	165.73	165.73	165.76	165.76	165.84
1180	1170.00	2.74	0.73	165.72	165.72	165.75	165.75	165.80
1530	1520.00	1.86	0.50	165.72	165.72	165.74	165.74	165.77
1980	1970.00	1.26	0.33	165.72	165.72	165.73	165.73	165.75
2570	2560.00	0.90	0.24	165.71	165.71	165.72	165.72	165.74
R^2Value with Decay Heat Model				.99996	.99996	.99996	.99996	.99996

Appendix C: Nuclide Dissolution Pourbaix Diagrams and Calculations

This appendix gives the calculations and figures created as a part of the Waste Form Dissolution Analysis in Chapter 5. The stable form of each nuclide in the borehole environment described in Table 4.1 was found using Pourbaix diagrams. These diagrams are shown below for 10 nuclides with the largest contribution to the initial radioactivity of the defense waste. Iodine was also included in this analysis even though it is not one of the largest contributors to radioactivity because it is the only nuclide not already included in the analysis that, historically, has been found in groundwater associated with non-vitrified defense waste storage locations[248].

For Americium, Antimony, Cesium, Nickel, Plutonium, and Technetium the maximum nuclide concentrations of a soluble species was calculated. Americium, Cesium, and Plutonium maximum soluble species concentrations were calculated using the procedure outlined in Section 5.3. To summarize, the reaction for each stable form was found and the temperature adjusted solubility product for each reaction was found using linear interpolation from the known solubility products at standard temperatures. Then the solubility product was used to find the concentration of the soluble species associated with the stable form of the nuclide.

The stable forms of Antimony, Nickel, and Technetium found in using the Pourbaix diagrams for each element below were not included in the Common Thermodynamic Database.[249] Therefore, a predicted balanced reaction was created using general knowledge of each species. The temperature adjusted Gibbs free energy values (found in HSC 6.0 Software) for each species in the predicted reaction were then used to find the solubility products.

The maximum nuclide concentrations for Cadmium, Europium, Iodine, Strontium, and Yttrium were not found because there were too many soluble ions in the predicted reaction for the

standard form. However, the Pourbaix diagrams and predicted reactions for these nuclides were included to show the stable forms.

Additional research is necessary to validate these calculations with experimental data. Also, only 11 of the over 40 nuclides in defense waste were included in this analysis due to time constraints; therefore, a similar analysis should be performed for each of the nuclides listed in Appendix A. This is because the nuclides analyzed were chosen because of their contribution to radioactivity. This does not correlate with solubility and was merely used as a quantitative method of selecting nuclides to analyze. Finally, The Pourbaix diagrams and predicted reactions should also be verified before using them in design applications.

C.1 Americium

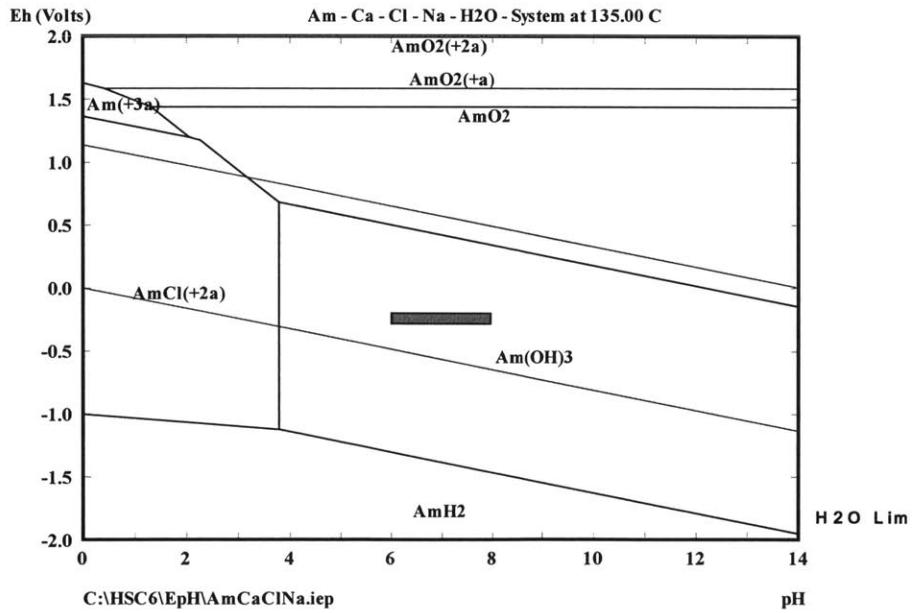

Figure C.1:Pourbaix Diagram for Americium in Borehole Environment (shaded area bounds the expected borehole conditions outlined in table 4.1)

Predicted Reaction from Common Thermodynamic Database:

$$\boldsymbol{Am^{3+}(aq) + 3H_2O(aq) \leftrightarrow Am(OH)_3(s) + 3H^+(g)}$$

Solubility Products from Common Thermodynamic Database:

$$logK(75^0C) = -12.5563$$

$$logK(100^0C) = -11.34015$$

Linear Interpolation to Find Solubility Product at 135□C:

$$\frac{-12.5563 - logK(135^0C)}{75^0C - 135^0C} = \frac{-11.34015 - logK(135^0C)}{100^0C - 135^0C}$$

$$logK(135^0C) = -9.6375$$

Calculation of Maximum Soluble Concentration from Solubility Product:

$$K = \frac{[Am(OH)_3][H^+]^3}{[Am^{3+}][H_2O]^3} = \frac{1 * [10^{-pH}]^3}{[Am^{3+}] * 1} = \frac{1 * [10^{-7}]^3}{[Am^{3+}] * 1} = 10^{-9.6375}$$

$$[Am^{3+}] = 10^{-11.363} = \mathbf{4.340 * 10^{-12} M}$$

$$\text{M} = \frac{\text{moles}}{\text{L of water in borehole}}$$

Figure C.2: Maximum Concentration of Soluble Species of Americium Calculation

C.2 Antimony

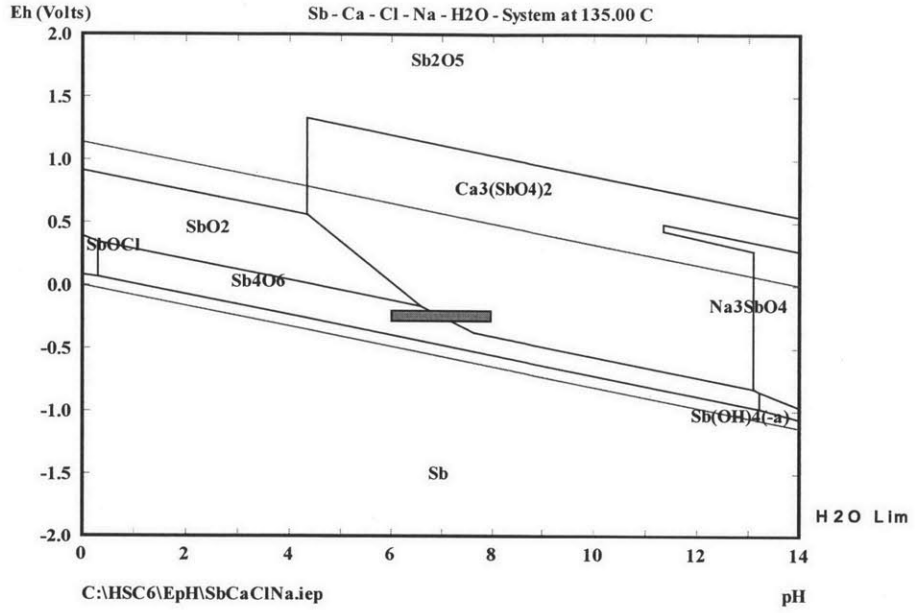

Figure C.3:Pourbaix Diagram for Antimony in Borehole Environment

(shaded area bounds the expected borehole conditions outlined in table 4.1)

There are 2 possible stable species in the predicted borehole environment. Therefore, there are two predicted reactions and corresponding maximum soluble species concentration calculations.

First Predicted Reaction (not given in Common Thermodynamic Database):

$$\mathbf{Ca_3(SbO_4)_2(aq) + 4H^+(aq) \leftrightarrow Ca(SbO_3)_2(s) + 2Ca^{2+}(aq) + 2H_2O(aq)}$$

This reaction is not given in CTDP; therefore, the temperature-specific Gibbs free energy values were used (from HSC 6.0 Software and CTPD).

$$\Delta G^0\left(Ca_3(SbO_4)_2(aq)\right) = -2893.23\frac{kJ}{mol}, \qquad \Delta G^0\left(H_2O(aq)\right) = -315.286\frac{kJ}{mol},$$

$$\Delta G^0\left(Ca(SbO_3)_2(s)\right) = -1471.98\frac{kJ}{mol}, \Delta G^0\left(Ca^{2+}(aq)\right) = -556.198\frac{kJ}{mol}, \ \Delta G^0\left(H^+(aq)\right) = 0\frac{kJ}{mol},$$

$$\Delta G^0{}_{reaction} = \Delta G^0(Ca(SbO_3)_2) + 2\,\Delta G^0(Ca^{2+}) + 2\Delta G^0(H_2O) - \Delta G^0(Ca_3(SbO_4)_2) - 2\Delta G^0(H^+)$$

$$\Delta G^0{}_{reaction} = -1471.98 + 2 * -556.198 + 2 * -315.286 - -2893.23 - 4 * 0$$

$$\Delta G^0{}_{reaction} = -321.718\frac{kJ}{mol}$$

Calculate Solubility Product from Gibbs Free Energy:

$$K(135^0C) = e^{-\frac{\Delta G^0(reaction)}{RT}} = e^{\frac{--321.718\frac{kJ}{mol}*1000\frac{J}{kJ}}{8.3145\frac{J}{mol*K}*(135°C+273.15)K}} = e^{94.802} = 10^{41.1722}$$

Calculation of Maximum Soluble Concentration from Solubility Product:

$$K = \frac{[Ca(SbO_3)_2][H_2O]^2[Ca^{+2}]^2}{[\,Ca_3(SbO_4)_2][H^+]^4} = \frac{1 * 1 * [60\ M]^2}{[\,Ca_3(SbO_4)_2][10^{-7}]^4} = 10^{41.1722}$$

$$[\,Ca_3(SbO_4)_2] = 10^{-9.6159} = \mathbf{2.422 * 10^{-10}M}$$

Second Predicted Reaction (not given in Common Thermodynamic Database):

$$\mathbf{Sb_4O_6(s) + 2H_2O(aq) \leftrightarrow 4SbO_2{}^-(aq) + 4H^+(aq)}$$

This reaction is not given in CTDP; therefore, the temperature-specific Gibbs free energy values were used (from HSC 6.0 Software and CTPD).

$\Delta G^0(Sb_4O_6(s)) = -1213.29\frac{kJ}{mol}$, $\Delta G^0(H_2O(aq)) = -315.286\frac{kJ}{mol}$, $\Delta G^0(SbO_2^-(aq)) = -298.187\frac{kJ}{mol}$,

$\Delta G^0(H^+(aq)) = 0\frac{kJ}{mol}$,

$\Delta G^0{}_{reaction} = 4 * \Delta G^0(SbO_2^-) + 4 * \Delta G^0(H^+) - \Delta G^0(Sb_4O_6) - 2 * \Delta G^0(H_2O)$

$\Delta G^0{}_{reaction} = 4 * -298.187 + 2 * 0 - -1213.29 - 2 * -315.286$

$\Delta G^0{}_{reaction} = 651.114\frac{kJ}{mol}$

Calculate Solubility Product from Gibbs Free Energy:

$$K(135^0C) = e^{-\frac{\Delta G^0(reaction)}{RT}} = e^{\frac{-651.114\frac{kJ}{mol}*1000\frac{J}{kJ}}{8.3145\frac{J}{mol*K}*(135°C+273.15)K}} = e^{-191.867} = 10^{-83.327}$$

Calculation of Maximum Soluble Concentration from Solubility Product:

$$K = \frac{[SbO_2^-]^4[H^+]^4}{[Sb_4O_6][H_2O]^2} = \frac{[SbO_2^-]^4[10^{-7}]^4}{1 * 1} = 10^{-83.327}$$

$[SbO_2^-] = 10^{-13.832} = 1.473 * 10^{-14}M$

Because this concentration value is so small, for simplicity it will be recorded at $<10^{-12}$M.

$[SbO_2^-] = 1.473 * 10^{-14}M \rightarrow \ < 10^{-12}\mathbf{M}$

Figure C.4: Maximum Concentration of Soluble Species of Antimony Calculation

C.3 Cadmium

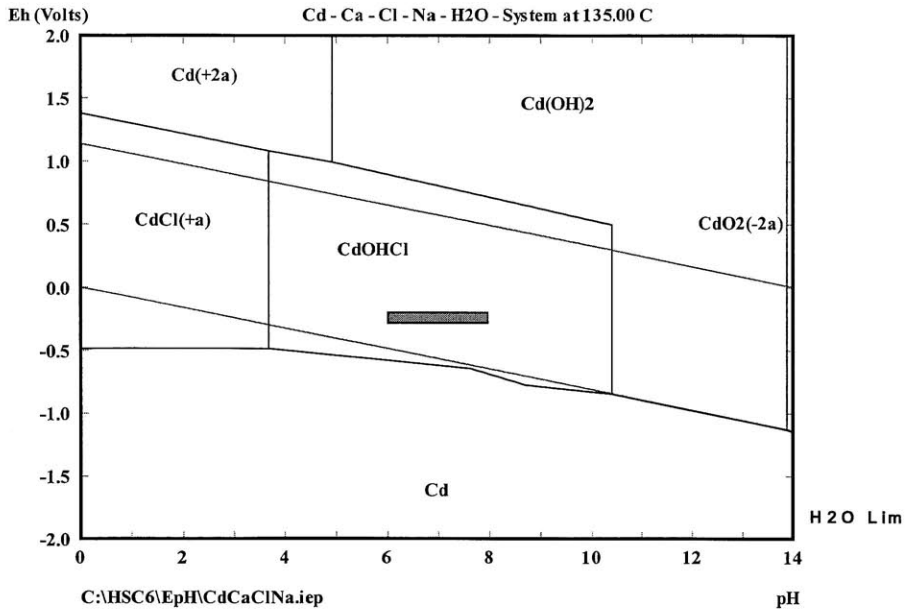

Figure C.5:Pourbaix Diagram for Cadmium in Borehole Environment

(shaded area bounds the expected borehole conditions outlined in table 4.1)

Predicted Reaction from Common Thermodynamic Database:

$$\boldsymbol{Cd^{2+}(aq) + Cl^{-}(aq) + H_2O(aq) \leftrightarrow CdOHCl(aq) + 3H^{+}(g)}$$

Calculation not possible because there are too many unknown variables; both Cd^{2+} and CdOHCl are aqueous species.

Figure C.6:Maximum Concentration of Soluble Species of Cadmium Calculation

C.4 Cesium

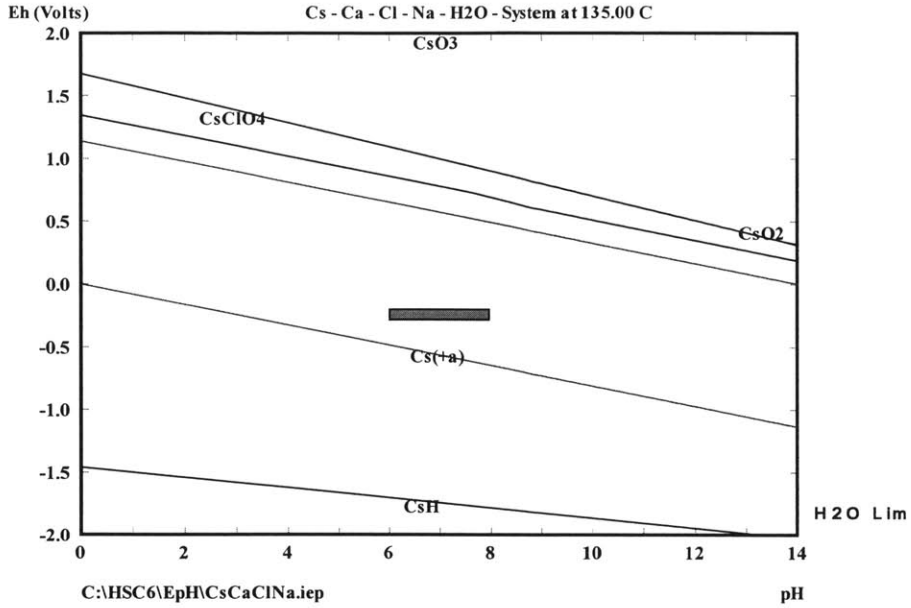

Figure C.7:Pourbaix Diagram for Cesium in Borehole Environment

(shaded area bounds the expected borehole conditions outlined in table 4.1)

Predicted Reaction from Common Thermodynamic Database:

$$\boldsymbol{Cs^{+}(aq) + Cl^{-}(aq) \leftrightarrow CsCl(s)}$$

Solubility Products from Common Thermodynamic Database:

$$logK(75^{0}C) = -1.98676$$

$$logK(100^{0}C) = -2.15995$$

Linear Interpolation to Find Solubility Product at 135□C:

$$\frac{-1.98676 - logK(135^{0}C)}{75^{0}C - 135^{0}C} = \frac{-2.15995 - logK(135^{0}C)}{100^{0}C - 135^{0}C}$$

$$logK(135^{0}C) = -2.4024$$

Calculation of Maximum Soluble Concentration from Solubility Product:

$$K = \frac{[CsCl]}{[Cs^+][Cl^-]} = \frac{1}{[Cs^+][100\ \mathrm{M}]} = 10^{-2.4024}$$

$$[\mathrm{Cs}^+] = 10^{.4024} = \mathbf{2.5258\ M}$$

Figure C.8:Maximum Concentration of Soluble Species of Cesium Calculation

C.5 Europium

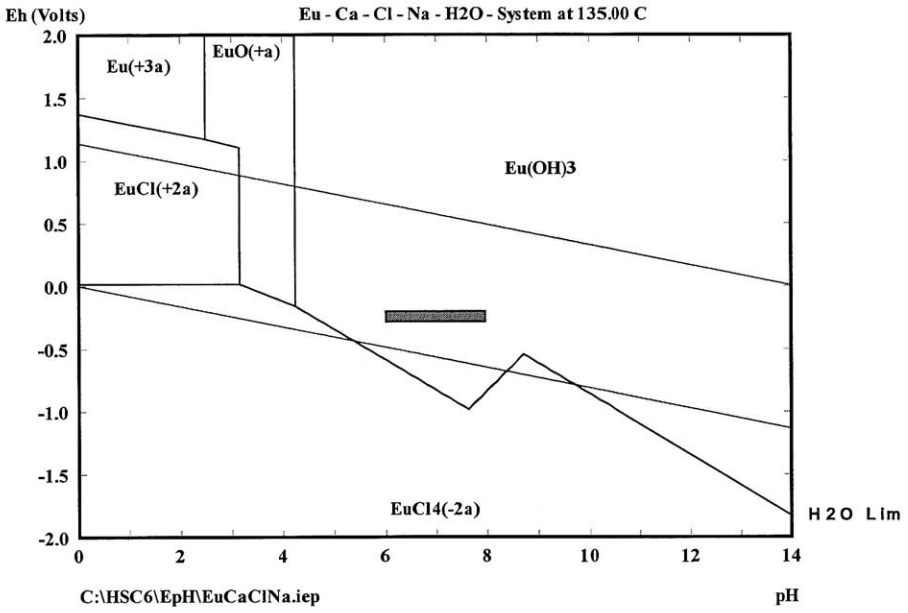

Figure C.9:Pourbaix Diagram for Europium in Borehole Environment

(shaded area bounds the expected borehole conditions outlined in table 4.1)

Predicted Reaction from Common Thermodynamic Database:

$$\boldsymbol{Eu^{3+}(aq) + 3H_2O(aq) \leftrightarrow Eu(OH)_3(aq) + 3H^+(aq)}$$

Calculation not possible because there are too many unknown variables; both Eu^{3+} and $\mathrm{Eu(OH)_3}$ are aqueous species.

Figure C.10:Maximum Concentration of Soluble Species of Europium Calculation

C.6 Iodine

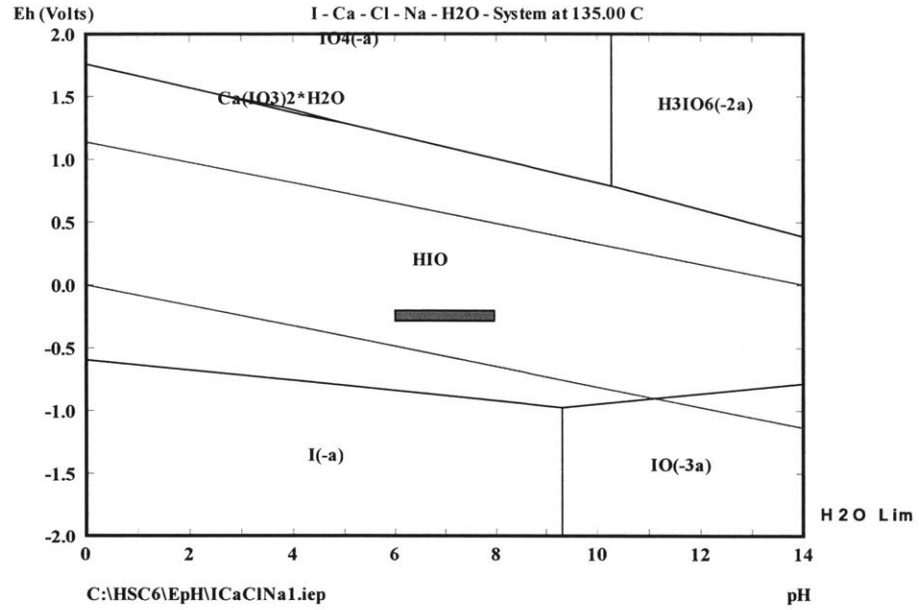

Figure C.11:Pourbaix Diagram for Iodine in Borehole Environment

(shaded area bounds the expected borehole conditions outlined in table 4.1)

Predicted Reaction from Common Thermodynamic Database:

$$\boldsymbol{IO^-(aq) + H^+(aq) \leftrightarrow HIO(aq)}$$

Calculation not possible because there are too many unknown variables; both IO^- and HIO are aqueous species with unknown concentrations.

Figure C.12:Maximum Concentration of Soluble Species of Iodine Calculation

C.7 Nickel

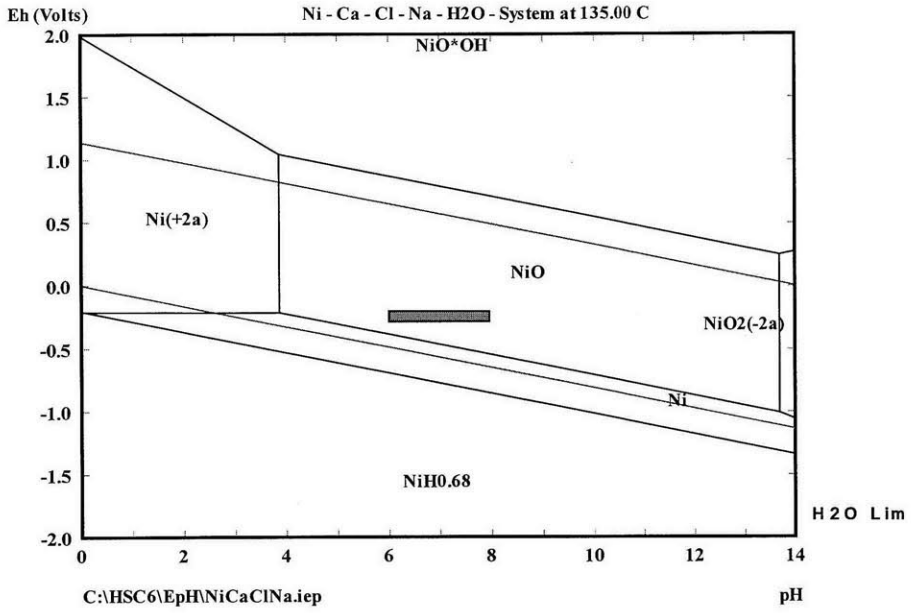

Figure C.13:Pourbaix Diagram for Nickel in Borehole Environment

(shaded area bounds the expected borehole conditions outlined in table 4.1)

Predicted Reaction (not given in Common Thermodynamic Database):

$$\mathbf{NiO(s) + H_2O(aq) \leftrightarrow NiO_2{}^{-2}(aq) + 2H^+(aq)}$$

This reaction is not given in CTDP; therefore, the temperature-specific Gibbs free energy values were used (from HSC 6.0 Software and CTPD).

$\Delta G^0(\mathrm{NiO(s)}) = -201.394\frac{kJ}{mol}$, $\Delta G^0(\mathrm{H_2O(aq)}) = -315.286\frac{kJ}{mol}$, $\Delta G^0\left(\mathrm{NiO_2{}^{-2}(aq)}\right) = -207.339\frac{\mathrm{kJ}}{\mathrm{mol}}$,

$\Delta G^0(\mathrm{H^+(aq)}) = 0\frac{kJ}{mol}$,

$$\Delta G^0{}_{reaction} = \Delta G^0(\mathrm{NiO_2{}^{-2}}) + 2 * \Delta G^0(\mathrm{H^+}) - \Delta G^0(\mathrm{NiO}) - \Delta G^0(\mathrm{H_2O})$$

$$\Delta G^0{}_{reaction} = -207.339 + 2 * 0 - -201.394 - -315.286$$

$$\Delta G^0{}_{reaction} = 309.341\frac{kJ}{mol}$$

Calculate Solubility Product from Gibbs Free Energy:

$$K(135^0C) = e^{-\frac{\Delta G^0(reaction)}{RT}} = e^{\frac{-309.341\frac{kJ}{mol}*1000\frac{J}{kJ}}{8.3145\frac{J}{mol*K}*(135°C+273.15)K}} = e^{-91.155} = 10^{-39.588}$$

Calculation of Maximum Soluble Concentration from Solubility Product:

$$K = \frac{[\mathrm{NiO_2{}^{-2}}][H^+]^2}{[\mathrm{NiO}][\mathrm{H_2O}]} = \frac{[\mathrm{TcO_4{}^-}][10^{-7}]^2}{1 * 1} = 10^{-39.588}$$

$$[\mathrm{NiO_2{}^{-2}}] = 10^{-25.588} = 2.581 * 10^{-26}M$$

Because this concentration value is so small, for simplicity it will be recorded at $<10^{-12}$M.

$$[\mathrm{NiO_2{}^{-2}}] = 2.581 * 10^{-26}M \rightarrow \ < 10^{-12}\mathbf{M}$$

Figure C.14: Maximum Concentration of Soluble Species of Nickel Calculation

C.8 Plutonium

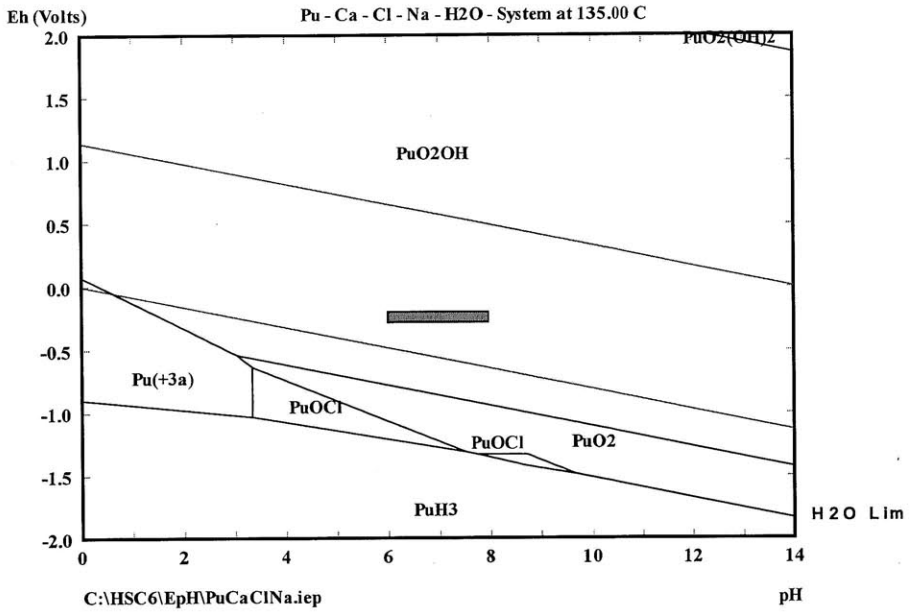

Figure C.15:Pourbaix Diagram for Plutonium in Borehole Environment

(shaded area bounds the expected borehole conditions outlined in table 4.1)

Predicted Reaction from Common Thermodynamic Database:

$$\boldsymbol{PuO_2{}^+(aq) + H_2O(aq) \leftrightarrow PuO_2OH(s) + H^+(g)}$$

Solubility Products from Common Thermodynamic Database:

$logK(75^0C) = -4.08929$

$logK(100^0C) = -3.72575$

Linear Interpolation to Find Solubility Product at 135□C:

$$\frac{-4.08929 - logK(135^0C)}{75^0C - 135^0C} = \frac{-3.72575 - logK(135^0C)}{100^0C - 135^0C}$$

$logK(135^0C) = -3.2168$

Calculation of Maximum Soluble Concentration from Solubility Product:

$$K = \frac{[PuO_2OH][H^+]}{[PuO_2^+][H_2O]} = \frac{1 * [10^{-pH}]}{[PuO_2^+] * 1} = \frac{1 * [10^{-7}]}{[PuO_2^+] * 1} = 10^{-3.2168}$$

$$[PuO_2^+] = 10^{-3.783} = \mathbf{1.647 * 10^{-4} M}$$

Figure C.16:Maximum Concentration of Soluble Species of Plutonium Calculation

C.9 Strontium

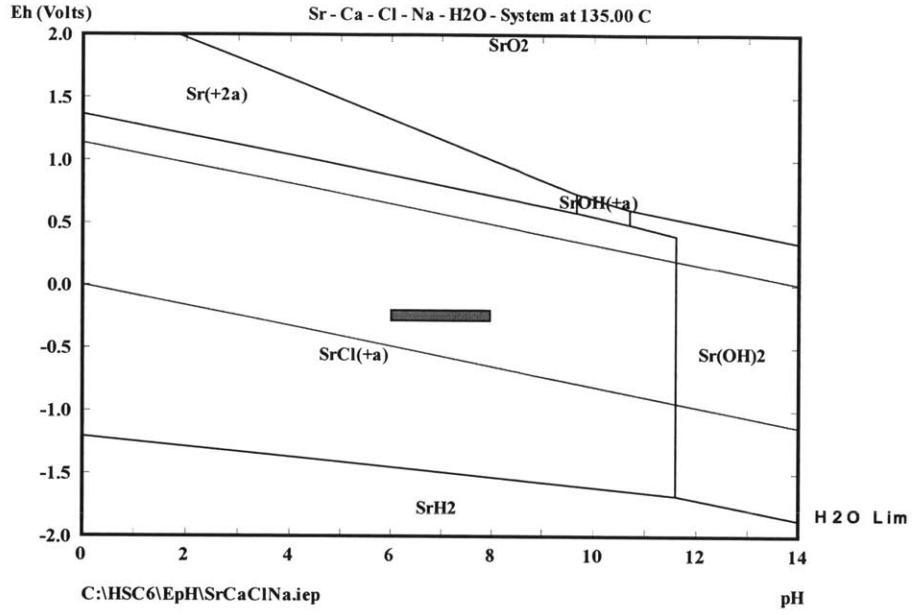

Figure C.17:Pourbaix Diagram for Strontium in Borehole Environment

(shaded area bounds the expected borehole conditions outlined in table 4.1)

Predicted Reaction from Common Thermodynamic Database:

$$\mathbf{Sr^{2+}(aq) + Cl^-(aq) \leftrightarrow SrCl^+(aq)}$$

Calculation not possible because there are too many unknown variables; both Sr^{2+} and $SrCl^+$ are aqueous species of unknown concentrations.

Figure C.18:Maximum Concentration of Soluble Species of Strontium Calculation

C.10 Technetium

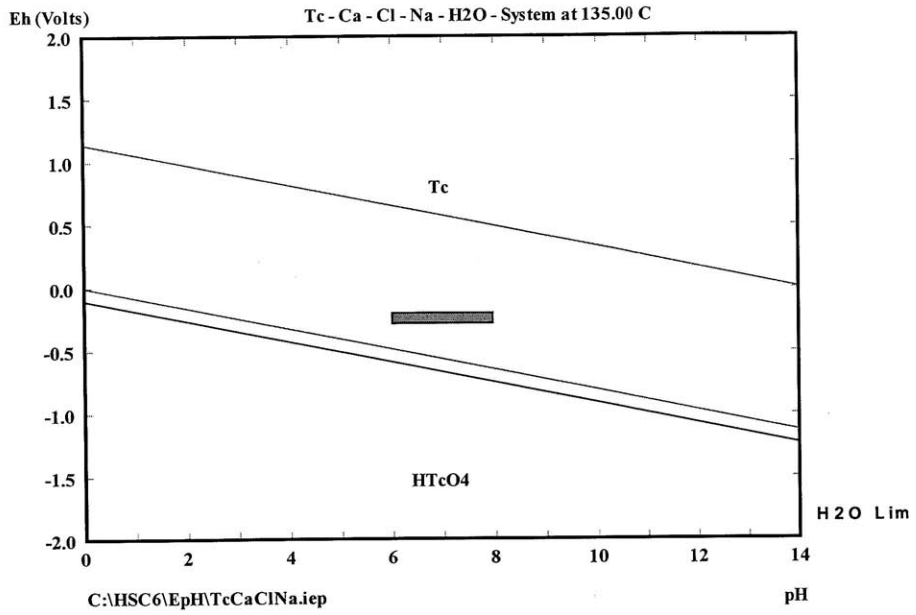

Figure C.19:Pourbaix Diagram for Technetium in Borehole Environment

(shaded area bounds the expected borehole conditions outlined in table 4.1)

Predicted Reaction from Common Thermodynamic Database:

$$\mathbf{Tc(s) + 4H_2O(aq) \leftrightarrow TcO_4^-(aq) + 8H^+(aq) + 7e^-}$$

Note: the reaction given in CTDP is a half reaction. Therefore, it is combined with the most probable half cell in a very low oxygen water system: $2H_2O + 2e^- \leftrightarrow H_2 + OH^-$, to form the full reaction:

$$\mathbf{Tc(s) + 7H_2O(aq) \leftrightarrow TcO_4^-(aq) + 8H^+(aq) + \frac{7}{2}H_2(g) + 7OH^-(aq)}$$

This reaction is not given in CTDP; therefore, the temperature-specific Gibbs free energy values were used (from HSC 6.0 Software and CTPD).

$\Delta G^0(\mathrm{Tc(s)}) = 0\frac{kJ}{mol}$, $\Delta G^0(\mathrm{H_2O(aq)}) = -315.286\frac{kJ}{mol}$, $\Delta G^0(\mathrm{TcO_4^-(aq)}) = -599.987\frac{\mathrm{kJ}}{\mathrm{mol}}$,

$\Delta G^0(\mathrm{H^+(aq)}) = 0\frac{kJ}{mol}$, $\Delta G^0(\mathrm{H_2}(g)) = -53.861\frac{kJ}{mol}$,

$\Delta G^0(OH^-(aq)) = -157.220\frac{kJ}{mol}$ *(temperature specific value not avialble)*

$$\Delta G^0{}_{reaction} = \Delta G^0(\mathrm{TcO_4^-}) + 8 * \Delta G^0(\mathrm{H^+}) + \frac{7}{2} * \Delta G^0(\mathrm{H_2}) + 7 * \Delta G^0(OH^-) - \Delta G^0(\mathrm{Tc}) - 8 * \Delta G^0(\mathrm{H_2O})$$

$$\Delta G^0{}_{reaction} = -599.987 + 8 * 0 + \frac{7}{2} * -53.861 + 7 * -157.220 - 0 - 8 * -315.286$$

$$\Delta G^0{}_{reaction} = 633.248 \frac{kJ}{mol}$$

Calculate Solubility Product from Gibbs Free Energy:

$$K(135^0C) = e^{-\frac{\Delta G^0(reaction)}{RT}} = e^{\frac{-633.248\frac{kJ}{mol}*1000\frac{J}{kJ}}{8.3145\frac{J}{mol*K}*(135℃+273.15)K}} = e^{-186.603} = 10^{-81.0405}$$

Note: Partial Pressure of Hydrogen[250] = 0.1

Calculation of Maximum Soluble Concentration from Solubility Product:

$$K = \frac{[\mathrm{TcO_4^-}][H^+]^8[OH^-]^7[H_2]^{7/2}}{[\mathrm{Tc}][\mathrm{H_2O}]^7} = \frac{[\mathrm{TcO_4^-}][10^{-7}]^8[10^{-7}]^7[.1]^{7/2}}{1 * 1} = 10^{-81.0405}$$

$$[\mathrm{TcO_4^-}] = 10^{-27.4595} = 3.474 * 10^{-28} M$$

Because this concentration value is so small, for simplicity it will be recorded at $<10^{-12}$M.

$$[\mathrm{TcO_4^-}] = 3.474 * 10^{-28} M \rightarrow \ < 10^{-12}\ \mathbf{M}$$

Note that because the initial reaction was given as a half cell reaction, the reaction used in this calculation may not be the only reaction occurring. However, this value for the soluble technetium ion makes sense because technetium is known to react with water at extremely low rates.[251] Therefore, the soluble ion concentration resulting from technetium metal in water should be very small.

Figure C.20:Maximum Concentration of Soluble Species of Technetium Calculation

C.11 Yttrium

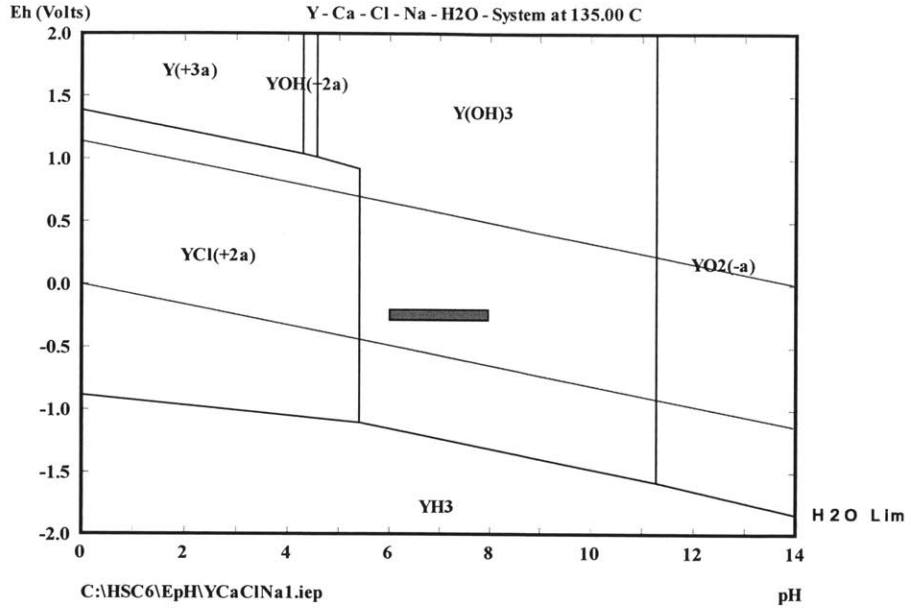

Figure C.21:Pourbaix Diagram for Yttrium in Borehole Environment

(shaded area bounds the expected borehole conditions outlined in table 4.1)

Predicted Reaction from Common Thermodynamic Database:

$$\boldsymbol{Y^{3+}(aq) + 3H_2O(aq) \leftrightarrow Y(OH)_3(aq) + 3H^+(aq)}$$

Calculation not possible because there are too many unknown variables; both Y^{3+} *and* $Y(OH)_3$ are aqueous species of unknown concentrations.

Figure C.22:Maximum Concentration of Soluble Species of Yttrium Calculation

Appendix D: Disposal Time and Cost Code and Calculations

D.1 Appendix Introduction

This appendix contains the calculations and MATLAB code that were used to calculate the drilling and emplacement cost data in Chapter 6. Section D.2 gives the specific data used to correlate borehole diameter size and the resulting drilling and emplacement costs. Sections D.3-D.5 give the input, functions, and command script that compose V-DeepBoRe-II. A code listing for V-DeepBoRe can be found in Jonathan Gibbs' MIT Master's thesis.[252] If the user is an MIT student, copies of V-DeepBoRe and V-DeepBoRe-II are on CD available through the MIT Department of Nuclear Science and Engineering administrative staff. Please note that external verification and validation is required on V-DeepBoRe and V-DeepBoRe-II before it can be used for professional purposes.

D.2 Diameter Dependent Cost Calculations

Section 6.4.2 explains the process by which the costs calculated in V-DeepBoRe are extended to larger diameter holes. Two methods were possible, depending on the assumptions on drill bit or pipe combinations.

Table D.1:Gibbs' Pipe Combinations Costs

Associated Liner Inner Diameter (m)	Pipe Combinations (correspond to ODs and IDs matrix values)			Cost from V-DeepBoRe-II ($/kg vitrified waste)
0.2027174	1	5	9	37.16
0.1783842	2	6	10	36.47
0.154051	3	7	11	35.68
0.1281938	4	8	12	34.95
0.1144524	5	9	13	34.45
0.1022604	6	10	14	33.9

Table D.2:Table D.2: Hoag Pipe Combinations Costs

Associated Liner Inner Diameter (m)	Pipe Combinations (correspond to ODs and IDs matrix values)			Cost from V-DeepBoRe-II ($/kg vitrified waste)
0.38735	1	2	3	41.1884
0.33655	2	3	4	39.7643
0.3048	3	4	5	38.8295
0.2794	4	5	6	38.1688
0.254508	5	6	7	37.5417
0.2271014	6	7	8	36.6221
0.2027174	7	8	9	35.8162
0.1783842	8	9	10	35.1598
0.154051	9	10	11	34.438
0.1281938	10	11	12	33.8753
0.1144524	11	12	13	33.4452
0.1022604	12	13	14	32.9929

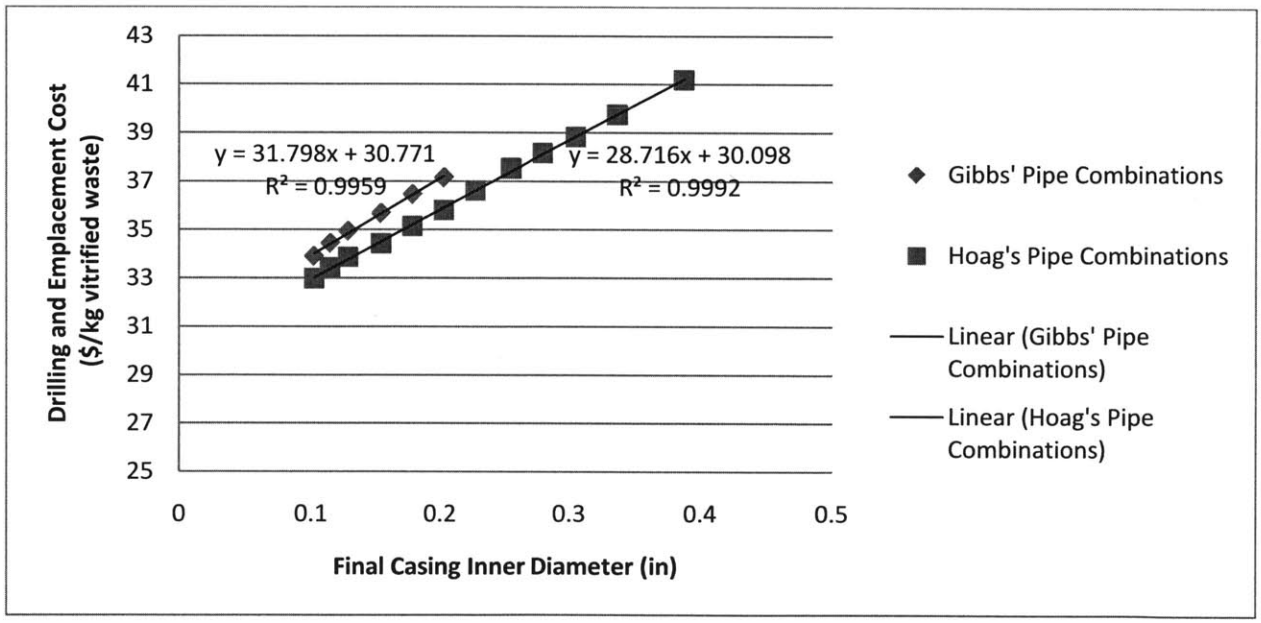

Figure D.1:Gibbs and Hoag Pipe Combinations Cost for Drilling and Emplacement

The Gibbs pipe combinations were used to produce equation 6.4, which is used for the expected cost for disposal of WTP and DWPF canisters. The Hoag pipe combinations were used to produce equation 6.5.

D.3 Drop-in Emplacement Velocity Calculations

This thesis was written concurrently with Ethan Bates' SM thesis.[253] Therefore, Bates was able to use his terminal velocity spreadsheet to calculate the terminal velocities for the Hoag and DOE canisters in borehole conditions (100°C, water density = 980.41 kg/m³, and viscosity of 2.955E-4 Pa-s). Tables D.3 and D.4 gives the values that he used as well as the dimensionless numbers he calculated to find the terminal velocities. The process by which he calculated these velocities is outlined in Chapter 4 of his thesis.

Table D.3: Values used by Bates to Calculate Canister Terminal Velocities:

Canister Design	Mass (kg)	Length (m)	Outer Diameter (m)	Lining Diameter (m)	Specific Gravity
Hoag Canister, vitrified	1128	5	0.34	0.387	2.487
DOE Canister, vitrified	4138	4.5	0.61	0.661	3.15

Table D.4: Dimensionless Numbers used by Bates to Calculate Terminal Velocity

Canister Design	Archimedes Number	Friction Factor	Reynolds Number	**Terminal Velocity (m/s)**
Hoag Canister, vitrified	1.70×10^{10}	1.14×10^{-2}	1.12×10^{6}	**1.63**
DOE Canister, vitrified	3.07×10^{10}	1.09×10^{-2}	1.46×10^{6}	**1.28**

D.3 Input Matrix

The following variables are necessary to use V-DeepBoRe-II. These variables should be input into the MATLAB command window and the work space should be saved in a matrix file and entitled in.mat. These variables could also be input manually into drilling_costs_II. Details on

the input matrices for V-DeepBoRe, including hexarray.mat, squarepacking.mat, pipes.mat, and radii.mat are included in Jonathan Gibbs' thesis.

Table D.5:Input Variables for V-DeepBoRe-II

Holes = [	IDs = [	ODs = [	bit_cost = ...	pipecombos = [
26.0000	19.2500	20.0000	1.0e+005 * [	1 4 8;
24.0000	17.2500	18.0000	0.7202	1 4 9;
20.0000	15.2500	16.0000	0.6477	1 5 9;
17.5000	13.2500	14.0000	0.5057	2 5 9;
17.0000	12.0000	12.7500	0.4189	1 4 10;
15.5000	11.0000	11.7500	0.4017	1 5 10;
14.5000	10.0200	10.7500	0.3506	2 5 10;
12.2500	8.9410	9.6250	0.3168	1 6 10;
11.6250	7.9810	8.6250	0.2417	2 6 10;
10.7500	7.0230	7.6250	0.2210	1 4 11;
9.0000	6.0650	6.6250	0.1923	1 5 11;
8.7500	5.0470	5.5630	0.1354	2 5 11;
7.8750	4.5060	5.0000	0.1273	1 6 11;
6.2500	4.0260	4.5000	0.0992	2 6 11;
48.0000	39.1250	40.0000	0.0475	1 7 11;
36.0000];	29.1250];	30.0000];	1.5830	2 7 11;
			1.0976];	3 7 11;
casing_mass = [	lam_sed = [	lam_gran = [	mu_sed = [	1 4 12;
116.9697	0.0100	0.0250	10	1 5 12;
105.0495	0.0100	0.0250	10	2 5 12;
92.9805	0.0100	0.0250	10	1 6 12;
81.2091	0.0100	0.0250	10	2 6 12;
73.7534	0.0100	0.0250	10	1 7 12;
67.8007	0.0100	0.0250	10	2 7 12;
60.2409	0.0100	0.0250	10	3 7 12;
50.4636	0.0100	0.0250	10	1 8 12;
42.4871	0.0100	0.0250	10	2 8 12;
35.0314	0.0100	0.0250	10	3 8 12;
28.2305	0.0100	0.0250	10	4 8 12;
21.7570	0.0100	0.0250	10	1 4 13;
18.6616	0.0100	0.0250	10	1 5 13;
16.0573	0.0100	0.0250	10	2 5 13;
275.1022	0.0100	0.0250	10	1 6 13;
205.5661];	0.0100];	0.0250];	10];	2 6 13;
mu_gran = [	radii = [	sd_gran = [	sd_sed = [	1 7 13;
3.9000	270.6875	0.3900	1	2 7 13;
3.9000	242.4084	0.3900	1	3 7 13;
3.9000	234.5111	0.3900	1	1 8 13;
3.9000	305.6486	0.3900	1	2 8 13;

3.9000	230.5941	0.3900	1	3 8 13;
3.9000	250.3056	0.3900	1	4 8 13;
3.9000	392.0508];	0.3900	1	1 9 13;
3.9000		0.3900	1	2 9 13;
3.9000		0.3900	1	3 9 13;
3.9000		0.3900	1	4 9 13;
3.9000		0.3900	1	5 9 13;
3.9000		0.3900	1	1 4 14;
3.9000		0.3900	1	1 5 14;
3.9000		0.3900	1	2 5 14;
3.9000		0.3900	1	1 6 14;
3.9000];		0.3900];	1];	2 6 14;
				1 7 14;
				2 7 14;
				3 7 14;
				1 8 14;
				2 8 14;
				3 8 14;
				4 8 14;
				1 9 14;
				2 9 14;
				3 9 14];
				4 9 14;
				5 9 14;
				1 10 14;
				2 10 14;
				3 10 14;
				4 10 14;
				5 10 14;
				6 10 14;

D.4 Functions

D.4.1 Function to Calculate Mass of Vitrified Waste

This function estimates the total mass of vitrified waste that can fit in the borehole and is called vit_waste.m.

```
function [vit_wasteparam]=vit_wastemass(emplacementlength,no_laterals,...
pipeschedule,IDs,PWR_frac,Vit_frac,vit_load)
%%%%%%%%%%%%%%%%%%%%%%%%%%%%%%%%%%%%%%%%%%%%%%%%%%%%%%%%%%%%%%%%%%%%%%%%%%%
% This function estimates the total mass of vitrified waste in the %
% repository once completely loaded %
%%%%%%%%%%%%%%%%%%%%%%%%%%%%%%%%%%%%%%%%%%%%%%%%%%%%%%%%%%%%%%%%%%%%%%%%%%%
% calculate the density of heavy metal in vitrified waste
```

```
rho_vit=2.81; % MT/m^3 from Hamel and Eschenberg
% Calculate the number of canisters in repository (5 m canister length)
no_canisters=(emplacementlength/5)*no_laterals;
% Calculate the interior diameter of the waste package
% (based on inner diameter of liner and Diam_frac above)
canID=0.318; %Figure 2.1
% Calculate the volume of the waste canister (L*pi*d^2/4)
V_can=4.46*(canID^2)/4*pi; % (in m^3)
% Divide up the total number of canisters by waste form
Vit_no=ceil(no_canisters*Vit_frac);
% Calculate mass of fuel in Vitrified waste canister
m_Vit=V_can*rho_vit;
% Calculate # of intact BWR assemblies per cannister
m_HM=Vit_no*m_Vit;
% Output key results back to the drilling script for 'scoring' repository
vit_wasteparam=[m_HM 0 0 0 0];
```

D.4.2 Function to Simulate Drilling and Emplacement

This function executes a Monte Carlo simulation of drilling a single vertical shaft of a borehole repository based on the inputs from the drilling_costs.m script described in Section D.3. This function outputs the simulated drilling progress in cost and time vs. depth as well as material (cement and casing) used, and how the waste is accommodated (canister packing, whether reconstitution is required, etc.). This function must be saved is drill_bit_life_II.m (note that the last two characters are roman numerals and therefore are letters, not numbers).

```
function [depthtimecosthistII,drillparamII,vit_wasteparam] = ...
    drill_bit_life_II(pluglength,emplacementlength,...
    declination,no_laterals,pipeschedule,ODs,Holes,IDs,mu_sed,...
    mu_gran,sd_gran,sd_sed,PWR_frac,Vit_frac,rho_vit,casing_mass,...
    bit_cost,radii)
%%%%%%%%%%%%%%%%%%%%%%%%%%%%%%%%%%%%%%%%%%%%%%%%%%%%%%%%%%%%%%%%%%%%%%%%%%%%
% This function executes a Monte Carlo simulation of drilling a single %
% vertical shaft of a borehole repository based on the inputs from the %
% drilling_costs.m script
%%%%%%%%%%%%%%%%%%%%%%%%%%%%%%%%%%%%%%%%%%%%%%%%%%%%%%%%%%%%%%%%%%%%%%%%%%%%
%% Drilling Parameters
backhaul=350; % backhaul speed (m/hr)
surfdepth=200; % depth of surface hole (m)
changeoutcost=[bit_cost(pipeschedule... % additional cost associated
(1)),bit_cost(pipeschedule(2)),... % with repair/replacement
bit_cost(pipeschedule(3))]; % of damaged drill bit ($)
cementcost=(80*.75*1.506); % cost for concrete poured
```

```
% ($/m^3), [25% by weight H2O, 1.506 kg/m^3 wet]
billingrate=4852; % cost factor of time($/hr), From Bates thesis
casingspeed=350; % speed of lowering casing (m/hr)
casingcost=6; % steel casing material cost ($/kg)
lowerspeed=350; % speed of lowering bits (m/hr)
cementspeed=10; % cement speed (m^3/hr)
cementcure=84; % curetime needed for cement (hr)
overburden=1000; % depth to granite formation (m)
lateraloffset=0; % required vertical spacing between lateral kickoffs (m)
kickoffdepth=(no_laterals-1)*... % calculate the depth of deepest
lateraloffset+overburden+... % lateral start (m)
pluglength+100;
kickcement=48; % time to cement for kickoff
latplug=72; % time to plug the lateral (hr)
boreholeplug=240; % time to plug the borehole (hr)
plugcost=1000000; % Additional plug cost
phasedelay=192; % Additional completion time at end of each phase
closeoutcosts=2000000; % Final cleanup/closure costs ($)
wastespeed2=casingspeed*.5; % Handling speed of waste once 100m
% into hole (no remote handling)
%% Determine the turn radius to permit 10 meter lateral liner to make bend
% minimum radius of curvature for lateral to allow casing placement (m)
turnradius=0; %radii(pipeschedule(3)-7);
% calculate distance drilled during transition to lateral
kickoffarc=turnradius*(90-declination)*pi/180;
%% Initialize Parameters
cementtally=0; % Total volume of cement (m^3)
casingtally=0; % Total mass of casing steel (kg)
depthtimecosthistII=zeros(20,3); % Time and cost history matrix
% (depth, time, cost)
depthtimecosthistII(1,3)=changeoutcost(1);
index=2; % for indexing the hist matrix
%% Drill surface shaft
disttogo=surfdepth;
% Determine the time to drill the surface shaft
while 1==1
surfspeed=normrnd(mu_sed(pipeschedule(1)),sd_sed(pipeschedule(1)));
if surfspeed >= 0
break
end
end
while 1==1
% Determine if failure occurs during the drilling of the surface shaft
ttf=200-lognrnd(log(100),.15);
if ttf>(disttogo/surfspeed)
depthtimecosthistII(index,:)=[surfdepth,depthtimecosthistII(index-1,...
2)+disttogo/surfspeed,depthtimecosthistII(index-1,3)+disttogo/...
surfspeed*billingrate];
index=index+1;
break
else
disttogo=disttogo-ttf*surfspeed;
depthtimecosthistII(index,:)=[depthtimecosthistII(index-1,1)+ttf*...
surfspeed,depthtimecosthistII(index-1,2)+ttf,...
depthtimecosthistII(index-1,3)+ttf*billingrate];
index=index+1;
depthtimecosthistII(index,:)=[depthtimecosthistII(index-1,1),...
```

```
depthtimecosthistII(index-1,2)+depthtimecosthistII(index-1,1)...
/backhaul+depthtimecosthistII(index-1,1)/lowerspeed,...
depthtimecosthistII(index-1,3)+(depthtimecosthistII(index-1,1)...
/backhaul+depthtimecosthistII(index-1,1)/lowerspeed)*...
billingrate+changeoutcost(1)];
index=index+1;
end
end
%% Back out surface drill string
depthtimecosthistII(index,:)=depthtimecosthistII(index-1,:)+[0,...
    (surfdepth/backhaul),(surfdepth/backhaul*billingrate)];
index=index+1;
%% Emplace surf casing
casingmass=surfdepth*casing_mass(pipeschedule(1));
depthtimecosthistII(index,:)=depthtimecosthistII(index-1,:)+[0,...
    (surfdepth/casingspeed),(surfdepth/casingspeed)*billingrate+...
    casingmass*casingcost];
casingtally=casingtally+casingmass;
index=index+1;
%% Cement surf casing
% Calculate cement volume (annulus)
Vsurfcement=(Holes(pipeschedule(1))^2 - ODs(pipeschedule(1))^2)*...
surfdepth*0.00064516/4*pi;
depthtimecosthistII(index,:)=depthtimecosthistII(index-1,:)+[0,...
    (cementcure+Vsurfcement/cementspeed),(cementcure+...
    Vsurfcement/cementspeed)*billingrate+cementcost*Vsurfcement];
cementtally=cementtally+Vsurfcement;
index=index+1;
%% Lower vertical drill string
depthtimecosthistII(index,:)=depthtimecosthistII(index-1,:)+[0,...
    (surfdepth/lowerspeed),(surfdepth/lowerspeed*billingrate)+...
    changeoutcost(2)];
index=index+1;
%% Drill main vertical shaft
% Determine the time to drill the main shaft
% Sedimentary Overburden portion
while 1==1
mainspeedsed=normrnd(mu_sed(pipeschedule(2)),sd_sed(pipeschedule(2)));
if mainspeedsed >= 0
break
end
end
disttogo=overburden-surfdepth;
while 1==1
% Determine if failure occurs during the drilling of the main shaft
ttf=200-lognrnd(log(100),.15);
if ttf>(disttogo/mainspeedsed)
depthtimecosthistII(index,:)=[overburden,...
depthtimecosthistII(index-1,2)+disttogo/mainspeedsed,...
depthtimecosthistII(index-1,3)+disttogo/mainspeedsed*...
billingrate];
index=index+1;
break
else
disttogo=disttogo-ttf*mainspeedsed;
depthtimecosthistII(index,:)=[depthtimecosthistII(index-1,1)+ttf*...
mainspeedsed,depthtimecosthistII(index-1,2)+ttf,...
```

```
depthtimecosthistII(index-1,3)+ttf*billingrate];
index=index+1;
depthtimecosthistII(index,:)=[depthtimecosthistII(index-1,1),...
depthtimecosthistII(index-1,2)+depthtimecosthistII(index-1,1)/...
backhaul+depthtimecosthistII(index-1,1)/lowerspeed,...
depthtimecosthistII(index-1,3)+(depthtimecosthistII(index-1,1)/...
backhaul+depthtimecosthistII(index-1,1)/lowerspeed)*...
billingrate+changeoutcost(2)];
index=index+1;
end
end
% Granite portion
while 1==1
mainspeedgran=normrnd(mu_gran(pipeschedule(2)),...
sd_gran(pipeschedule(2)));
if mainspeedgran >= 0
break
end
end
disttogo=kickoffdepth-overburden;
while 1==1
% Determine if a failure occurs during the drilling of the main shaft
ttf=76-lognrnd(log(38),.1);
if ttf>(disttogo/mainspeedgran)
depthtimecosthistII(index,:)=[kickoffdepth,...
depthtimecosthistII(index-1,2)+disttogo/mainspeedgran,...
depthtimecosthistII(index-1,3)+disttogo/mainspeedgran*...
billingrate];
index=index+1;
break
else
disttogo=disttogo-ttf*mainspeedgran;
depthtimecosthistII(index,:)=[depthtimecosthistII(index-1,1)+ttf*...
mainspeedgran,depthtimecosthistII(index-1,2)+ttf,...
depthtimecosthistII(index-1,3)+ttf*billingrate];
index=index+1;
depthtimecosthistII(index,:)=[depthtimecosthistII(index-1,1),...
depthtimecosthistII(index-1,2)+depthtimecosthistII(index-1,1)/...
backhaul+depthtimecosthistII(index-1,1)/lowerspeed,...
depthtimecosthistII(index-1,3)+(depthtimecosthistII(index-1,1)/...
backhaul+depthtimecosthistII(index-1,1)/lowerspeed)*...
billingrate+changeoutcost(2)];
index=index+1;
end
end
%% Back out drill string
depthtimecosthistII(index,:)=depthtimecosthistII(index-1,:)+[0,...
    (kickoffdepth/backhaul),(kickoffdepth/backhaul*billingrate)];
index=index+1;
%% Emplace casing
casingmass=(kickoffdepth-surfdepth)*casing_mass(pipeschedule(2));
depthtimecosthistII(index,:)=depthtimecosthistII(index-1,:)+[0,...
    (kickoffdepth/casingspeed),(kickoffdepth/casingspeed)*billingrate+...
    casingmass*casingcost];
casingtally=casingtally+casingmass;
index=index+1;
%% Cement lower casing
```

```
% Calculate cement volume (annulus) (only portions below plug zone)
Vmaincement=(Holes(pipeschedule(2))^2 - ODs(pipeschedule(2))^2)*...
(kickoffdepth-pluglength-surfdepth)*0.00064516/4*pi;
depthtimecosthistII(index,:)=depthtimecosthistII(index-1,:)+[0,...
    (cementcure+Vmaincement/cementspeed),(cementcure+Vmaincement/...
    cementspeed)*billingrate+cementcost*Vmaincement];
cementtally=cementtally+Vmaincement;
index=index+1;
%% Repeat for laterals:
for j=1:no_laterals
%% Cement for kickoff
depthtimecosthistII(index,:)=depthtimecosthistII(index-1,:)+[0,...
(kickcement),(kickcement*billingrate)+changeoutcost(3)];
index=index+1;
%% Lower lateral drill string
depthtimecosthistII(index,:)=depthtimecosthistII(index-1,:)+[0,...
(kickoffdepth/lowerspeed),(kickoffdepth/lowerspeed*billingrate)];
index=index+1;
%% Drill through to lateral declination
% Determine the time to drill the radial shaft
while 1==1
latspeed=normrnd(mu_gran(pipeschedule(3)),...
sd_gran(pipeschedule(3)));
if latspeed >= 0
break
end
end
latspeed=latspeed/2; % a factor of 2 is included to incorporate
% difficultly of turning radius
disttogo=kickoffarc;
while 1==1
% Determine if a failure occurs during the drilling of the radial
% kickoff
ttf=76-lognrnd(log(38),.1);
if ttf>(disttogo/latspeed)
depthtimecosthistII(index,:)=[kickoffdepth+kickoffarc,...
depthtimecosthistII(index-1,2)+disttogo/latspeed,...
depthtimecosthistII(index-1,3)+disttogo/latspeed...
*billingrate];
index=index+1;
break
else
disttogo=disttogo-ttf*latspeed;
depthtimecosthistII(index,:)=[depthtimecosthistII(index-1,1)+...
ttf*latspeed,depthtimecosthistII(index-1,2)+ttf,...
depthtimecosthistII(index-1,3)+ttf*billingrate];
index=index+1;
depthtimecosthistII(index,:)=[depthtimecosthistII(index-1,1),...
depthtimecosthistII(index-1,2)+depthtimecosthistII(index-...
1,1)/backhaul+depthtimecosthistII(index-1,1)/lowerspeed,...
depthtimecosthistII(index-1,3)+(depthtimecosthistII(index-...
1,1)/backhaul+depthtimecosthistII(index-1,1)/lowerspeed)...
*billingrate+changeoutcost(3)];
index=index+1;
end
end
%% Drill lateral
```

```
% Determine the time to drill the remainder of the lateral shaft
latspeed=latspeed*2; % factor of 2 removed
disttogo=emplacementlength;
while 1==1
% Determine if a failure occurs during the drilling of the lateral
ttf=76-lognrnd(log(38),.1);
if ttf>(disttogo/latspeed)
depthtimecosthistII(index,:)=[kickoffdepth+kickoffarc+...
emplacementlength,depthtimecosthistII(index-1,2)+disttogo/...
latspeed,depthtimecosthistII(index-1,3)+disttogo/latspeed*...
billingrate];
index=index+1;
break
else
disttogo=disttogo-ttf*latspeed;
depthtimecosthistII(index,:)=[depthtimecosthistII(index-1,1)+ttf...
*latspeed,depthtimecosthistII(index-1,2)+ttf,...
depthtimecosthistII(index-1,3)+ttf*billingrate];
index=index+1;
depthtimecosthistII(index,:)=[depthtimecosthistII(index-1,1),...
depthtimecosthistII(index-1,2)+depthtimecosthistII(index-...
1,1)/backhaul+depthtimecosthistII(index-1,1)/lowerspeed,...
depthtimecosthistII(index-1,3)+(depthtimecosthistII(index-...
1,1)/backhaul+depthtimecosthistII(index-1,1)/lowerspeed)*...
billingrate+changeoutcost(3)];
index=index+1;
end
end
%% Back out drill string
depthtimecosthistII(index,:)=depthtimecosthistII(index-1,:)+[0,...
(kickoffdepth+kickoffarc+emplacementlength)/backhaul,...
((kickoffdepth+kickoffarc+emplacementlength)/backhaul...
*billingrate)];
index=index+1;
%% Emplace lateral casing
casingmass=(emplacementlength+kickoffarc)*casing_mass(pipeschedule(3));
depthtimecosthistII(index,:)=depthtimecosthistII(index-1,:)+[0,...
(kickoffdepth/casingspeed+(kickoffarc+emplacementlength)/...
(casingspeed))+phasedelay,(kickoffdepth/casingspeed+...
((kickoffarc+emplacementlength)/(casingspeed)+phasedelay)*...
billingrate)+casingmass*casingcost];
casingtally=casingtally+casingmass;
index=index+1;
%% Emplace waste canisters
% values taken from Ethan Bates thesis
depthtimecosthistII(index,:)=[depthtimecosthistII(index-1,1),...
    depthtimecosthistII(index-1,2)+...
    10/(60*24)*(emplacementlength/5)*no_laterals,... %10 min/canister
    depthtimecosthistII(index-1,3)+700000]; %$700,000/borehole
    % accounts for $10,500/hr radworker emplacement billing rate
%% Plug lateral
depthtimecosthistII(index,:)=depthtimecosthistII(index-1,:)+[0,latplug,...
latplug*billingrate];
depthtimecosthistII(index,1)=kickoffdepth;
index=index+1;
kickoffdepth=kickoffdepth-lateraloffset;
end
```

```
%% Back out vertical casing (above cemented region)
depthtimecosthistII(index,:)=depthtimecosthistII(index-1,:)+[0,...
(pluglength+surfdepth)/backhaul,(pluglength+surfdepth)/...
backhaul*billingrate+closeoutcosts];
depthtimecosthistII(index,1)=pluglength+surfdepth;
index=index+1;
%% Plug borehole
depthtimecosthistII(index,:)=depthtimecosthistII(index-1,:)+[0,...
boreholeplug,boreholeplug*billingrate+plugcost];
depthtimecosthistII(index,1)=0;
vit_wasteparam=vit_wastemass(emplacementlength,no_laterals,...
    pipeschedule,IDs,PWR_frac,Vit_frac,rho_vit);
drillparamII=[casingtally cementtally];
```

D.5 Drilling Costs Script

This script specifies the input parameters to drill_bit_life_II.m. This script is the one that is typed into the MATLAB command window to start the calculations (once the functions and input matrices are saved in 'Current Folder' specified in the MATLAB window). This script is saved as drilling_costs_II.m.

```
%%%%%%%%%%%%%%%%%%%%%%%%%%%%%%%
% Drilling Cost Script %
% Edited by Frances Dozier %
% 2010-2011 %
% Created by Jonathan S Gibbs %
%%%%%%%%%%%%%%%%%%%%%%%%%%%%%%%
clear
clc
close all
format compact
%% Parameter Initialization
load in.mat % loads parameters
Vit_frac= 1; % fraction of canisters with vitrified wasteform
%For this thesis, all canisters are vitrified DNW
PWR_frac=0; %.64*(1-Vit_frac); % fraction of canisters with PWR waste
vit_load=.45; % waste loading of vitrified waste by mass (i.e. 25% of
% Bounding Value from Hamel and Eschenberg p. 8
output=0; % determines whether trial is plotted
index=1; % tracking parameter
% Vertical plug length required (m) from Figure 2.1
pluglength=1000;
% Shaft length of lateral required (m)
```

```
emplacementlength=2000;
% Declination angle of lateral emplacement (degrees from horizontal)
% For this thesis, only 1 vertical shaft is analyzed.
declination=90;
% Number of lateral emplacements used per main shaft
no_laterals=1;
% Pipe schedule combinations to study, values correspond to inner and
% outer diameters of casings and bits
pipeschedule=[1 2 3];
% Number of individual realizations for each combination
no_realizations=1000;
% Total size of the trade-space
spacesize=1;
% Initialize the tracker matrix
tracker=zeros(spacesize,16); % output matrix for key results
% from each trial
%% Trade-space study
if output==1
figure('Position',[100 100 750 900])
end
% For each trial in the trade-space (for each realization) calculate the
% results from the drill_bit_life_II.m and vit_wastemass.m scripts

for n=1:no_realizations
[depthtimecosthistII,drillparamII,vit_wasteparam]=drill_bit_life_II...
    (pluglength,    emplacementlength,declination,no_laterals,...
    pipeschedule(:),ODs,Holes,IDs,mu_sed,mu_gran,sd_gran,sd_sed,...
    PWR_frac,Vit_frac,vit_load,casing_mass,bit_cost,radii);
time=depthtimecosthistII(size(depthtimecosthistII,1),2)/24/...
    vit_wasteparam(1);
cost=depthtimecosthistII(size(depthtimecosthistII,1),3)/vit_wasteparam(1);
tracker(index,:)=[time,cost,drillparamII,vit_wasteparam ,pluglength,...
    emplacementlength,declination,no_laterals,Holes(pipeschedule(1)),...
    Holes(pipeschedule(2)), Holes(pipeschedule(3))];
%% Output
% If plotting is desired, plot the history of depth
% vs. time and cost for the most recent trial
if output==1
depthtimecosthistII(:,2)=depthtimecosthistII(:,2)/24;
subplot(3,1,1)
figure(1)
hold on
plot(depthtimecosthistII(:,2),-depthtimecosthistII(:,1),'LineWidth',2)
xlabel('\fontsize{10}\bfTime (days)')
ylabel(['\fontsize{10}\bfTotal Pathlength, Hole Depth (m)'])
grid on
title(['\fontsize{14}\bfSample Repository'...
    ' Drilling Cost and Time Simulation'])
subplot(3,1,2)
hold on
plot(depthtimecosthistII(:,3)/1e6,-depthtimecosthistII(:,1),'LineWidth',2)
xlabel('\fontsize{10}\bfCost (millions of US dollars)')
ylabel(['\fontsize{10}\bfTotal Pathlength, Hole Depth (m)'])
grid on
subplot(3,1,3)
hold on
plot(depthtimecosthistII(:,2),depthtimecosthistII(:,3)/vit_wasteparam(1)...
```

```
    /1e3,'LineWidth',2)
xlabel('\fontsize{10}\bfTime (days)')
ylabel('\fontsize{10}\bfCost ($/kg of vitrified waste)')
grid on
end
index=index+1;
end
% Find Statistics
averagecost=mean(tracker(:,2)/1000) %average cost in $/kg vit waste
stdevcost=std(tracker(:,2)/1000);
averagetime=mean(tracker(:,1)); %average time in days
stdevtime=std(tracker(:,1));
```

D.6 Disposal Time and Cost Calculation Sample Problem using V-DeepBoRe-II

This section is included so that a V-DeepBoRe-II user can verify correct application of the code. This section includes instructs on implementing the codes and verifying the results. The instructions are worded appropriately for MATLAB beginners.

1. Copy each cell of table D.3 into the MATLAB command window. There should be 14 names of variables in the workspace. Save the workspace as in.mat in the current folder listed at the top of the MATLAB window.
2. Copy vit_wastemass.m, drill_bit_life_II.m, and drilling_costs_II.m into new m files and save them in the current folder listed at the top of the MATLAB window.
3. Open drilling_costs_II.m. Set the variable 'output' equal to 0. This suppresses the plotting function. Set the 'no_realizations' variable equal to 1000. This conducts 1000 trials of the Monte Carlo simulation. Leave all other variables as they are given in Appendix D. The rational for these variables are given in table 6.1.
4. Type drilling_costs_II in the MATLAB command window. After a few seconds, a value for 'averagecost' should print. The average cost should be $37.28 < \text{averagecost} < 45.05$ with a 99.9% confidence.

5. From here, 'no_realizations' can be increased to get a more accurate result. Other variables (pluglength, emplacement length, vit_load, etc.) can also be changed to reflect the specific borehole configuration to be analyzed.

References

1 Kolar, Michael J., "Midweek Perspectives: Waste that won't go away," Pittsburgh Post-Gazette, August 15, 2001.
2 Sapiie, Benyamim, and Michael J. Driscoll, "A Review of Geology-Related Aspects of Deep Borehole Disposal of Nuclear Wastes," MIT Center for Advanced Nuclear Energy Systems, MIT-NFC-TR-109, Cambridge, 2009.
3 Forsberg, Charles, "Radioactive Waste Disposal: Radionuclide Transport in Groundwater." Lecture notes from MIT Course 22.78: Nuclear Chemical Engineering and Waste Management, Cambridge, MA, April 8, 2011.
[4] Sapiie and Driscoll, p. 23.
[5] Sapiie and Driscoll, p. 19.
[6] Sapiie and Driscoll, p. 19.
[7] Hoag, Christopher Ian, "Canister Design of Deep Borehole Disposal of Nuclear Waste," SM Thesis, MIT Dept. Nuclear Science and Engineering, Sept. 2004, p. 31.
[8] Sapiie and Driscoll.
[9] Forsberg, Charles, "Radioactive Waste Disposal: Institutions and Waste Management-I." Lecture notes from MIT Course 22.78: Nuclear Chemical Engineering and Waste Management, Cambridge, MA, April 22, 2011.
[10] Sapiie and Driscoll.
[11] Sapiie and Driscoll, p. 10.
[12] Hoag.
[13] Gibbs, Jonathan S., "Feasibility of Lateral Emplacement in Very Deep Borehole Disposal of High Level Nuclear Waste." Nuclear Eng. Thesis, MIT Dept. Nuclear Science and Engineering, June 2010.
[14] Bates, Ethan A., "A Drop-in Concept for Deep Borehole Canister Emplacement." SM Thesis, MIT Dept. Nuclear Science and Engineering, June 2011.
[15] Sizer, Calvin. "Minor Actinide Waste Disposal in Deep Geologic Boreholes," BS Thesis, MIT Dept. Nuclear Science and Engineering, May 2006.
[16] Shaikh, Samina, "Effective thermal conductivity measurements relevant to deep borehole nuclear waste disposal." SM Thesis, MIT Dept. Nuclear Science and Engineering, February 2007.
[17] Hobbs, Linn W., "Waste Forms and their Behavior I," Lecture notes from MIT Course 22.78: Nuclear Chemical Engineering and Waste Management, Cambridge, MA, April 11, 2011.
[18] Forsberg, Charles, "Radioactive Waste Disposal Overview." Lecture notes from MIT Course 22.78: Nuclear Chemical Engineering and Waste Management, Cambridge, MA, March 16, 2011.
[19] Common Thermodynamic Database Project, www.ctdp.org, accessed May 11, 2011.
[20] Gibbs, p. 25.
[21] "Linking Legacies: Connecting the Cold War Nuclear Weapons Production Processes to Their Environmental Consequences." U.S. Department of Energy Office of Environmental Management, DOE/EM-0319, January 1997.
[22] U.S. Department of Energy Office of Environmental Management, "Linking Legacies."
[23] Murray, Raymond L., *Understanding Radioactive Waste*, 3rd ed., Columbus: Battelle Press, 1989 p. 57.
[24] U.S. Department of Energy Office of Environmental Management, "Linking Legacies."
[25] U.S. Department of Energy Office of Environmental Management, "Linking Legacies," p. 6.
[26] Murray, p. 114.
[27] Hill, R. C. Philip, "A Comparison of Hanford and Savannah River Site High-Level Wastes" Paper presented at 13th International High-Level Radioactive Waste Management Conference, Albuquerque, NM, April 10-14, 2011.
[28] Murray, p. 115.
[29] Murray, p. 115.
[30] Vienna, John D., "Nuclear Waste Vitrification in the United States: Recent Developments and Future Options," *International Journal of Applied Glass Science*, Vol. 1, No. 3, (2010).
[31] U.S. Department of Energy Office of Environmental Management, "Linking Legacies p. 2.
[32] Murray, p. 114.
[33] Hamel, William F., and John F. Eschenberg, "Waste Treatment and Immobilization Plant High-Level Waste Canister Production Estimates to Support Analyses by the Yucca Mountain Project," Department of Energy Office of River Protection, Richland, WA, Sept. 2004.
[34] Hamel and Eshenberg, p. 6.
[35] Hamel and Eshenberg.
[36] Hamel and Eshenberg.

[37]Regalbuto, Monica, "Spent Nuclear Fuel Reprocessing Lecture 1," Lecture notes from MIT Course 22.78: Nuclear Chemical Engineering and Waste Management, Cambridge, MA, March 5, 2011.
[38] Hill.
[39] Hill.
[40] Hobbs.
[41] Hobbs.
[42] Hobbs.
[43] Hamel and Eshenberg.
[44] Hoag.
[45] Anderson, Victoria K. "An Evaluation of the Feasibility of Disposal of Nuclear Waste in Very Deep Boreholes," SM Thesis, MIT Dept. Nuclear Science and Engineering, Sept. 2004, p. 15.
[46] Hoag.
[47] Hamel and Eschenberg.
[48] Hoag, p. 32.
[49] Hoag, p. 44.
[50] Driscoll, M. J., and K. G. Jensen. "Deep Boreholes: Attributes and Performance Requirements", MIT Center for Advanced Nuclear Energy Systems, MIT-NFC-PR-120, Cambridge, MA, May 2010.
[51] Hemond, Harold, and Elizabeth Fechner-Levy, *Chemical Fate and Transport in the Environment*, Academic Press, San Diego, 2000.
[52] Jussila, Petri, "Geosphere Transport of Radionuclides in Safety Assessment of Spent Fuel Disposal," Radiaction and Nuclear Safety Authority, Helsinki, Finland, 2000.
[53]Jussila.
[54] Driscoll, Michael J. "A Case for Disposal of Nuclear Waste in Deep Boreholes," Massachusetts Institute of Technology, Presentation, March 2010.
[55] Jensen, K. G., M. J. Driscoll. "HLW Deep Borehole Design and Assessment: Notes on Technical Performance," MIT Center for Advanced Nuclear Energy Systems, MIT-NFC-PR-116, Cambridge, MA, April 2010.
[56] Anderson.
[57] Sapiie, Benyamim, and Michael J. Driscoll. "A Review of Geology-Related Aspects of Deep Borehole Disposal of Nuclear Wastes," MIT Center for Advanced Nuclear Energy Systems, MIT-NFC-TR-109, Cambridge, 2009.
[58] Driscoll.
[59] Sapiie and Driscoll, p. 41.
[60] Sapiie and Driscoll.
[61] Anderson.
[62] Anderson.
[63] Khristoforova, et al, "Temperature Distribution and Anomalies in the Crystalline Basement of the Tataria Arch," *Physics and Chemistry of the Earth Part A*, Vol. 25, Issues 6-7 (2000), p. 597-604.
[64] Anderson.
[65] Anderson.
[66] Tester, Jefferson W., et al., "The Future of Geothermal Energy: Impact of Enhanced Geothermal Systems (EGS) on the United States in the 21st Century," MIT Interdisciplinary Panel, 2006.
[67] Brady, Patrick V., et al, "Deep Borehole Disposal of High-Level Radioactive Waste," Sandia National Laboratories, SAND2009-4401, July 2009.
[68] Anderson.
[69] Driscoll.
[70] Anderson.
[71] Arnold, Bill W., Peter N. Swift, Patrick V. Brady, S. Andrew Orrell, and Geoff A. Freeze. "Radwaste Management: Deep Boreholes," *Nuclear Engineering International* (February 2010), p. 18-22.
[72] Sapiie and Driscoll.
[73] Cadelli, N., et al. "Performance Assessment of Geological Isolation Systems for Radioactive Waste." Commission of the European Communities, Luxemburg, 1988.
[74] Sapiie and Driscoll, p. 14.
[75] Sapiie and Driscoll, p. 14.
[76] Sapiie and Driscoll, p. 14.
[77] Anderson.
[78] Sapiie and Driscoll.

[79] Anderson, p. 37.
[80] Rebak, Raul B. "Selection of Corrosion Resistant Materials for Nuclear Waste Repositories." *Materials Science and Technology*, Cincinatti, October 15-19, 2006.
[81] Rebak.
[82] Sapiie and Driscoll, p. 14.
[83] Sapiie and Driscoll, p. 14.
[84] Gibbs.
[85] Gibbs.
[86] Gibbs.
[87] Carslaw, H. S., and J. C. Jaeger, *Conduction of Heat in Solids,* 2nd ed. Oxford University Press Inc., New York, 1959, pg. 204.
[88] Scale 6.0, Radiation Safety Information Computational Center, Oak Ridge, TN.
[89] Hill.
[90] Hill.
[91] Miller, Holly. "Initial Radionuclide Inventories," Bechtel SAIC Company, LLC., presented to U.S. Department of Energy, Doc. No. 20040921.0003, Sept. 2004, p. 4-11.
[92] Miller, p. 4-11.
[93] Miller, p. 4-11.
[94] Miller, p. 4-11.
[95] Gibbs, p. 66.
[96] Ranade, Raj. "Thermal Simulation of a Deep-Borehole Storage Facility for Nuclear Waste". Report, MIT Research Science Institute, August 2005, pg. 8-9.
[97] Gibbs, p. 74-80.
[98] Gibbs, p. 66.
[99] Sapiie and Driscoll, p. 52.
[100] Kuo, W.-S., "Evaluation of Deep Drillholes for High Level Nuclear Waste Disposal." SM Thesis, MIT Dept. Nuclear Science and Engineering, October 1991.
[101] Gibbs, p. 66.
[102] Sizgek, G.D., "Thermal Considerations in a Very Deep Borehole Nuclear Waste Repository for Synroc," Materials Research Society Symp. Proc., Vol. 663 (2001).
[103] Kuo.
[104] Gibb, F. G. F., et al., "Modeling Temperature Distribution around Very Deep Borehole Disposal of HLW," Nuclear Technology, Vol. 163, No. 1, July 2008.
[105] Kuo.
[106] Sapiie and Driscoll, p. 51.
[107] Sapiie and Driscoll, p. 51.
[108] Sapiie and Driscoll, p. 14.
[109] Shaikh.
[110] Hoag.
[111] Shaikh.
[112] Perry, John H. and Robert H. Perry, "Engineering Manual: A Practical Reference of Data and Methods in Architectural, Chemical, Civil, Electrical, Mechanical, and Nuclear Engineering," New York: McGraw-Hill Book Company, 1959.
[113] Moore, Ronald W., Hongyan Marr and Michael J. Anderson, "Evaluation of the Thermal Responce of the 5-DHLW Waste Package-Hypothetical Fire Accident," Office of Civilian Radioactive Waste Management, CAL-WIS-TH-000008, October, 2000.
[114] Gibbs, p. 67.
[115] Shaikh, p. 60.
[116] Hoag, p. 61.
[117] Gibbs, p. 67.
[118] Crawford, Charles L., et al., " Overview of Research on Glass and Ceramic Wasteforms for Fuel Cycle Research & Development." *Transactions of the American Nuclear Society*, Vol. 103, No. 1, (November 2010).
[119] Hobbs.
[120] Forsberg, Charles, "Radioactive Waste Disposal Overview."
[121] HSC 6.0 Chemistry Software Package, version 6.06, Outokumpu Research Oy, Pori, Finland.

[122] Revie, R. Winston, and Herbert H. Uhlig, *Corrosion and Corrosion Control; An Introduction to Corrosion Science and Engineering,* 4th ed., Hoboken, NJ:John Wiley & Sons Inc., 2008, pg. 43.
[123] Anderson.
[124] Anderson.
[125] Anderson, p. 37.
[126] Rebak.
[127] Rebak.
[128] Anderson, p. 29.
[129] Forsberg, "Radioactive Waste Disposal Overview."
[130] Hänninen, Hannu. " Factors Affecting the Safe Life of Copper Canisters." Lecture notes from MIT Course 22.78: Nuclear Chemical Engineering and Waste Management, Cambridge, MA, April 20, 2011.
[131] Hänninen.
[132] Hoag.
[133] Anderson.
[134] Revie and Uhlig, p. 156.
[135] Rebak.
[136] Rebak.
[137] Anderson.
[138] Roberge, Pierre R., Handbook of Corrosion Engineering, New York: McGraw-Hill, 2000, p. 653.
[139] Revie and Uhlig, p. 238.
[140] "The Copper Controversy," *Nuclear Energy International*, Article based on "Mechanisms of Copper Corrosion in Aquous Environments" from the Swedish National Council for Nuclear Waste, October 2010.
[141] Braithwaite, Jeffrey W., and Martin A. Molecke. "Nuclear Waste Canister Corrosion Studies Pertinent to Geologic Isolation." *Nuclear and Chemical Waste Mangement*, Vol. 1 (1980). p. 37-50.
[142] Carter, John P., and Stephen D. Cramer. *Materials of Construction for High-Salinity.* United States Department of the Interior Bureau of Mines, 1988.
[143] McCright, R. D. "Corrosion Behavior of Materials Exposed to Hypersaline Geothermal Brine." Presentation at the International Corrosion Forum, Toronto, April 6-10. 1981.
[144] Revie and Uhlig, p. 100
[145] Braithwaite, p. 39
[146] Ballinger, Ronald. "Kinetics - Polarization and Corrosion Rates" Lecture notes from MIT Course 22.72: *Corrosion: The Environmental Degredation of Materials*, Cambridge, MA, March 2, 2011.
[147] Rebak.
[148] Rebak.
[149] Braithwaite.
[150] Rebak.
[151] Maiya, P. S., et al. "Microstructural Characterization, Mechanical Properties, and Corrosion Resistance of the CaO-TiO2 System." Materials and Components Technology Division, Argonne National Laboratory, Argonne, 1993.
[152] Anderson.
[153] Braithwaite.
[154] Braithwaite.
[155] Rebak. p. 6.
[156] Verdes, Giles, et al. "Thermodynamic Properties of the Aluminate Ion and of Bayerite, Boehmite, Diaspore and Gibbsite." *European Journal of Mineralogy*, Vol. 4 (1992), p. 767-792.
[157] Suciu, Dan F., and Penny M. Wikoff. "An Evaluation of Materials for Systems Uing Cooled, Treated, Geothermal or High-Saline Brines." U.S. Department of Energy Idaho Operations Office, Idaho Falls, 1982.
[158] Anderson.
[159] Braithwaite.
[160] Anderson.
[161] Braithwaite.
[162] Rebak.
[163] Rebak.
[164] Braithwaite.
[165] Suciu, p. 8

[166] Roberge, p. 653.
[167] Braithwaite.
[168] Suciu, p. 16
[169] Braithwaite.
[170] MetalPrices.com. *Metal Prices.* May 1, 2011. http://www.metalprices.com/FreeSite/index.asp.
[171] Hill.
[172] Hill.
[173]Randall, Chris T., et al., " The Defense Waste Processing Facility, from Vision to Reality." Westinghouse Savannah River Company, Document WSRC-MS-2000-00111.
[174] Hamel and Eschenberg
[175] Akgunduz, Nina, et al., "Waste Vitrification Systems Lessons Learned," Department of Energy, March 1999.
[176] Akgunduz et al.
[177] Ahn, Joonhong, and Michael J. Apted, *Geologic Repository Systems for Safe Disposal of Spent Nuclear Fuels and Radioactive Waste*, Abington Hall, UK: Woodhead Publishing Ltd., 2010.
[178] Hobbs.
[179] Ledieu, Aurelien, et al., "Contribution of Monte Carlo Modeling to Understanding the Alteration of Nuclear Glasses by Water". *Nuclear Science and Engineering*, Volume 153, Number 3, July 2006. p. 285-300.
[180] Ledieu et al.
[181] Ledieu et al.
[182]Donald, Ian W., *Waste Immobilization in Glass and Ceramic Based Hosts: Radioactive, Toxic and Hazardous Wastes*, Southern Gate, UK: John Wiley & Sons Inc., 2010. p. 285.
[183] Ledieu et al.
[184] Ledieu et al.
[185] Donald, p. 277.
[186] Donald, p. 277.
[187] Crawford, Charles L., et al., " Overview of Research on Glass and Ceramic Wasteforms for Fuel Cycle Research & Development." *Transactions of the American Nuclear Society*, Vol. 103, No.1, (November 2010), p. 168.
[188] Anderson.
[189] Ringwood, A. E., and P. Willis, "Stress Corrosion in a Borosilicate Glass Nuclear Wasteform," *Nature*, Vol. 311, October (1984), p. 735-737.
[190] Ringwood and Willis.
[191] Bickford, D. F., and C. M. Jantzen. "Devitrification of Defense Nuclear Waste Glasses: Role of Melt Insolubles," *Journal of Non-Crystalline Solids,* Volume 84, 1986. p. 299-307.
[192] Ray, J.W., et al., "DWPF Glass Product Control Program," Department of Energy, Document WSRC-IM-91-116-6, Revision 5, August 2004.
[193] Bickford et al.
[194] Spilman, D. B., et al., "Devitrification and Subsequent Effects on the Leach Behavior of a Simulated Borosilicate Nuclear Waste Glass," *Nuclear and Chemical Waste Management*, Vol. 6 (1986), p. 107-119.
[195] Hobbs.
[196] Anderson.
[197] HSC 6.0 Chemistry Software.
[198] Revie and Uhlig, pg. 43.
[199] Common Thermodynamic Database Project, www.ctdp.org, accessed June 23, 2011.
[200] "Tank Closure and Waste Management Environmental Impact Statement," Department of Ecology: State of Washington, Publication 10-05-002, January 2010.
[201] Brady, Patrick V., et al., p. 32.
[202] Arnold, et al., p. 18-22.
[203] Anderson.
[204] Ringwood and Willis.
[205] Spilman et al.
[206] Anderson.
[207] Department of Ecology: State of Washington, Tank Closure and Waste Management Environmental Impact Statement."
[208] Gibbs.

[209] Gibbs, p. 25.
[210] Gibbs, p. 84.
[211] Gibbs, p. 99.
[212] Gibbs, p. 28.
[213] Hamel and Eschenberg, p. 8.
[214] Hoag, p. 38.
[215] Gibbs.
[216] Bates, p. 37.
[217] Bates.
[218] Bates, p. 63.
[219] Bates.
[220] Bates, E. A., M. J. Driscoll, and J. Buongiorno, "Drop-in Concept for Deep Borehole Canister Emplacement" Paper presented at 13th International High-Level Radioactive Waste Management Conference, Albuquerque, NM, April 10-14, 2011.
[221] Bates.
[222] Bates.
[223] Bates
[224] Bates.
[225] Gibbs.
[226] Bates, p. 77.
[227] Bates, p. 78.
[228] Schneider and Bathke.
[229] Schneider and Bathke.
[230] Schneider and Bathke.
[231] Hamel and Eschenberg.
[232] Gibbs, p. 99.
[233] Hamel and Eshenberg.
[234] Andrews, M.K., C.A. Cicero-Herman, and D.T. Herman, "Results of the DWPF Melter Drain Canister, S00209," WSRC-RP-98-00555, Westinghouse Savannah River Company, July 1998
[235] Plodinec, M. D., "DWPF Product Qualification Programs," *Nuclear Waste Technical Review Board Meeting*, February 1992.
[236] Hoag.
[237] Gibbs, p. 135.
[238] Moffett, Matt. "Foot-Wide Shaft Reaches Miners: U.S. Drill Bit Provides a Breakthrough in Chile; Next Phase Poses New Challenge," *The Wall Street Journal*, New York, September 18, 2010.
[239] Anderson.
[240] Ringwood and Willis.
[241] Spilman et al.
[242] Anderson.
[243] Hoag.
[244] Hill.
[245] Hamel and Eschenberg.
[246] Miller, p. 4-11.
[247] Miller.
[248] Buske, Norm and Linda Josephson. "Accounting a Few Radionuclides in Hanford Growndwater," Search Technical Services, Data Report 3, Davenport, WA, Fall 1987, Reprinted November 2002.
[249] Common Thermodynamic Database Project, www.ctdp.org, accessed June 23, 2011.
[250] Anderson, p. 113.
[251] http://www.webelements.com/technetium/chemistry.html
[252] Gibbs.
[253] Bates.